University of Alberta

Seismic response of coal seams in the Western Canadian Basin

by

Verónica L. Martinez

A thesis submitted to the Faculty of Graduate Studies and Research in partial fulfillment of the requirements for the degree of Master of Science

in

Geophysics

Department of Physics

Edmonton, Alberta

Fall 2002

National Library of Canada
Acquisitions and Bibliographic Services
395 Wellington Street
Ottawa ON K1A 0N4
Canada

Bibliothèque nationale du Canada
Acquisitions et services bibliographiques
395, rue Wellington
Ottawa ON K1A 0N4
Canada

Your file Votre référence

Our file Notre référence

The author has granted a non-exclusive licence allowing the National Library of Canada to reproduce, loan, distribute or sell copies of this thesis in microform, paper or electronic formats.

L'auteur a accordé une licence non exclusive permettant à la Bibliothèque nationale du Canada de reproduire, prêter, distribuer ou vendre des copies de cette thèse sous la forme de microfiche/film, de reproduction sur papier ou sur format électronique.

The author retains ownership of the copyright in this thesis. Neither the thesis nor substantial extracts from it may be printed or otherwise reproduced without the author's permission.

L'auteur conserve la propriété du droit d'auteur qui protège cette thèse. Ni la thèse ni des extraits substantiels de celle-ci ne doivent être imprimés ou autrement reproduits sans son autorisation.

0-612-81439-4

Canada

University of Alberta

Library Release Form

NAME OF AUTHOR:	Verónica L. Martinez
TITLE OF THESIS:	Seismic response of coal seams in the Western Canadian Basin
DEGREE:	Master of Science
YEAR THIS DEGREE GRANTED:	2002

Permission is hereby granted to the University of Alberta Library to reproduce single copies of this thesis and to lend or sell such copies for private, scholarly or scientific research purposes only.

The author reserves all other publication and other rights in association with the copyright in the thesis, and except as hereinbefore provided neither the thesis nor any substantial portion thereof may be printed or otherwise reproduced in any material form whatever without the author's prior written permission.

Verónica L. Martinez
Department of Physics
University of Alberta
Edmonton, AB
Canada T6G 2J1

April 22,2002

University of Alberta

Faculty of Graduate Studies and Research

The undersigned certify that they have read, and recommend to the Faculty of Graduate Studies and Research for acceptance, a thesis entitled **Seismic response of coal seams in the Western Canadian Basin** submitted by **Verónica L. Martinez** in partial fulfillment of the requirements for the degree of Master of Science in Geophysics.

Dr. Mauricio D. Sacchi (Supervisor)

Dr. Moritz Heimpel

Dr. Gerhard Reuter

Dr. Doug Schmitt

DATE: April 22, 2002

Progreso y retroceso

Inventaron un cristal que dejaba pasar las moscas. La mosca venia, empujaba un poco con la cabeza y, pop, ya estaba del otro lado. Alegria enormisima de la mosca.

Todo lo arruino un sabio hungaro al descubrir que la mosca podia entrar pero no salir, o viceversa a causa de no se sabe que macana en la flexibilidad de las fibras de este cristal, que era muy fibroso. En seguida inventaron el cazamoscas con un terron de azucar dentro, y muchas moscas morian deseperadas. Asi acabo toda confraternidad con estos animales dignos de mejor suerte.

Julio Cortázar : Cuentos completos/I

Abstract

Seismic exploration has been proven to be a powerful tool for imaging the subsurface of the Earth. There are cases, however, where although sonic logs exhibit significant velocity stratification, seismic processing is unable to obtain a well defined image of the reflectors. Coal seams in the Western Canadian Basin are an example of such a problem. Non-resolvable layers of coal cause large reflection coefficients due to the strong impedance contrast with the background. This behaviour, typical for a cyclic reflectivity causes apparent attenuation of the transmitted signal due to intrabed multiples. The interference between primaries and mutiples will be destructive for certain frequencies. Therefore, the amplitude spectrum of the transmitted signal will exhibit notches for such frequencies. This thesis is intended to propose a processing sequence that helps to compensate for that loss of frequency and therefore achieve a better image of the subsurface.

Acknowledgements

I would like to thank my supervisor, Dr. Mauricio D. Sacchi, for his support and guidance along my research. Also, I would like to thank his family for being somehow my Argentinian family in Edmonton.

I would like to recognize my friends and colleagues Carrie Youzwishen, Henning Kühl and Ulrich Theune for their encouragement and many useful technical conversations. I am also very grateful to my friends Lara De Nardo and Nathalie Lara for their support and great sense of humor.

I would like to thank my good friends from Argentina, especially Mercedes Gil and Cecilia Zarpellon for giving me strength during this time far away from my home country.

Finally, I would like to recognize my family, who shared every single moment of this master, for their constant encouragement and dedication.

To

my parents

Table of Contents

1 Introduction **1**

1.1 Seismic reflectivity sequences. 1

1.1.1 A Western Canadian Sedimentary Basin (WCB) case study: the Rosebud data set 4

1.2 Motivation 4

1.3 Thesis outline 5

2 Cyclic and transitional reflectivities **8**

2.1 Introduction 8

2.1.1 Cyclic and transitional layering 9

2.1.2 Power spectrum and amplitude distribution for primary reflection coefficients 18

2.1.3 Stochastic reflectivity modeling 19

2.2 Fitting ARMA models to WCB log data 24

2.3 Summary 30

3 Stratigraphic filtering **31**

3.1 Introduction 31

3.1.1 Interface transmission losses 32

3.1.2 Multiple reflection effects 33

3.1.3 Layering Filtering 35

3.1.4 Layering Filtering in the Western Canadian Basin 36
3.1.5 Analysis of the impulse response for a single layer using the Z transform 37
3.2 Impulse response for transitional and cyclic reflectivities. 41
3.3 Seismic attenuation due to layering 51
3.4 Summary 54

4 Deconvolution **55**
4.1 Introduction 55
4.2 Deconvolution 56
4.3 Least squares deconvolution 57
4.4 Deconvolution for non-white reflectivity 61
4.4.1 Reflectivity whitening filter 63
4.4.2 Frequency domain filtering 64
4.4.3 Double filtering 64
4.4.4 Spectral compensation filter 65
4.5 Deconvolution in the presence of layering filtering 66
4.6 Non-stationarity of the signal 67
4.7 Examples 68
4.8 Summary 81

5 Modeling techniques **83**
5.1 Synthetic seismograms at zero offset 83
5.1.1 Interface equations 83
5.1.2 Full response model 87
5.2 The reflectivity method (including offset) 89
5.2.1 Homogeneous differential system 91
5.2.2 Layered medium 93

5.2.3 The Source term 97
5.2.4 Complete solution 100
5.2.5 Inverse Transforms 103

6 Conclusions **105**

References **110**

A The reflectivity method **115**
A.1 Non-zero elements of the eigenvector matrix 115
A.2 Reflection and transmission coefficients 117

B O'Doherty-Anstey formula **121**
B.1 Derivation of the O'Doherty-Anstey formula 121

List of Tables

2.1 Values of the autoregressive parameter ϕ_1 and the moving average parameter θ_1 for cyclic and transitional reflectivities found by Walden and Hosken. 22

2.2 Parameters p, λ_1, λ_2 for a Laplace distribution corresponding to a cyclic and a transitional reflectivities found by Walden and Hosken. 22

List of Figures

2.1 Reflectivity corresponding to a well in the Western Canadian Basin 11

2.2 Sonic logs corresponding to three wells from Rosebud area in the WCB. Layers of coal are identified by their high sonic values compared to the background. 13

2.3 Top: Reflectivity series computed from three well sites in the WCB. The presence of coal seams is evidenced by large reflection coefficients (OWT stands for one way time). Bottom: Autocorrelation function (acf). Non-whiteness is exhibited by the oscillatory behavior of the acf at small lags. 14

2.4 Reflectivity series and windowed amplitude spectrum corresponding to cyclic and transitional impedance layering for Well 1 from the WCB. 15

2.5 Reflectivity series and windowed amplitude spectrum corresponding to cyclic and transitional impedance layering for Well 2 from the WCB. 16

2.6 Reflectivity series and windowed amplitude spectrum corresponding to cyclic and transitional impedance layering for Well 3 from the WCB. 17

2.7 Left: cyclic reflectivity series using ARMA(1,1). Right: Corresponding amplitude spectrum computed using the periodogram and the theoretical power spectrum (smooth line). 23

2.8 Left: transitional reflectivity series using ARMA(1,1). Right: Corresponding amplitude spectrum computed using the periodogram and the theoretical power spectrum (smooth line). 23

2.9 Top: Reflectivity series and windowed amplitude spectrum of Well 1 and the fitted ARMA model. Bottom: parameters ϕ and θ found from minimum error. 26

2.10 Top: Reflectivity series and windowed amplitude spectrum of Well 1 and the fitted ARMA model. Center: Comparison of parameters ϕ and θ for the window 0.3-0.4 sec, using bigger search interval. Bottom: Log(J) is plotted in this case for better visualization of the minimum. 27

2.11 Top: Reflectivity series and windowed amplitude spectrum of Well 2 and the fitted ARMA model. Bottom: parameters ϕ and θ found from minimum error. 28

2.12 Top: Reflectivity series and windowed amplitude spectrum of Well 3 and the fitted ARMA model. Bottom: parameters ϕ and θ found from minimum error. 29

3.1 Reflected signal in a layered media. 33

3.2 Intrabed multiple reflected signal for a layered media. 34

3.3 The cumulative effect of the multiple reflections for a sequence of thin layers. 34

3.4 Reflection and transmission coefficients for a wave traveling through a single layer. 37

3.5 Amplitude spectrum for the impulse response of a single layer system as the one presented in figure 3.4. Case 1 : reflection coefficients at the interfaces have opposite signs. 41

3.6 Amplitude Spectrum for the impulse response of a single layer system as the one presented in figure 3.4. Case 2 : reflection coefficients at the interfaces have same signs. 42

3.7 Model for coal seams. 43

3.8 Ray path for primaries, 1st order multiple and 2nd order multiple. 43

3.9 Top: impulse response with transmission loss but no multiples. Bottom: corresponding amplitude spectrum. 44

3.10 Top: impulse response with transmission loss and 1st order multiples. Bottom: corresponding amplitude spectrum. 45

3.11 Top: impulse response with transmission loss and with 2nd order multiples. Bottom: corresponding amplitude spectra. 46

3.12 Top: transitional and cyclic reflectivity sequences. Bottom: corresponding amplitude spectra. 48

3.13 Top: impulse response with transmission loss and no multiples for a transitional and cyclic reflectivity sequences. Bottom: corresponding amplitude spectra. 49

3.14 Top: impulse response with transmission loss and all multiples for a transitional and cyclic reflectivity sequence. Bottom: corresponding amplitude spectra. 50

3.15 Attenuation due to layering only. Attenuation due to transmission loss computed as the spectra ratio of primary time trace to input time trace. Attenuation due to multiples only computed as the spectra ratio of multiple time trace to primary time trace. Attenuation due to layering (transmission + multiples) computed as multiple time trace to input time trace. 53

4.1 Earth model for a transmission filter. 69

4.2 Top: reflectivity model. Middle: zero offset-impulse response (only primaries). Bottom: zero offset-full response. Window A stands for 'Above the transmission filter' and B stands for 'Below the transmission filter'. . . . 70

4.3 Top: O'Doherty and Anstey theoretical amplitude spectrum for the transmitted signal.Bottom: amplitude spectrum A for data between 0.1-0.3 sec overlying amplitude spectrum B for data between 0.5-0.7 sec. 71

4.4 Full impulse response with offset. Window A stands for 'Above the transmission filter' and B stands for 'Below the transmission filter'. 72

4.5 Top: amplitude spectrum for data between 0.1-0.3 sec. Bottom: amplitude spectrum for data between 0.5-0.7 sec, below transmission filter 73

4.6 Full impulse response-stack data. Window A stands for 'Above the transmission filter' and B stands for 'Below the transmission filter'. Stacked trace was repeated for plotting purposes. 74

4.7 Top left: data A (Above transmission filter). Top right: amplitude spectrum A for data A. Bottom left: data B (Below transmission filter). Bottom right: amplitude spectrum B for data B. 75

4.8 Right: data A (Above transmission filter). Left top: extrated wavelet from data A by conventional deconvolution. Left bottom: amplitude spectrum of extracted wavelet A. 76

4.9 Right: data B (Below transmission filter). Left top: extrated wavelet from data B by conventional deconvolution. Left bottom: amplitude spectrum of extracted wavelet B overlying amplitude spectrum of extracted wavelet A. . . 77

4.10 Left:seismic data B, Below transmission filter. Right: seismic data Bf, Below transmission Filter after applying compensatory filter to overcome the loss in frequency content trf_{min} (equation 4.5.4). 78

4.11 Amplitude spectrum A for the data above the transmission filter, overlying the amplitude spectrum B for data below the transmission filter and amplitude spectrum Bf for data below transmission filter after applying compensatory filter trf_{min}. 79

4.12 Top left: extrated wavelet B from data below the transmission filter. Bottom left: amplitude spectrum of the extracted wavelet B overlying amplitude spectrum from extracted wavelet A (Above transmission filter). Top right:extrated wavelet Bf from data below the transmission filter, after compensatory filter. Bottom right: amplitude spectrum of the extracted wavelet Bf, overlying amplitude spectrum from extracted wavelet A. 80

5.1 Reflection coefficient model. 84

5.2 Reflection and transmission coefficients. 84

5.3 Waves at a layer j, time t. 85

5.4 Reflected and transmitted waves at interface j. 85

5.5 Reflected and transmitted ray at an interface z_t. Subscript indicates the incident wave direction. 95

5.6 The generation of the ray expansion when an extra layer $z_{n-1} < z < z_n$ is added to a stack of layers $z_m < z < z_{n-1}$. One ray in each set of reverberations is illustrated. 96

Chapter 1

Introduction

1.1 Seismic reflectivity sequences.

The goal in seismic exploration is to obtain an accurate description of geological formations using seismic wave fields generated and recorded at the surface of the Earth. However, there are cases where, despite sonic logs show significant velocity stratification, seismic processing is not able to generate a well defined image of the reflectors. The key word in those cases is resolution. Some areas present a stratification that is so fine that cannot be resolved by the seismic frequency band. Non resolvable sections in which the impedance structure is cyclic present an apparent attenuation which differs from the linear frequency dependence commonly attributed to absorption. One main cause for this attenuation is the presence of short-path multiples. In cyclic systems, the impedances tend to alternate rapidly between high and low values. Consequently, the reflection coefficients tend to be large and transmission losses are important. Short delay multiples do not show a distinct arrival, but overlays the primary and modifies it by superposition. As more and more multiples are superposed, the primary itself is decreased by transmission losses until the propagating wavelet is purely

multiple energy. The main concept to understand this effect is that the time difference between primary and first multiple is less than the width of the propagating wavelet. Therefore, we are dealing with a problem that it is beyond seismic resolution and as a consequence seismic processing fails to eliminate the multiple energy.

O'Doherty and Anstey (1971) have shown that short path multiples exert an important influence on the amplitude and character of the reflected waves in systems in which the impedance stratification is cyclic. Schoenberger and Levin (1974) attempt to separate the apparent attenuation due to this layering effect from the common attenuation known due to absorption. Based on the latter work, Mateeva (2001) tried to understand the *coloring effect* intrabed multiples have on seismic trace spectra. Still it is a confusing subject, since on top of the big processing limitation due to seismic resolution, there is the problem of non-white reflectivity series. Conventional seismic processing assumes a white earth's reflectivity; hardly ever in the processing flow non-whiteness is taking into account. Cyclic impedance layering presents an amplitude spectrum that is far away of being white (Walden and Hosken, 1985). This property implies another challenge for seismic processing in areas with this type of reflectivities.

Seismic data have to be properly processed in order to obtain a good representation of the subsurface. Processing parameters and assumptions made at this stage have to be coherent with the geological knowledge of the area under study. The difficult task, however, it is to determine how should the right set of parameters be chosen? General assumptions about the seismic model are made during seismic processing so as to simplify the problem under study.

The processing step that needs a significant assumption about the Earth's response is the deconvolution step. Deconvolution is a process that improves the temporal resolution of seismic data by compressing the basic seismic wavelet

(Yilmaz, 1987). A recorded seismogram can be modeled as a convolution of the Earth's impulse response with the seismic wavelet. The Earth's impulse response comprises primary reflections (reflectivity series) and all possible multiples. Ideally, deconvolution should compress the wavelet components and eliminate multiples, leaving only the Earth's reflectivity in the seismic trace. Of course, to be able to compress the wavelet, first it has to be known or approximately estimated. Generally, the wavelet is assumed to be minimum phase, although this is not enough to solve the problem. An extra assumption should be made; the Earth's response is white. Such a significant assumption becomes necessary in order to find the wavelet through the autocorrelation of the trace. The immediate question would be, is this a valid assumption? Computation of the autocorrelation function of primary reflection coefficients from real well logs identifies them as a non-white process evidenced by the presence of significant negative values of autocorrelation at small lags (O'Doherty and Anstey, 1971). Investigations on the spectral properties of primary reflection coefficients were made for a wide variety of rock sequences around the world. It was found (Walden and Hosken, 1985) that each sequence has a 'pseudo white' spectrum above a corner frequency f_c. The power spectrum below f_c fell off as f^{β} where β is between 0.5 and 1.5. After Walden and Hosken (1985), it is clear that the whiteness assumption was invalid.

This thesis is intended to deal with these two main effects, the apparent frequency attenuation due to short path multiples in a cyclic impedance layering and the property of nonwhiteness associated with this type of stratification.

1.1.1 A Western Canadian Sedimentary Basin (WCB) case study: the Rosebud data set

Data from the Western Canadian Sedimentary Basin (WCB) gives a good example of the two effects mentioned in the previous section. Data from the Rosebud area present a challenge at the time of being processed. Thin layers of coal cause large reflection coefficients due to the strong impedance contrast with the background. As it will be explained in chapters 2 and 3, this behavior, typical from a cyclic reflectivity, cause apparent attenuation due to intrabed multiples. The interference between primaries and multiples will be constructive for some frequencies but destructive for others. As a consequence, the amplitude spectrum of the transmitted signal will exhibit notches for certain frequencies. All these effects will change the waveform of the signal as it propagates through the layers, arising then the problem of non-stationarity of the wavelet. At this stage is where the conventional processing fail to get a good image of the subsurface due to two main factors. First, short delay multiples interfering with the primary energy, distorting not only its amplitude but also its phase spectrum. Second, the cyclic reflectivity implies certain order that deviates from the whiteness assumption. These two effects together cause the non-stationarity of the signal. Windowed processing of the data including filters to compensate for the loss of frequency content and the lack of adequate assumptions in seismic processing, seems to be the best way to approach this problem.

1.2 Motivation

As it was mentioned in the previous section, in the WCB thin coal layers act as a layering transmission filter. A notch at certain frequency would then appear in the amplitude spectrum of the transmitted signal just below the transmission

filter. This loss of high frequency content in the signal makes difficult to have a good image of the seismic horizons (reflectors) below the coal seams. Secondly, reflectivity in the presence of coal seams has a non-white correlation structure that should be taken into account at the moment of thinking in deconvolution.

The aim of this work is to propose a processing sequence that helps to compensate for the loss of frequency due to intrabed multiples and therefore achieve a better image of the reservoir. As well, techniques dealing with non-white reflectivity deconvolution will be considered.

1.3 Thesis outline

This thesis reviews the concept of cyclic and transitional layering. Stochastic modeling of reflectivity for these two types of layering systems will be used to model non-white reflectivities and will help at the moment of proposing a new deconvolution scheme for this kind of scenario.

The effect due to intrabed multiples for one simple layer will be presented analytically in order to understand the relation between the apparent attenuation and the characteristics of the layer. Zero offset acoustic deterministic modeling will help in understanding the idea of frequency notches in the transmitted signal through a cyclic layering. Once the zero offset case is introduced and understood, an analysis versus offset is presented. In order to have realistic simulations including effects due to transmission loss and multiples I investigate which modeling technique would be proper for this study. I found that for zero offset modeling the algorithm due to Mendel (1979) and extended by Wyatt (1981) is more flexible than the earlier approaches from Wuenschel (1960), Robinson (1968) and Claerbout (1976). Mendel's algorithm not only allows to place source and sensors at different depth but also the usage of non-equal one way time. This method treats all the equations for a layered-system media in the time domian.

In the case of offset dependent simulations I found that the reflectivity method, although its algorithm is complicated as much as its implementation, it is the best way to perform offset dependent seismic simulations. With this algorithm we overcome the computation difficulties from the traditional matrix methods introduced by Thompson (1950) and corrected and expanded by Haskell (1953) such as growing exponentials. The algortihm I used builds the whole response of an elastic half space in terms of the reflection and transmission properties of the stratified medium (Kennet, 1983). This method do not contain any growing solution and so completely avoid the loss of precision problems. Examples using these techniques are shown to visualize the layering filtering effect.

The structure of the thesis is as follows:

* Chapter 1 provides an introduction, motivation and scope of the thesis.

* Chapter 2 provides an introduction to the concepts of cyclic and transitional reflectivities. The main focus within this chapter resides on the cyclic impedance layering, being this the one that corresponds to coals layering in the WCB. Its probability distribution and autocorretalion structure are also discussed. Models and examples are provided.

* Chapter 3 deals with the impulse response for the two reflectivity types introduced in the previous chapter. Consequences of the short-period multiples associated with cyclic layering are explained theoretically and clarify with examples.

* Chapter 4 first, reviews the existing approaches for deconvolution with non-white reflectivity. Then, a new scheme is proposed to overcome the effects of the apparent attenuation due to cyclic impedance layering. An example is given to illustrate this technique.

* Chapter 5 explains the modeling techniques used to understand the impulse response of coal seams. Techniques involving all multiples and transmission loss are explained for zero offset and offset dependent seismograms.

* Chapter 6 it is a summary of my research and conclusions where I propose a way to face the problem of processing data in the presence of coal seams.

Chapter 2

Cyclic and transitional reflectivities

2.1 Introduction

This chapter deals with the concept of reflection coefficients and their influence in the propagation of waves. The subsurface can be characterized by changes due to different acoustic properties of successive layers. These changes are related to the reflectivity of the subsurface. One can distinguish two extreme types of reflectivity, *cyclic* and *transitional*. Several researchers have work in this problem and there are many publications about the statistical properties of these types of reflectivities as well as their effects on a propagating wavelet. The most important contributions published are those by O'Doherty and Anstey (1971) and Walden and Hosken (1985).

To introduce the subject, let us first start with a basic definition of reflection coefficients. The ratio of the amplitude of the displacement of a reflected wave to that of the incident wave is defined as the *reflection coefficient*. The normal incidence definition for an interface which separates media of densities ρ_1 and ρ_2

and velocities V_1 and V_2 , for a plane wave vertical incidence from medium 1 is given by:

$$R_{12} = \frac{\rho_2 V_2 - \rho_1 V_1}{\rho_2 V_2 + \rho_1 V_1}. \tag{2.1.1}$$

Many authors have studied the amplitude spectrum and distribution of the reflection coefficients of the earth. O'Doherty and Anstey (1971) made a complete analysis on the amplitudes of reflected signal. Their paper paid special attention to those variations in reflection amplitudes imposed by the subsurface geology. According to their research, the factors affecting reflection amplitudes can be enumerated as follows:

- ⇝ spherical divergence
- ⇝ absorption
- ⇝ interface reflection coefficients
- ⇝ interface transmission losses
- ⇝ multiple reflection effects

In this thesis, the focus is on those factors related with interface reflection coefficients, transmission losses and multiples reflections. This chapter deals with the reflectivity properties and how to model them, next chapter is a discussion of their effect in the impulse response.

2.1.1 Cyclic and transitional layering

A series of reflection coefficients as they were defined by equation 2.1.1 can be classified in two main categories *cyclic* and *transitional*. These types of reflectivity are associated with two extreme cases of layering. Cyclic layering is a

pattern of thin layers that alternate high and low velocity materials. Thin layers in this context are defined as those whose thickness is beyond the seismic resolution. This is to say, layers with thickness less than about $\lambda/8$, where λ is the (predominant) wavelength computed using the velocity of the layer. In the presence of noise the threshold of resolution is forced to thicker layers; less than $\lambda/4$ (Widess, 1973) .

Transitional layering would imply steady gradations of velocity within thick layers (O'Doherty and Anstey, 1971). In terms of reflectivity it is found that for the former type, the reflection coefficients tend to be large and with alternating sign due to the significant contrast of velocities at every interface. On the other hand, for the latter type, reflection coefficients are small since the contrast on the layer properties are not so drastic.

Real data, in many cases it is a mixture of these two types of layering. A clear example is shown by the reflectivity series corresponding to well data from the Rosebud area in the WCB. The cyclic pattern, in this case, is given by the presence of coals seams. These are thin layers of 1 to 10 m thickness with velocity and density half of the background in packages of 20 to 30 m. An example of these data is shown in figure 2.1 where sections of transitional and cyclic layering are identified.

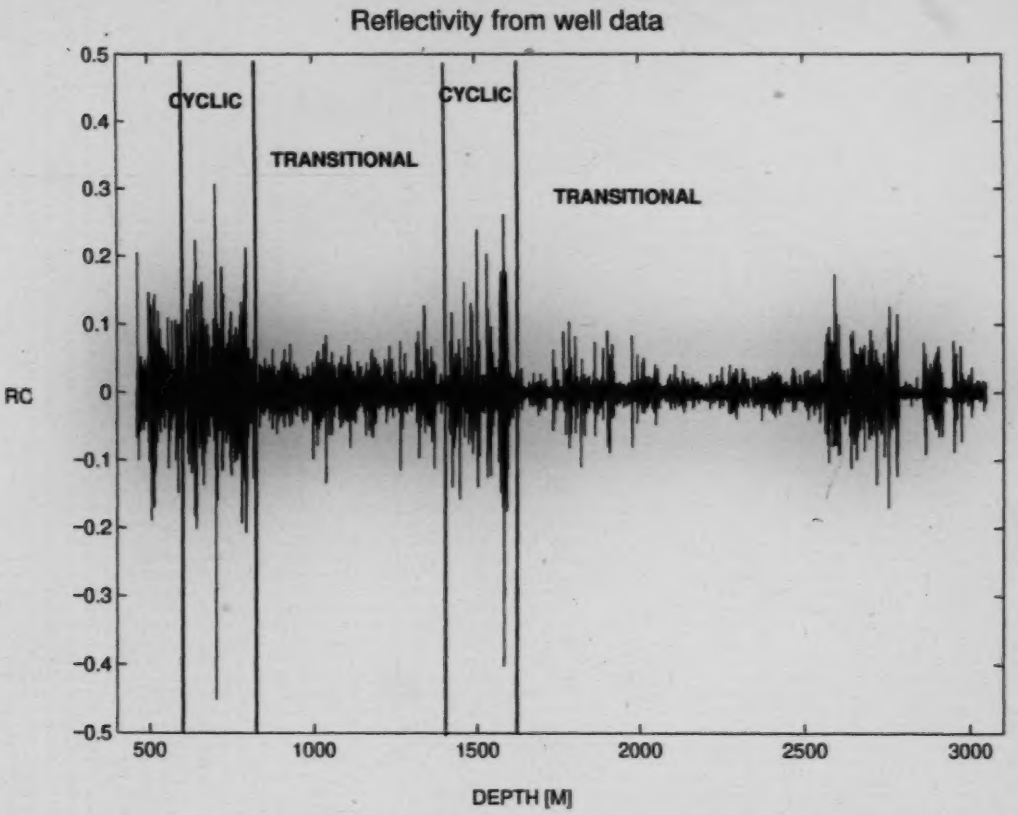

Figure 2.1: Reflectivity corresponding to a well in the Western Canadian Basin

The classification of these types of stratification helps to identify the analogous concept from the point of view of impedance contrast. I will refer from now and on to cyclic reflectivity as the one associated with cyclic layering and transitional reflectivity that associated with transitional layering. The auto-correlation function (acf) of each reflection coefficients series (rc) present different features. The acf for the transitional case, basically, has all positive values for small lags. Instead, for the cyclic case, it reveals a second value strongly negative. This behavior of the acf clearly reveals that reflectivity in neither case is white. A white reflectivity would have an acf with its maximum value at zero lag and zero at the rest of the lags.

Seismic processing, as it was mentioned in the introduction, often makes the assumption of white reflectivity to simplify the deconvolution problem. Real data generally deviate from the whiteness assumption.

The WCB presents clear examples of this type of non-white reflectivities. Data from three wells on the Rosebud area (WCB) help to visualize the characteristics just mentioned. All the wells include layers of coals (cyclic pattern) but as it is shown in the sonic logs for Well 1 the presence of coal seams seems to be stronger than in the other two wells.

As it is shown in figure 2.2 coal seams have a low velocity compared to the background (high values in the sonic log) giving rise to large reflection coefficients. The autocorrelation function shows strong negative values at small lags for well 1 remarking that for this well the influence of coals seams is quite important. The acf for wells 2 and 3 still show negative values at small lags but not as important as in well 1. Coal layers do not seem to have such a strong effect overall the reflection coefficient series in wells 1 and 2.

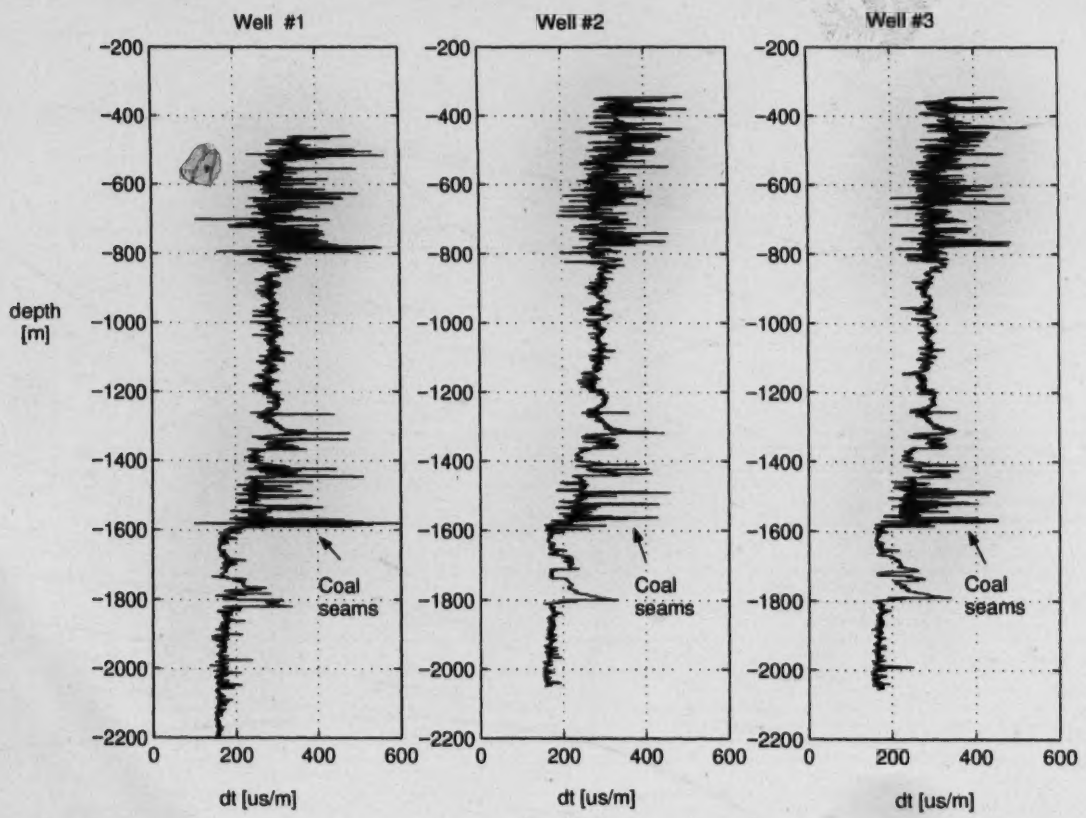

Figure 2.2: Sonic logs corresponding to three wells from Rosebud area in the WCB. Layers of coal are identified by their high sonic values compared to the background.

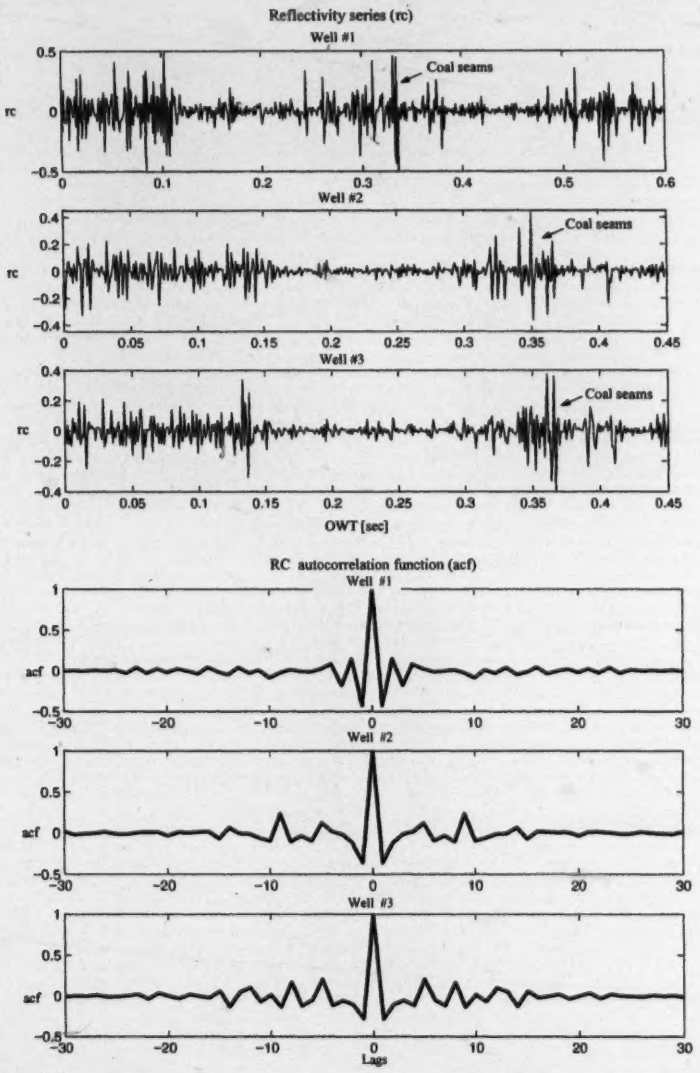

Figure 2.3: Top: Reflectivity series computed from three well sites in the WCB. The presence of coal seams is evidenced by large reflection coefficients (OWT stands for one way time). Bottom: Autocorrelation function (acf). Non-whiteness is exhibited by the oscillatory behavior of the acf at small lags.

It is interesting to visualize how the amplitude spectrum changes through different time windows taken from the reflectivity series of each well. Figures 2.4, 2.5, 2.6 illustrate the amplitude spectrum for windows containing transitional and cyclic reflectivity respectively. Note that reflectivity series are pseudo white as observed by Walden and Hosken (1985).

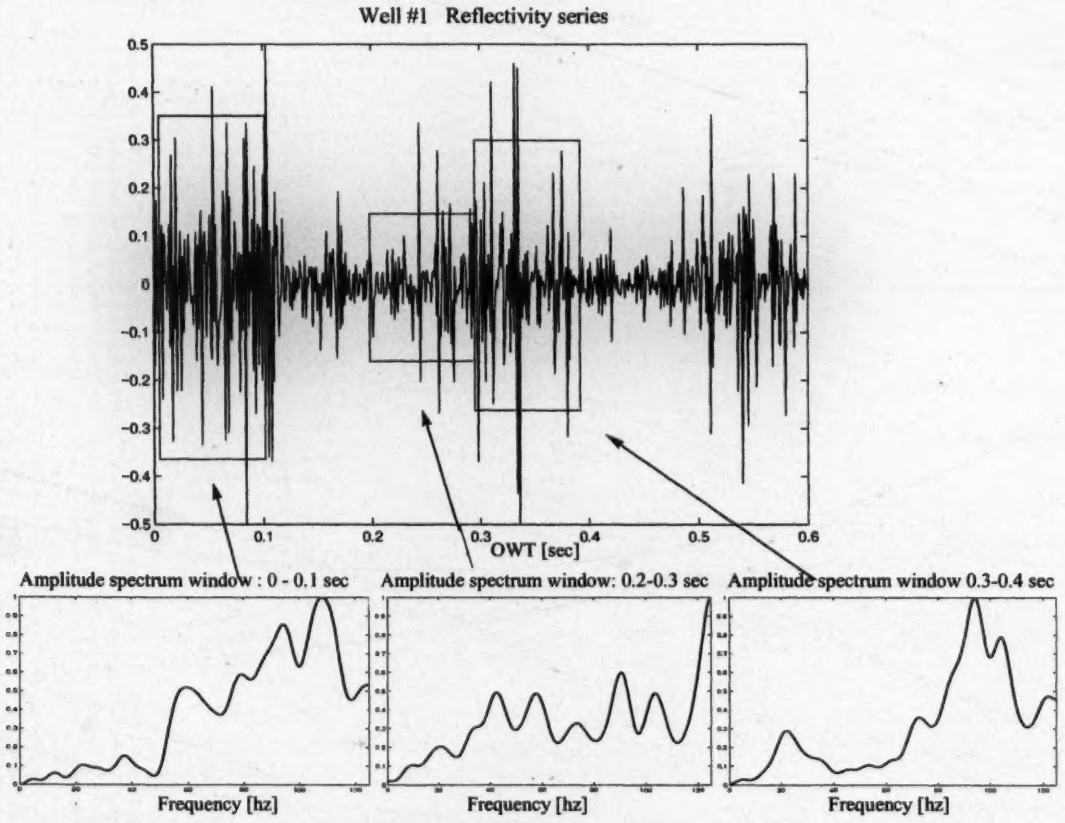

Figure 2.4: Reflectivity series and windowed amplitude spectrum corresponding to cyclic and transitional impedance layering for Well 1 from the WCB.

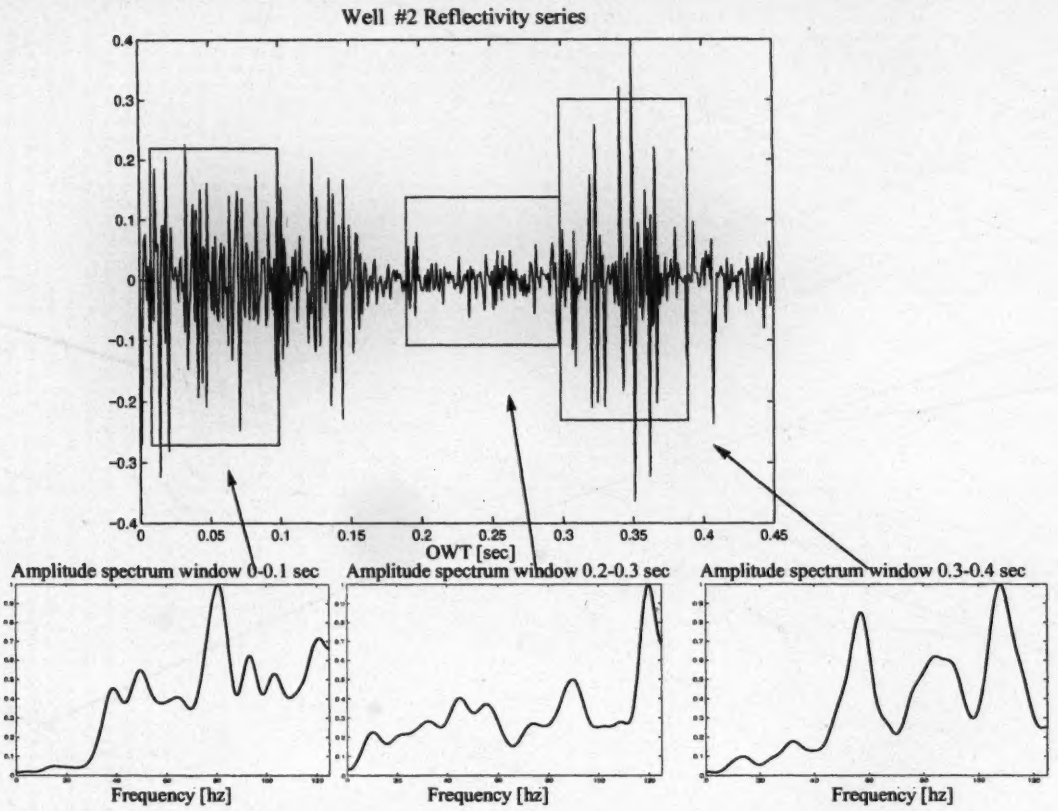

Figure 2.5: Reflectivity series and windowed amplitude spectrum corresponding to cyclic and transitional impedance layering for Well 2 from the WCB.

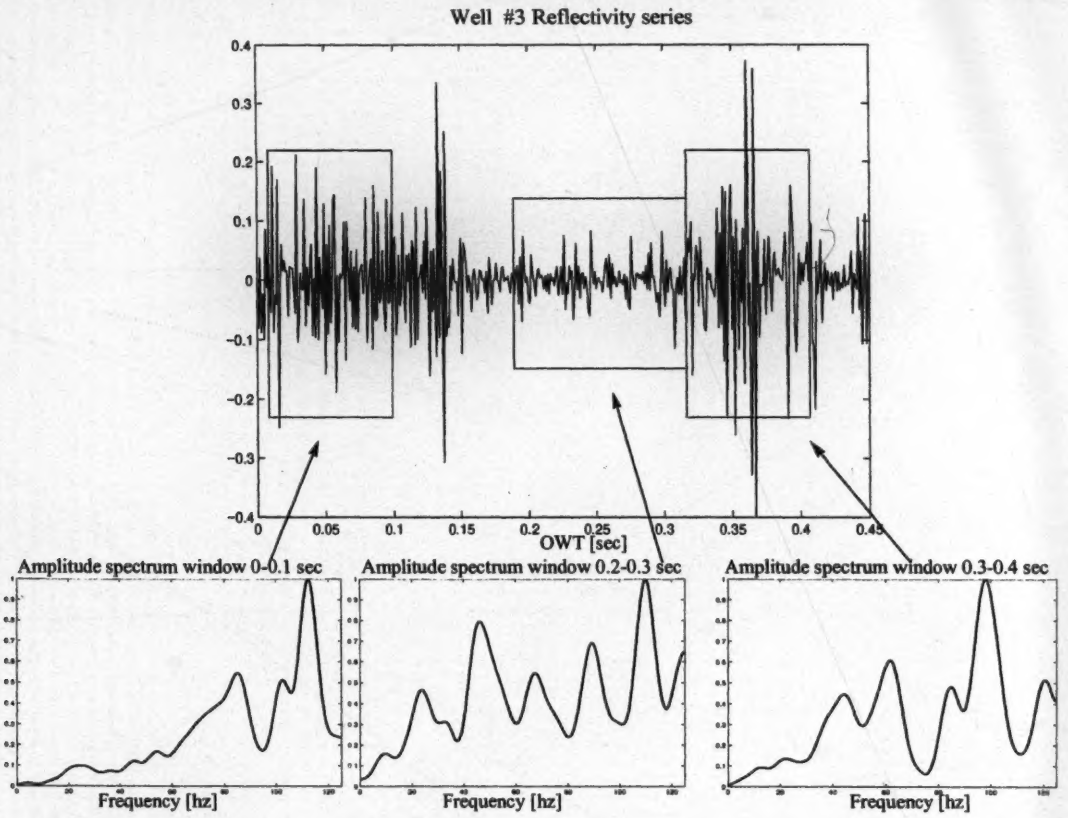

Figure 2.6: Reflectivity series and windowed amplitude spectrum corresponding to cyclic and transitional impedance layering for Well 3 from the WCB.

2.1.2 Power spectrum and amplitude distribution for primary reflection coefficients

Studies of the spectral properties of primary reflectivity have been published, an important contribution is the work done by Walden and Hosken (1985). They basically investigated the form of the non-whiteness encountered in the reflection coefficient series corresponding to different well data around the world.

It was found that the reflection series are pseudo-white only above a corner frequency below which their power spectrum falls away according to a power law f^{β}, where β is between 0.5 and 1.5. Cyclic reflectivity has a value of β which tend to be greater than in the case of transitional reflectivity. Examples illustrating this features can be seen in the figures from the previous analysis for the Rosebud data and also in the stochastic modeling presented in the following section (figures 2.7 and 2.8).

Another important property of the reflection coefficient series is its amplitude distribution. In general no assumption is made about the probability distribution of the reflection coefficients in conventional deconvolution, or if it is done, then is assumed to be Gaussian. Walden and Hosken (1986) also studied this property and they found that the distribution is essentially symmetric but has a sharper central peak and larger tails than a Gaussian distribution.

While in many cases Gaussianity is assumed for convenience, in wavelet phase estimation, it is necessary that the reflection coefficients are not Gaussian or else phase recovery is impossible (Sacchi and Ulrych, 2000). A Gaussian reflection coefficient series means that the trace is also Gaussian and its probability structure is completely determined by the modulus of the wavelet's transfer function at each frequency, that is to say, by the spectral density which carries no phase information.

Walden and Hosken (1986) proposed that a mixture of two Laplace distribu-

tions provides a good fit to the amplitude distribution of the primary reflection coefficients. They found that the single distribution representation of amplitudes of reflection coefficient always corresponds to an underlying kurtosis [1] of about six or above. They suggested that a suitable mixture model representation might be in terms of two-component distributions whose sum always corresponds to a kurtosis exceeding six whatever the mixing proportions. A model satisfying such a constraint is a mixture of two Laplace (or double-sided exponential) distributions, such a mixture always has a kurtosis exceeding six.

2.1.3 Stochastic reflectivity modeling

Based on what was observed in terms of the spectral properties of the reflection coefficient sequences, it was found (Walden and Hosken, 1985) that an ARMA(1,1) process would be a simple way for modeling the kind of spectrum described in the previous section.

An ARMA(1,1) is a mixed autoregressive/moving average process (Chatfield, 1996) and is given by:

$$x_t = \phi_1 \; x_{t-1} \; + \; \varepsilon_t - \theta_1 \; \varepsilon_{t-1}, \tag{2.1.3}$$

where x_t represent the reflection coefficients, ϕ_1 is the autoregressive parameter, θ_1 is the moving-average parameter, ε_t is a pure random process with zero mean and variance σ_ε^2 with a Laplace distribution.

The Power Spectrum of an ARMA(1,1) can be computed by means of the z-transform. Let us first introduce the concept of z transform (see for instance,

[1] Given a zero mean time series x_t kurtosis is defined as:

$$K_x = \frac{E[x_t^4]}{(E[x_t])^2} \tag{2.1.2}$$

where $E[.]$ stands for expected value.

Robinson and Treitel, (1980). Given a sequential collection of samples

$$x_0, x_1, x_2, ..., x_n. \tag{2.1.4}$$

where x_n indicate the sample at time $n\triangle t$. Then, the Z transform of x_k with $k = 0, 1, 2, 3...n$ is defined as

$$X(z) = \sum_{k=0}^{n} x_k \, z^k, \tag{2.1.5}$$

where z is known as the delay operator given by,

$$z = e^{i\omega}, \tag{2.1.6}$$

ω is the angular frequency given in radians.

Now, using the z-transform, equation 2.1.3 can be re written as:

$$X(z)\,[1 - \phi_1 z] = E(z)\,[1 - \theta_1 z]. \tag{2.1.7}$$

Then the power spectrum is defined by:

$$P(z) = X(z)\,X(z^{-1}), \tag{2.1.8}$$

by replacing $z = e^{i\omega}$,

$$P(z) = \sigma_\varepsilon^2 \frac{[1 - \theta_1 z][1 - \theta_1 z^{-1}]}{[1 - \phi_1 z][1 - \phi_1 z^{-1}]}, \tag{2.1.9}$$

$$P(\omega) = \sigma_\varepsilon^2 \frac{1 + \theta_1^2 - 2\theta_1 cos(\omega)}{1 + \phi_1^2 - 2\phi_1 cos(\omega)}. \tag{2.1.10}$$

The auto-covariance function $c_k = E(x_t x_{t+k})$ ($E(.)$ denoting expected value) is given by (Box and Jenkins, 1970)

$$c_0 = \sigma^2 = [(1 + \theta_1^2 - 2\phi_1\theta_1)/(1 - \phi_1^2)]\sigma_\varepsilon^2. \tag{2.1.11}$$

$$c_1 = [(1 - \phi_1\theta_1)(\phi_1 - \theta_1)/(1 - \phi_1^2)]\sigma_\varepsilon^2. \tag{2.1.12}$$

$$c_k = \phi_1 c_{k-1} \qquad k \geq 2. \tag{2.1.13}$$

Then, the autocorrelation function (acf) $\rho_k = c_k/\sigma^2$ is given by:

$$\rho_0 = 1. \tag{2.1.14}$$

$$\rho_1 = [(1 - \phi_1\theta_1)(\phi_1 - \theta_1)/(1 - \phi_1^2)]. \tag{2.1.15}$$

$$\rho_k = \phi_1 \rho_{k-1} \qquad k \geq 2. \tag{2.1.16}$$

The acf decays exponentially from the starting value ρ_1. The decay is smooth if ϕ_1 is positive and oscillatory if ϕ_1 is negative (Walden and Hosken, 1985). Notice that the sign of ρ_1 is given by the sign of $(\phi_1 - \theta_1)$. The process is correlated if $\phi_1 > \theta_1$ and anti-correlated (negatively correlated) if $\phi_1 < \theta_1$. When $\phi_1 = \theta_1$ the process is uncorrelated and it reduces to white noise.

The mixed Laplace distribution is given by:

$$f(r; p, \lambda_1, \lambda_2) = \frac{p}{2\lambda_1} e^{-\frac{|r|}{\lambda_1}} + \frac{1-p}{2\lambda_2} e^{-\frac{|r|}{\lambda_2}}, \tag{2.1.17}$$

p and $(1 - p)$ are the mixing proportions of the Laplace distributions

$$\tfrac{1}{2\lambda_1}\, e^{-\frac{|r|}{\lambda_1}} \text{ and } \tfrac{1}{2\lambda_2}\, e^{-\frac{|r|}{\lambda_2}},$$

where λ_1 and λ_2 are the scale parameters of the first population and second population, respectively. Values found by Walden and Hosken for the ARMA(1,1) and for the Laplace distribution for the cases of cyclic and transitional reflectivity are given in tables 2.1 and 2.2 respectively.

Notice that in both cases $\phi_1 < \theta_1$ showing that the process should be anti-correlated. In the cyclic case $\phi_1 << \theta_1$, thus it is expected to find important

rc sequence	ϕ_1	θ_1
cyclic	0.1	0.9
transitional	0.8	0.98

Table 2.1: Values of the autoregressive parameter ϕ_1 and the moving average parameter θ_1 for cyclic and transitional reflectivities found by Walden and Hosken.

rc sequence	p	λ_1	λ_2
cyclic	1	0.09	0
transitional	0.23	0.007	0.017

Table 2.2: Parameters p, λ_1, λ_2 for a Laplace distribution corresponding to a cyclic and a transitional reflectivities found by Walden and Hosken.

negative values for small lags in this case. Instead, the transitional case has a ϕ_1 which is closer to θ_1, though is still below it, but this reflects that this case is closer to a white process than the cyclic one.

The modeled reflectivity series for a cyclic and transitional case using ARMA(1,1) with Walden and Hosken parameters is shown in the figures 2.7 and 2.8.

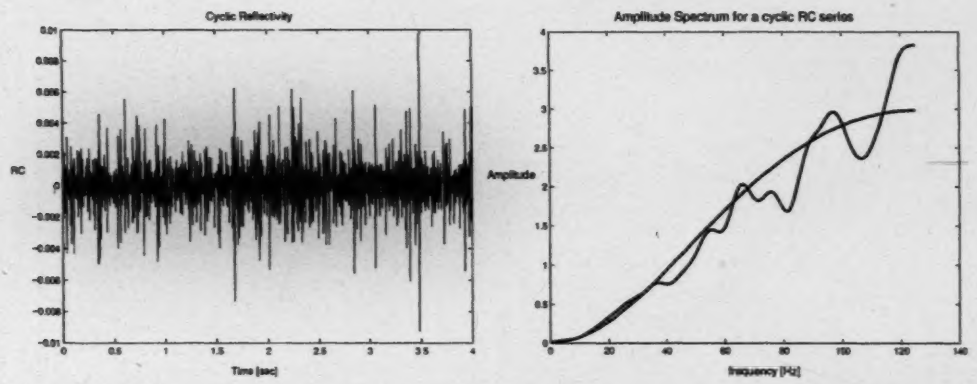

Figure 2.7: Left: cyclic reflectivity series using ARMA(1,1). Right: Corresponding amplitude spectrum computed using the periodogram and the theoretical power spectrum (smooth line).

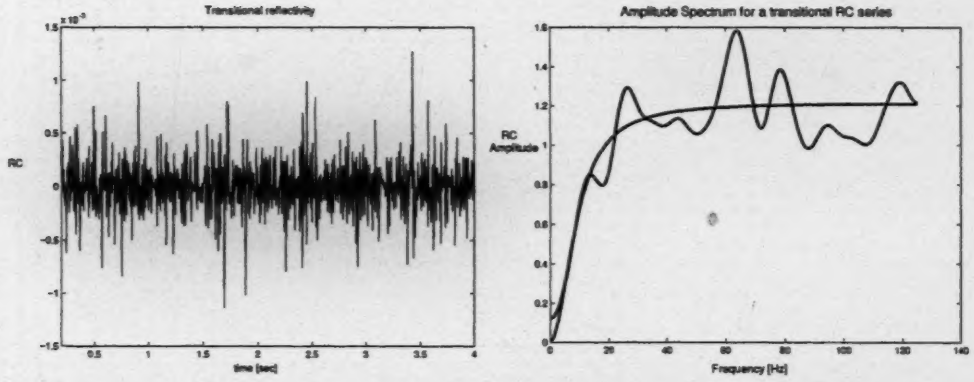

Figure 2.8: Left: transitional reflectivity series using ARMA(1,1). Right: Corresponding amplitude spectrum computed using the periodogram and the theoretical power spectrum (smooth line).

2.2 Fitting ARMA models to WCB log data

Based on the ideas of Walden and Hosken (1985), ARMA(1,1) models were fit to the well data from the WCB. Therefore, it is necessary to estimate the autoregressive parameter ϕ_1 and the moving-average parameter θ_1. This estimation is perfomed in an iterative way, the sum of squares of the residuals can be calculated at every point on a suitable grid of parameter values. The values which give the minimum sum of squares may then be the best estimated parameters (Chatfield, 1996). The model is given by:

$$x_t = \phi_1 \ x_{t-1} + \varepsilon_t - \theta_1 \ \varepsilon_{t-1}, \tag{2.2.1}$$

where x_t is the reflectivity series coming from log data. Given N observations $x_1, ...x_N$; values for ϕ_1 and θ_1 are found by grid search. Given an initial value for ε_0, the residuals are calculated recursively by:

$$\varepsilon_t = x_t - \phi_1 \ x_{t-1} + \theta_1 \ \varepsilon_{t-1}. \tag{2.2.2}$$

The residual sum of squares may then be calculated as:

$$J = \sum_{t=1}^{N} \varepsilon_t^2. \tag{2.2.3}$$

Then, several values of ϕ_1 and θ_1 are tried until the minimum of J is found. One fact to take into account when defining the range of values to test is that an ARMA(1,1) process is stationary if $\mid \phi_1 \mid < 1$ and invertible or minimum phase if $\mid \theta_1 \mid < 1$. This limits the range of parameters. In the case of fitting ARMA models to the Rosebud well data, I used the values found by Walden and Hosken (1985) as the reference values to set the limits. Therefore, the search was done with $0.05 < \phi_1 < 0.9$ and $0.5 < \theta_1 < 0.92$. Models were perfomed for sections corresponding to cyclic and transitional patterns present in each well. The sections chosen are time windows of 0.1 sec cointaining 100 samples. Figures

2.9, 2.11 and 2.12 illustrate the three wells with their amplitude spectra computed using a periodogram technique (Chatfield, 1996) and using ARMA models. The corresponding plot of the residual sum of squares to find the parameters ϕ_1 and θ_1 is shown at the bottom of those figures.

Notice that for well 1 the fitted model at window 0.3-0.4 sec does not give a good approximation of the amplitude spectrum because it overestimates the values. In this case, it was found that allowing ϕ_1 and θ_1 to vary between -1 to 1 a better fit is obtained. As a result it was found a value for $\phi_1 < 0$, that would agree with a more oscillatory acf as the one observed in this window due to the strong effect of the coal seams. On the other hand, it can be seen from the plot of the cost function J that the optimal parameters are in a wide region. Figure 2.10 illustrate this case, for better visualization of the minimum value $log(J)$ instead of J has been plotted.

In all the other windows changing the searching limits between -1 and 1 does not result in significant differences. Only for well 1 and the window 03-04 sec the parameters found in the larger interval were used. These parameters are $\phi_1 = -0.33$ and $\theta_1 = 0.2$.

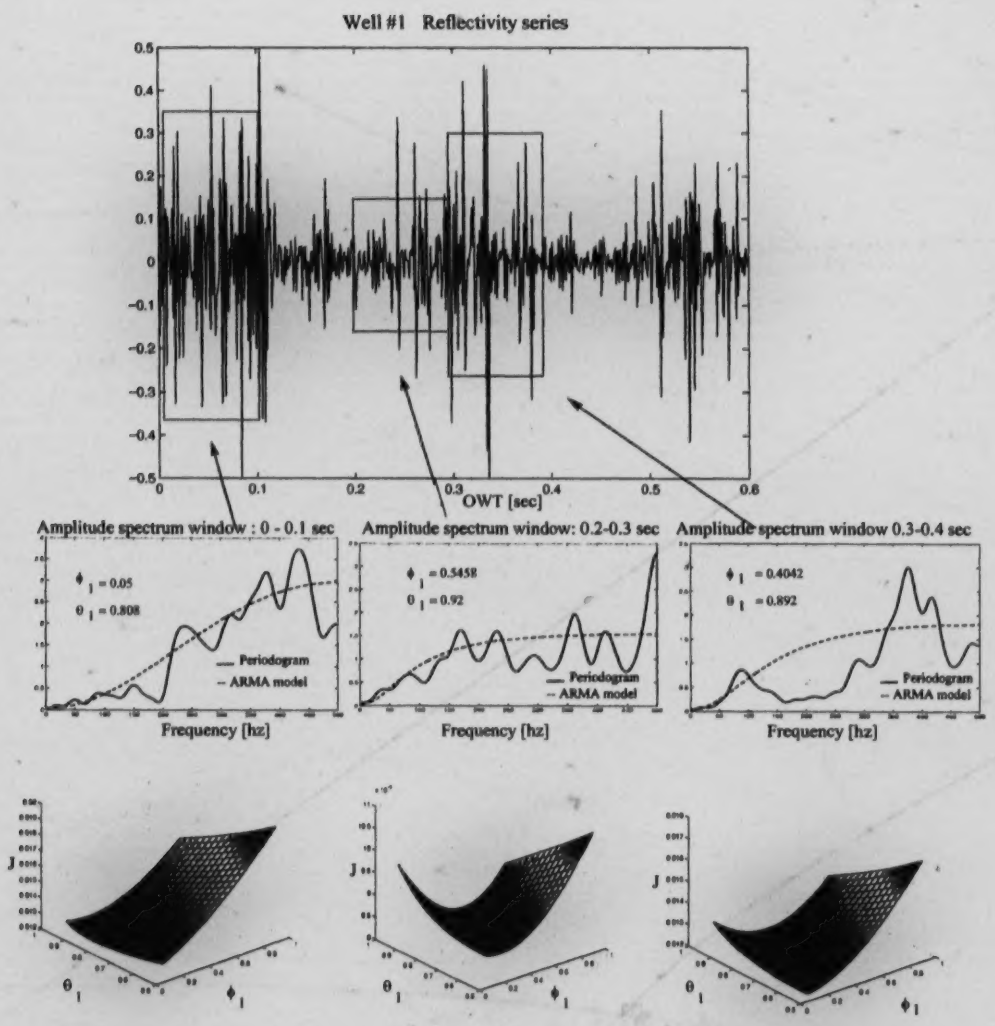

Figure 2.9: Top: Reflectivity series and windowed amplitude spectrum of Well 1 and the fitted ARMA model. Bottom: parameters ϕ and θ found from minimum error.

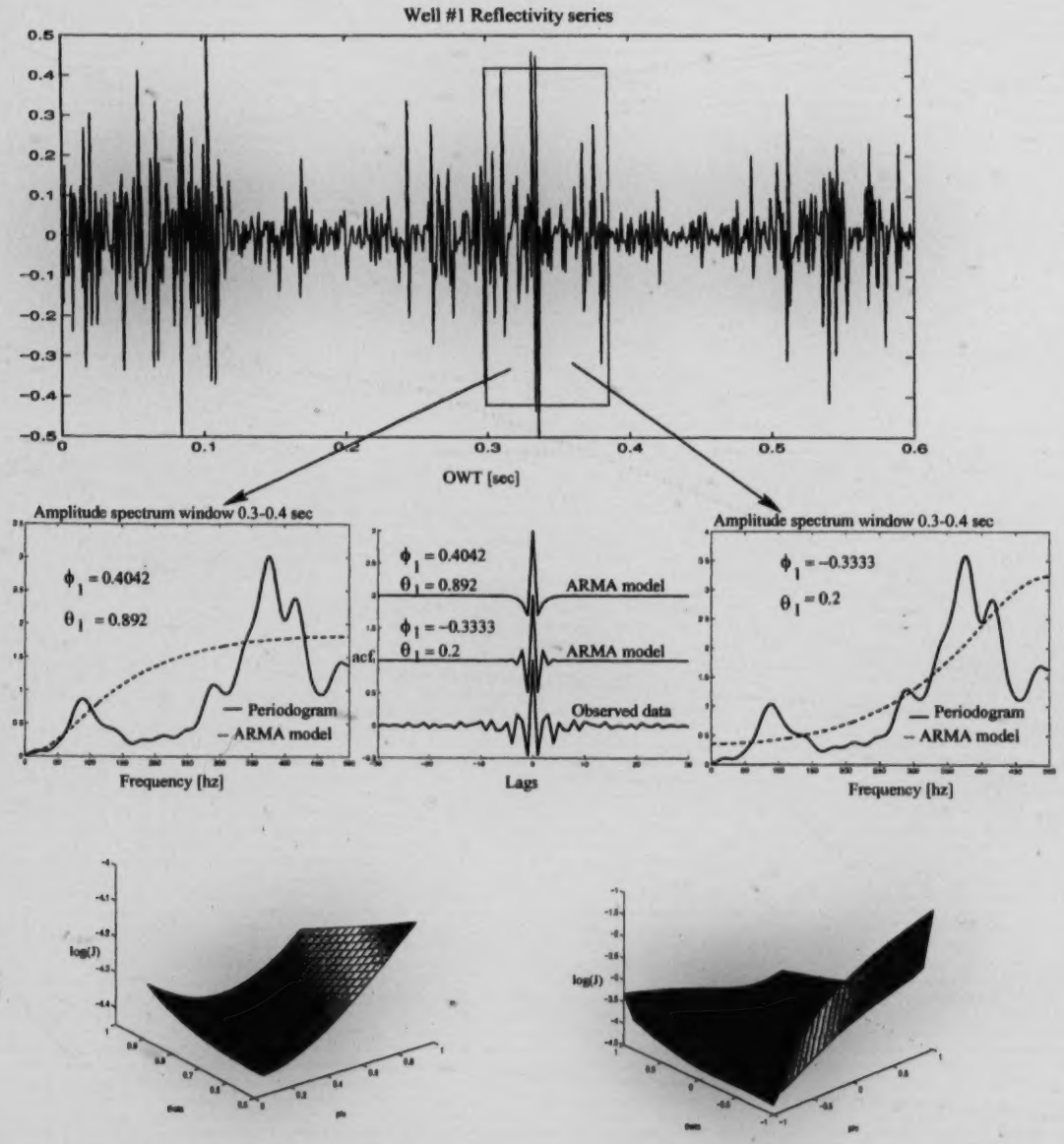

Figure 2.10: Top: Reflectivity series and windowed amplitude spectrum of Well 1 and the fitted ARMA model. Center: Comparison of parameters ϕ and θ for the window 0.3-0.4 sec, using bigger search interval. Bottom: Log(J) is plotted in this case for better visualization of the minimum.

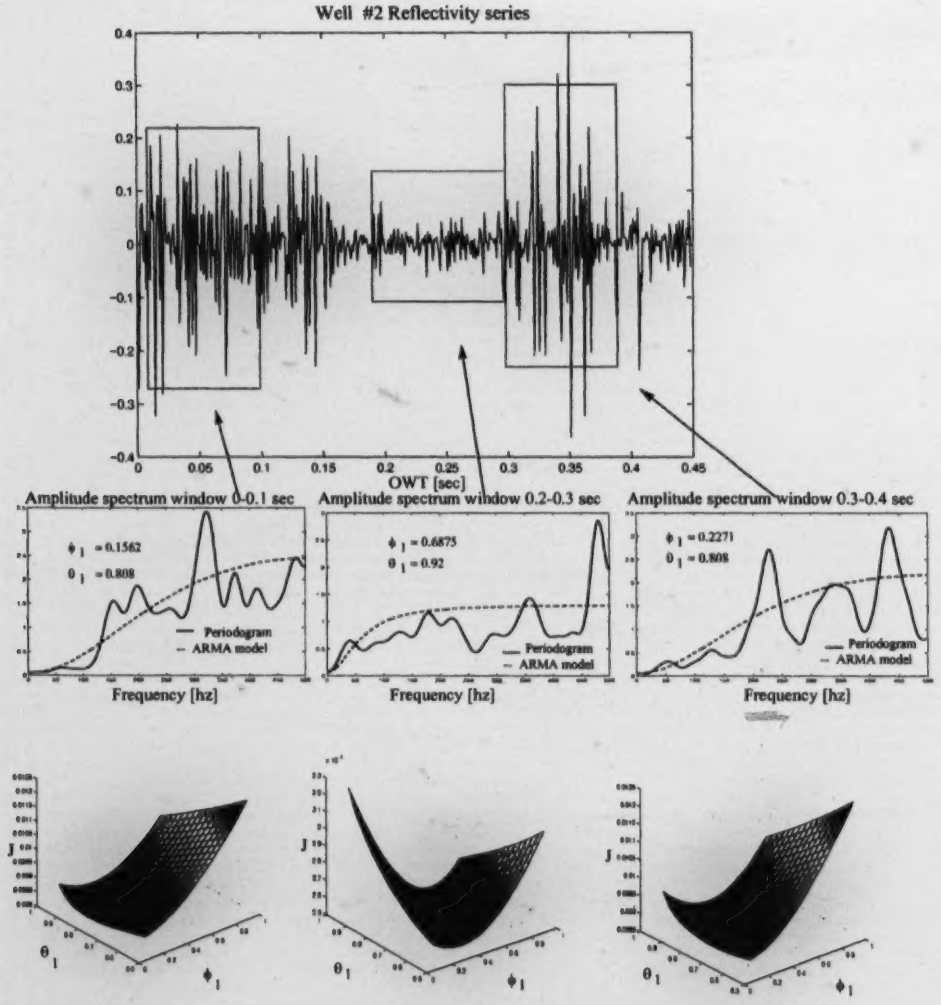

Figure 2.11: Top: Reflectivity series and windowed amplitude spectrum of Well 2 and the fitted ARMA model. Bottom: parameters ϕ and θ found from minimum error.

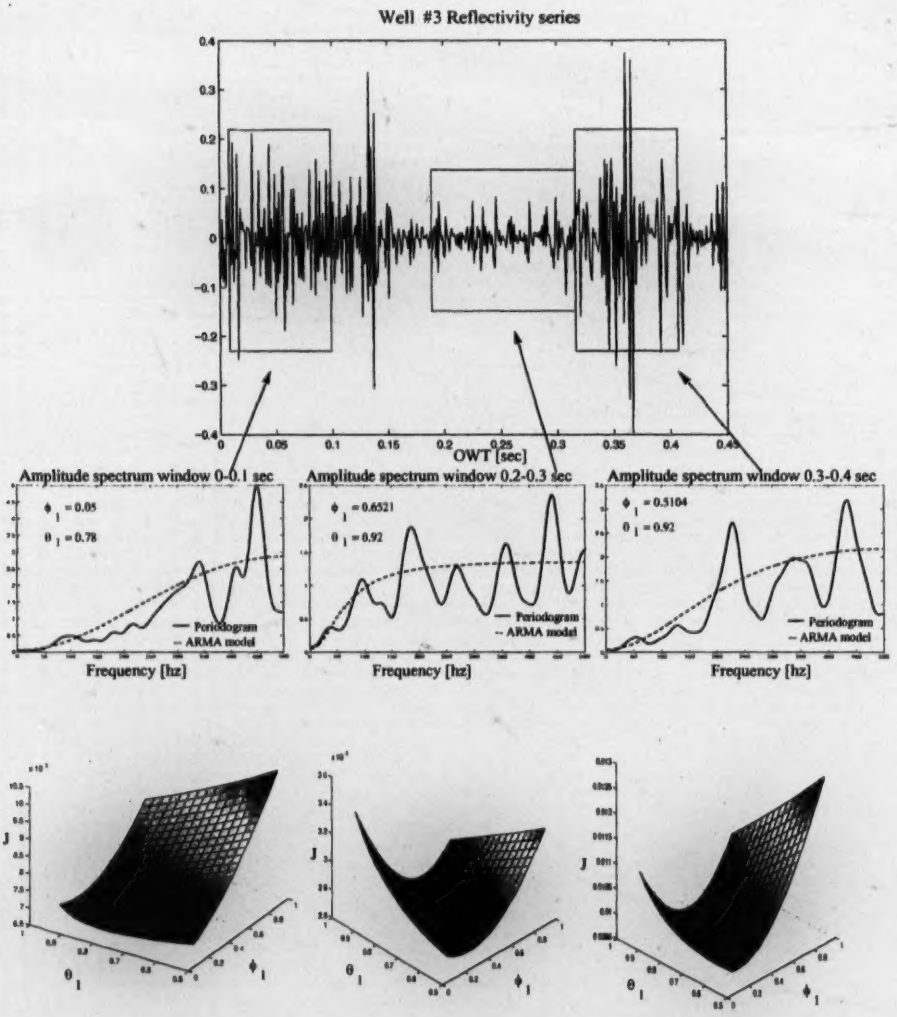

Figure 2.12: Top: Reflectivity series and windowed amplitude spectrum of Well 3 and the fitted ARMA model. Bottom: parameters ϕ and θ found from minimum error.

2.3 Summary

In this chapter, the concepts of cyclic and transitional reflectivities were reviewed.

A cyclic impedance layering is the one that corresponds to high reflection coefficients alternating signs. Its autocorrelation presents important negative values at small lags revealing its non-whiteness. Its power spectrum decays according to a power law f^{β}, where β tends to be greater than in the case of a transitional reflectivity.

The transitional case is described by small reflection coefficients. Its autocorrelation is smoother than in the cyclic case with positive values at small lags. Its power spectrum has a gently small slope.

Walden and Hosken (1985; 1986) have shown that reflectivity series, in general, are non-white and its amplitude distribution is not Gaussian. They have proposed that both types of reflectivity can be modeled by an ARMA(1,1) process. This kind of process is defined by two parameters, an autoregressive parameter ϕ and the moving-average parameter θ. Its autocorrelation function suggests that the process is uncorrelated when $\phi = \theta$. In the cyclic case the autoregressive parameter ϕ tends to be far away from the moving-average parameter θ, while in the transitional case they are closer. This fact clearly indicates that there is certain order or correlation being stronger in the cyclic case.

In the Western Canadian Basin, the presence of sections with coal seams perfectly fit into the definition of cyclic reflectivity. It is interesting to be able to model cyclic reflectivities for further applications during deconvolution as it will be explained in chapter 4.

Examples were given using well log data from the Western Canadian Basin. Several log sections corresponding to the two types of reflectivity were chosen and modeled using ARMA(1,1) processes.

Chapter 3

Stratigraphic filtering

3.1 Introduction

In the previous chapter I have discussed two types of reflectivitites that can be used to model seismic data. It is important to notice that, in general, reflectivity series exhibit segments that can be considered of either cyclic or transitional behavior. In this chapter, I will focus on the study of the Earth impulse response when the Earth consists of vertically stratified succession of layers. There are two main factors to consider. First, the interface transmission losses and secondly multiple reflection effects. As it was mentioned in the introduction of this thesis, these effects are critical in the case of a cyclic impedance stratification. Interference between primary and short path multiples is the key point to understand the frequency attenuation of the transmitted signal.

Apparent attenuation due to layering is often known as *stratigraphic filtering*, *layering filtering* or simply *transmission filtering*.

O'Doherty and Anstey (1971) proposed a connection between the amplitude spectrum of the pulse transmitted through the stratigraphic filtering and the power spectrum of the reflection coefficients corresponding to the layering filter.

After their work, many others authors focus on the problem of stratigraphic filtering and study different approaches to derive the O'Doherty and Anstey formula since their derivation seems to be too sketchy to follow. Banik (1985b) proposed a new derivation of O'Doherty and Anstey formula based on the mean field theory (see Appendix B). Schoenberger and Levin (1974) accept O'Doherty and Anstey derivation and focus on separating the apparent attenuation due to layering filtering from the common one known due to absorption. Mateeva (2001) follow this latter approach to explain the "color" imposed by the short-delay multiples in the spectrum of the seismic trace.

In this chapter the concept of layering filtering will be discussed. Examples are given in order to clarify the difference on the impulse response for transitional an cyclic reflectivities. Deterministics and stochastic reflectivity models are used to illustrate the effect of a cyclic layering. Finally, following Schoenberger and Levin (1974), an example will help to illustrate that the effects of layering filtering are a combination of transmission loss and multiple interference.

3.1.1 Interface transmission losses

The importance on the classification of cyclic and transitional reflectivity arises when we compare the interface transmission losses for each case. To clarify the idea let us write the two-way transmission loss for a normal incidence case:

$$T_{12} = 1 - R_{12}^2. \tag{3.1.1}$$

where R_{12} is the reflection coefficient between layers 1 and 2. T_{12} is the two way transmission coefficient between same layers as they are illustrated in figure 3.1.

From this expression it is easy to see that in the case of transitional reflectivity where the reflection coefficients are small, transmission loss is not significant. Instead, for a cyclic case, represented by high reflection coefficients, transmission losses becomes quite important.

Now, we consider the amplitude of a reflection coming from the third layer as shown in figure 3.1

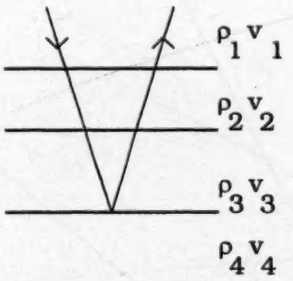

Figure 3.1: Reflected signal in a layered media.

Then, the amplitude of the reflected signal is given by:

$$R_{34} .(1 - R_{12}^2). (1 - R_{23}^2). \tag{3.1.2}$$

Since $R_{ij}^2 \approx 0$ for the transitional case, the amplitude would basically be the one of convolving the wavelet with the reflection coefficient series. In the case of a cyclic reflectivity amplitude would significantly be affected by transmission loss.

3.1.2 Multiple reflection effects

The most important effect to take in account when dealing with the computation of the impulse response is the one due to multiple reflections. There are two main effects involved: one is caused by the waves trapped inside thin layers, the other is the cumulative effect of multiple reflections from a sequence of thin layers (figures 3.2 and 3.3).

In the first case, it can be shown that for one layer its thickness plays an important role in determing the appeareance of a frequency notch in the amplitude spectrum

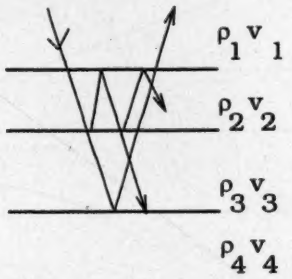

Figure 3.2: Intrabed multiple reflected signal for a layered media.

of the reflected signal. In the second case (figure 3.3), the multiply-reflected signal in a sequence of thin layers, which are bounded by interfaces of opposite polarity, it is always of the same sign as the direct transmitted signal and tends to overtake it in amplitude. The contribution of these multiples tend to compensate some of the large transmission loss that would otherwise occur.

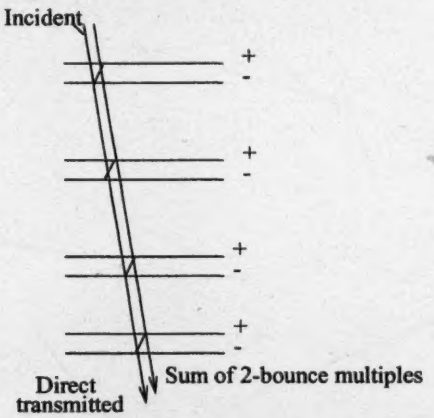

Figure 3.3: The cumulative effect of the multiple reflections for a sequence of thin layers.

The result of these two effects together is known as *layering filtering.*

3.1.3 Layering Filtering

The term *stratigraphic filtering* or *layering filtering* is used in the literature for the shaping of transmitted waves by superposition of multiples reverberating in beds too thin to be resolved individually (Banik et al., 1985a). O'Doherty and Anstey (1971) found an approximate relationship between the amplitude spectrum $T(\omega)$ of the transmitted pulse and the power spectrum $R(\omega)$ of the reflection coefficients series [1], given by

$$T(\omega) = e^{-R(\omega)\Delta t} \tag{3.1.3}$$

where Δt is the traveltime of the directly transmitted wave.

The key concept to understand the idea of stratigraphic filtering is the interference between primary and short-period multiples. The qualifier "short-period" means the time difference between primary and first multiple is less than the width of the propagating wavelet. Thus the multiple does not show as a distinct arrival but rather, it overlies and modifies the primary by superposition. Then, as more and more multiples are superposed, the primary itself is decreased by transmission losses until the propagating wavelet is purely multiple energy.

It is this transformation from primary to superposition of multiples that may be conceived as a filter. Since the cause of this filtering is the presence of successive beds too fine to be resolved, the term "stratigraphic filtering" or "layering filtering" is appropriate. Studies on this subject indicate that the qualitative effects of stratigraphic filtering are preferential attenuation of high frequencies. The apparent attenuation in stratigraphic filtering is due to loss of coherence not absorption of energy (Banik et al., 1985b) .

Schoenberg and Levin (1974) studied the apparent attenuation due to intrabed multiples and found that transmission losses attenuates amplitudes uniformly at all frequencies, while intrabed multiples tend to raise the amplitudes

[1] A derivation of this formula is given in Appendix B.

at the low-frequency end of the spectrum and lower those at the high frequency end. When the input pulse pass through a cyclic section, the transmitted signal appears broaden with a set of intrabed multiples following it.

3.1.4 Layering Filtering in the Western Canadian Basin

Examples of layering filtering can be found in the Western Canadian Basin. Coulombe and Bird (1996) were one of the first to publish on stratigraphic filtering caused by coals seams in the Western Canadian Basin.

The term coal refers to a rock that comprises mainly plant-derived carbonaceous material. Coal is formed from peat that appeared from the accumulation and decomposition of vegetal debris in the stagnant waters of swamps and marshes. In the Western Canadian Basin it was observed that coals from the Mannville formation in the lower Cretaceous act as a transmission filter. The Mannville group is a mainly non-marine succession with a middle interval of marine shale and limestones and glauconitic sandstones. Thin coal beds were originated in alluvial-plains and deltaic enviroments during the deposition of the Lower Mannville (Smith, 1989; Smith et al., 1994).

Coulombe and Bird (1996) examined zero offset data and noticed that layers on the Devonian (deeper than the Mannville coals) were lacking in frequencies above 50Hz even though the Cretaceous section (shallower than the coals) present plenty of signal up to 75 Hz. Their studies showed that the intrabed multiples created by coals were acting as transmission filter attenuating the higher frequency data.

More recently, Perz (2000) examined the angle-dependent transmission filtering effect introduced by high amplitude coal reflectors. His research reveals that the offset-dependence for amplitude attenuation was a small effect compared to the magnitude of the basic spectral notching effect common to all offsets.

Next sections will covered the problem of lack of high frequencies due to thin layers with high impedance contrast. The impulse response at zero offset for the simple case of one layer is modeled to understand which are the variables controlling the presence of notches. Next, stochastic reflectivity models (ARMA(1,1)) are used as input for zero offset simulations to study the impulse response of cyclic and transitional impedance layering.

3.1.5 Analysis of the impulse response for a single layer using the Z transform

As it was mentioned before, a simple way to visualize the effects of multiples is considering only one layer and writing the reflection response in terms of the Z transform. Where the delay operator z in this case is given by,

$$z = e^{-2i\omega\tau}. \tag{3.1.4}$$

with ω as the angular frequency given in [rad/sec] and τ is the transit time.

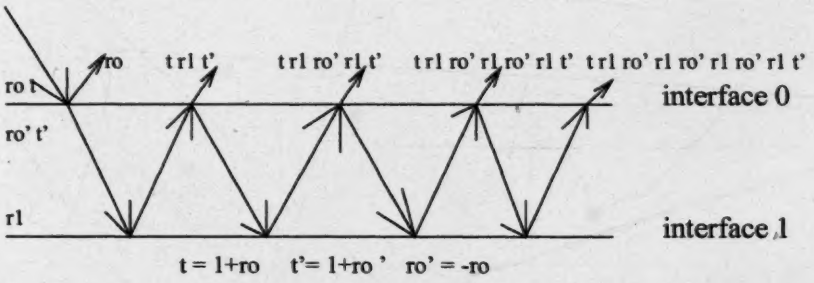

Figure 3.4: Reflection and transmission coefficients for a wave traveling through a single layer.

The reflection response for a single layer can be written as:

$$R(z) = z^d[r_0 + t_0 r_1 t_0' z + t_0 r_1^2 r_0' t_0' z^2 + t_0 r_1^3 r_0'^2 t_0' z^3 + ...]. \tag{3.1.5}$$

$$R(z) = z^d[r_0 + (1+r_0)r_1(1-r_0)z + (1+r_0)r_1^2 r_0'(1-r_0)z^2] \tag{3.1.6}$$

$$R(z) = z^d[r_0 + (1-r_0^2)r_1 z[1 - r_1 r_0 z + r_1^2 r_0^2 z^2 - ...]. \tag{3.1.7}$$

$$R(z) = z^d[r_0 + \frac{(1-r_0^2)r_1 z}{1 + r_1 r_0 z}]. \tag{3.1.8}$$

Finally, it can be written as:

$$R(z) = z^d \frac{r_0 + r_1 z}{1 + r_1 r_0 z}. \tag{3.1.9}$$

The power spectrum is given by:

$$P_R(z) = R(z)R(1/z). \tag{3.1.10}$$

To find the amplitude spectrum we replace the delay operator z by expression 3.1.6

$$P_R(\omega) = \frac{r_0^2 + r_1^2 + 2r_0 r_1 \cos(2\omega\tau)}{1 + (r_0 r_1)^2 + 2r_0 r_1 \cos(2\omega\tau)}. \tag{3.1.11}$$

Now, let us analyze the position of minima and maxima in 3.1.11. The condition to find the minimum on the spectrum is given by

$$\frac{dP_R(\omega)}{d\omega} = 0. \tag{3.1.12}$$

It can be shown that this will be true when

$$\sin(2\omega\tau) = 0. \tag{3.1.13}$$

The latter leads to the following condition

$$2\omega\tau = k\pi, \tag{3.1.14}$$

or

$$\tau = \frac{k\pi}{2\omega}, \tag{3.1.15}$$

and if the layer transit time is given by

$$\tau = \frac{h}{v}. \tag{3.1.16}$$

where h is the thickness and v the velocity of the layer, then replacing equation 3.1.16 into equation 3.1.15 with $\omega = 2\pi f$ we can write the condition for a stationary point as:

$$h = \frac{vk}{4f}. \tag{3.1.17}$$

where f is the nodal frequency and k an integer number.

If k is even, then the power spectrum for a stationary point can be written as:

$$P_R = \frac{(r_0 + r_1)^2}{(1 + r_0 r_1)^2}. \tag{3.1.18}$$

If k is odd then the power spectrum for a stationary point is given by:

$$P_R = \frac{(r_0 - r_1)^2}{(1 - r_0 r_1)^2}. \tag{3.1.19}$$

Then, the expression of the minimum of the power spectrum would depend on the relation between r_0 and r_1. When r_0 and r_1 have different signs, then minima will be given by equation 3.1.19. When they have the same signs, minima will be given by equation 3.1.18. This is shown in the figures 3.2 and 3.3 where the reflection response was computed using the previous formula for a layer with a velocity of 1200 m/s, and the thickness was calculated using equation 3.1.17 for $f_0 = 50\ Hz$. In figure 3.2 $r_0 = -0.9$ and r_1 varying from 0.1 up to 0.9, then

minima are given by equation 3.1.15 and the nodal frequencies are at multiples of f_0. Figure 3.3 illustrates the case of $r_0 = -0.9$ and r_1 varying from -0.1 down to -0.9; notice how the minima from the previous case changed into maxima. As it can be seen from these figures the closer the reflection coefficients from the two interfaces, the more pronounced the minima.

In the case of two layers the reflection response is given by:

$$R(z) = \frac{r_0 + [r_1 + r_0 r_1 r_2]z + r_2 z^2}{1 + [r_0 r_1 + r_1 r_2]z + r_0 r_1]z^2}. \tag{3.1.20}$$

The power spectrum is given by:

$$P(\omega) = \frac{r_0^2 + [r_0 r_1 + r_0^2 r_1 r_2 + r_1 r_2 + r_0 r_1 r_2^2]cos(2\omega\tau) + r_0 r_2 cos(4\omega\tau) + [r_1 + r_0 r_1 r_2]^2 + r_2^2}{1 + [r_0 r_1 + r_1 r_2 + r_0^2 r_1^2 + r_0 r_1^2 r_2]cos(2\omega\tau) + r_0 r_1 cos(4\omega\tau) + [r_0 r_1 + r_1 r_2]^2 + r_0^2 r_1^2}. \tag{3.1.21}$$

As it can be seen the expression gets more complicated as one adds more layers. Finding the minima of the spectrum, analytically, becomes quite cumbersome.

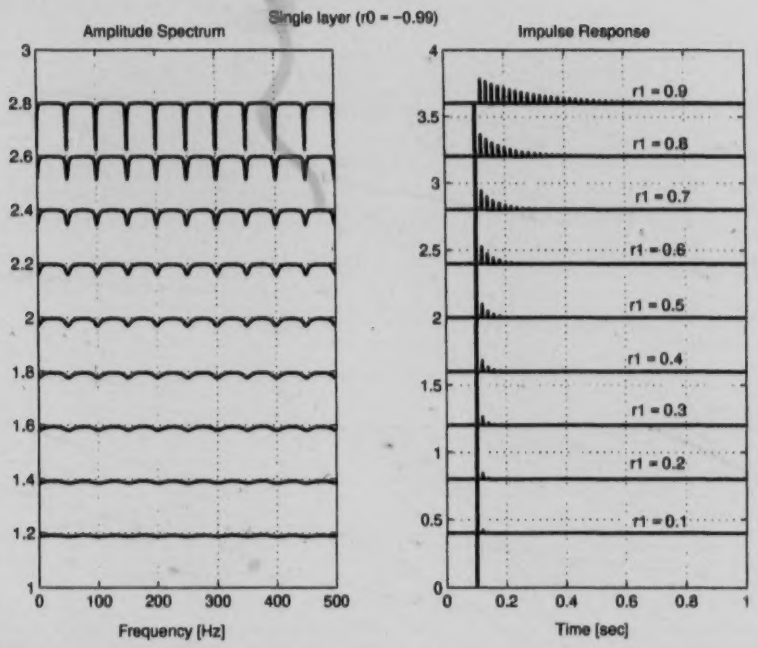

Figure 3.5: Amplitude spectrum for the impulse response of a single layer system as the one presented in figure 3.4. Case 1 : reflection coefficients at the interfaces have opposite signs.

3.2 Impulse response for transitional and cyclic reflectivities.

Let us start with an example where the reflection coefficient series was created in order to simulate a cyclic scenario with values representative for the coals seams described in section 2.1.1. The model is shown in figure 3.7.

With this simple example the idea is to illustrate step by step what happens when multiples are added one by one. It is important to clarify what is understood as primaries, first order multiples, second order and so on.

Zero offset simulations are generated with the algorithm developed by Mendel (1979) and extended by Wyatt (1981). Details of this algorithm are given in chapter five. In this example, I will consider the contribution of first and

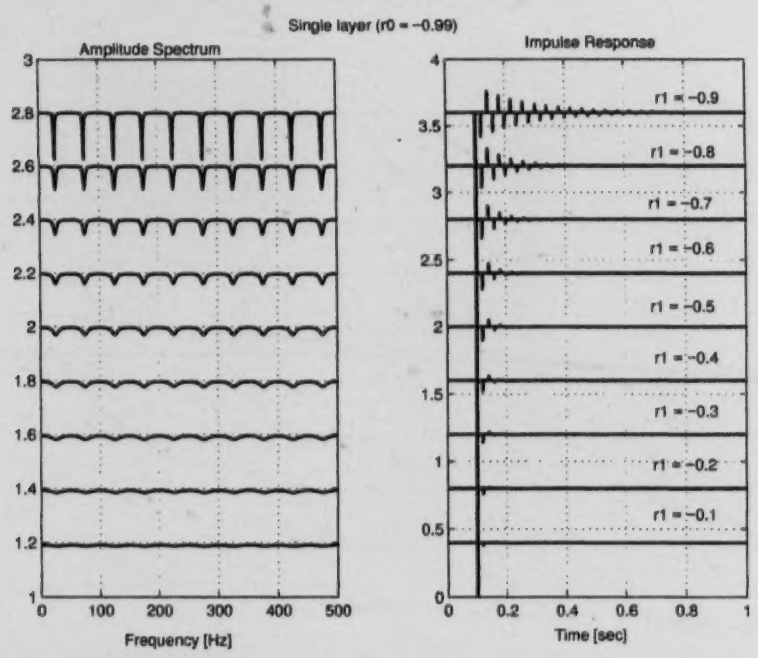

Figure 3.6: Amplitude Spectrum for the impulse response of a single layer system as the one presented in figure 3.4. Case 2 : reflection coefficients at the interfaces have same signs.

second order multiples only. First, let us see the impulse response for the model considering only primary reflection, transmission effects included. This is shown in the figure 3.9. As it can be seen amplitude decay quite quickly, it can also be seen from the the amplitude spectrum how some spectral amplitudes are slightly attenuated.

Now, let us see the case when all the first order multiples are included in the impulse response. Comparing with the previous case, it seems that all the minima are accentuated and some of the primaries amplitude are reinforced by the multiples as is shown in the seismogram (figure 3.10).

Finally, figure 3.11 shows the effect of adding the second order multiples in the impulse response. Again multiples reinforce primary reflection amplitudes as it was shown in section 3.1.2, figure 3.3, multiples coming from these thin

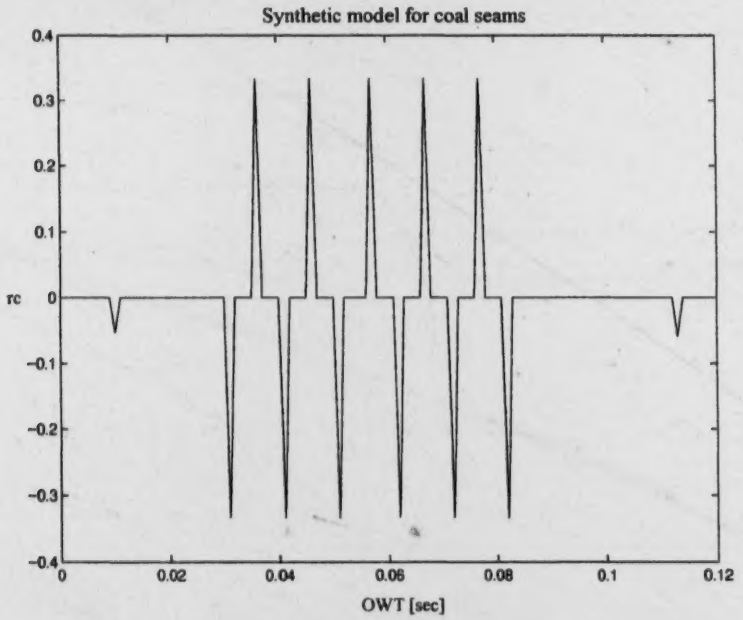

Figure 3.7: Model for coal seams.

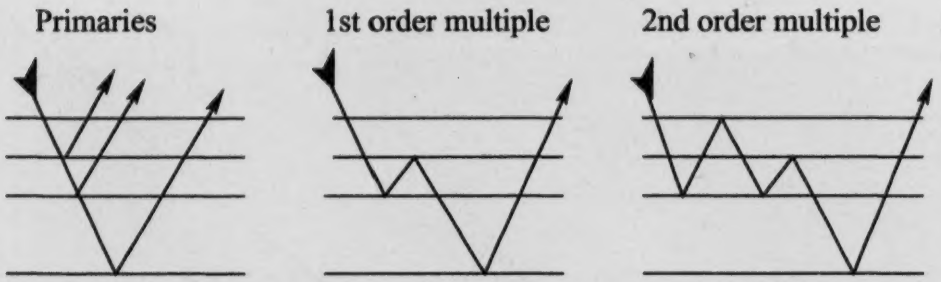

Figure 3.8: Ray path for primaries, 1st order multiple and 2nd order multiple.

layers overtake the amplitude of the direct waves. Also notice the presence of new notches on the amplitude spectrum in the minima sections. It is interesting to notice in this three cases the minimum at $100Hz$ for the first two cases, that turn out to be a local maximum in the third case. The idea behind this example is that when adding multiples of different order, the section between $75Hz$ and $125Hz$ exhibits the appereance of new minima caused by destructive

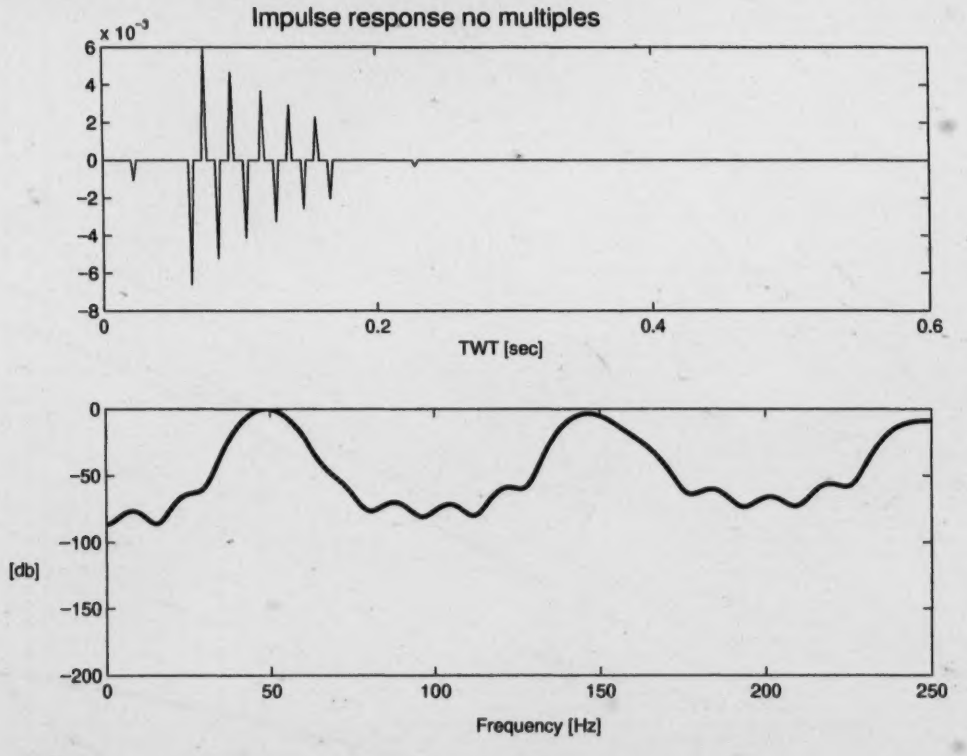

Figure 3.9: Top: impulse response with transmission loss but no multiples. Bottom: corresponding amplitude spectrum.

interference between primaries and multiples. Including higher order of multiples could slightly move the position of this minimum due to a new interference between the added multiple and the previous impulse response.

Let us now see two examples of impulse response where the reflectivity series is a little bit more complex. Using the ARMA(1,1) model described in the previous chapter, simulations of cyclic and transitional reflectivities were generated with a total of 200 samples (sampling inerval of 0.001 sec). Figure 3.12 illustrates the two reflection coefficient series with their corresponding amplitude spectra (periodogram in full line and ARMA model in dashed line).

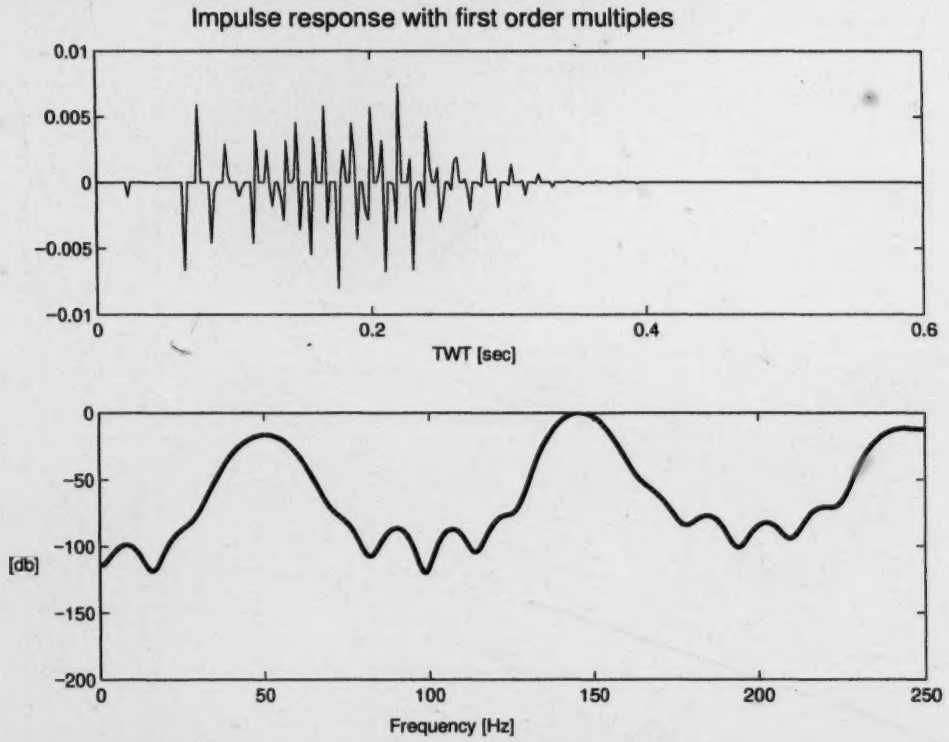

Figure 3.10: Top: impulse response with transmission loss and 1st order multiples. Bottom: corresponding amplitude spectrum.

Seismograms at zero offset were generated based on these rc series using a unit pulse as a source. First, the computation of the seismogram was made without any multiple, only primaries were included. Results are shown in figure 3.13. From this picture it can be corroborated what was explained in sections 3.1.1 and 3.1.2, the impulse response for a reflectivity "transitional type" is like convolving the source with the reflection coefficient itself. It can be seen that the corresponding amplitude spectrum is pretty similar to the one corresponding to the rc series itself and the impulse response looks like the rc series multiply by a scale factor. The reason for this is that since the reflection coefficients are small, the effects of transmission loss are also quite small. Conversely, for the impulse

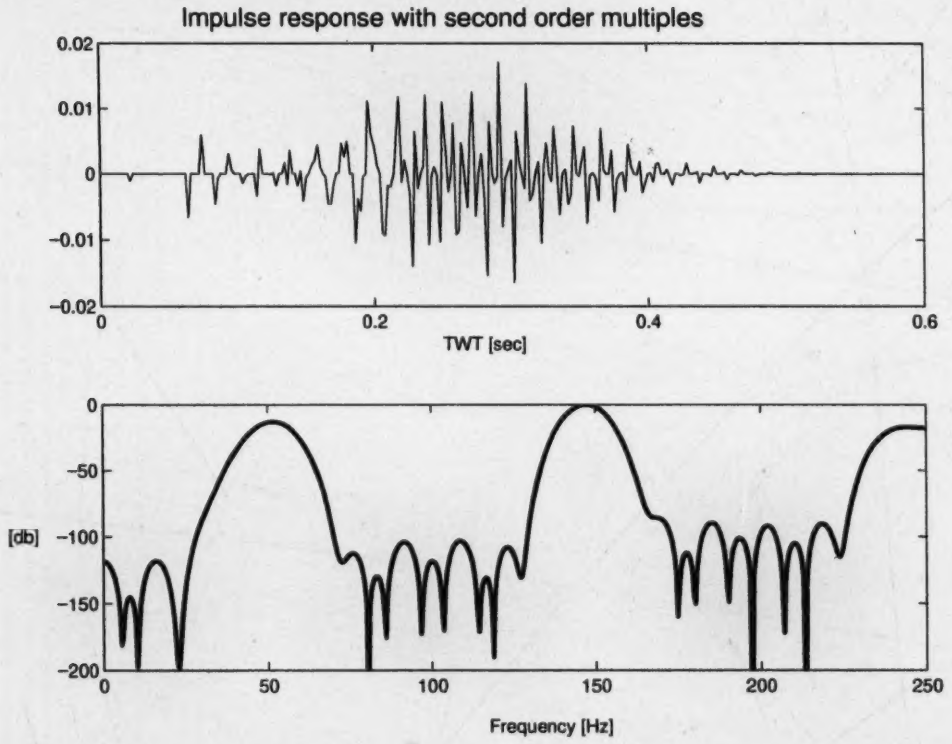

Figure 3.11: Top: impulse response with transmission loss and with 2nd order multiples. Bottom: corresponding amplitude spectra.

response of a cyclic reflectivity, the effects of transmission loss are quite strong and the amplitude of the signal decays rapidly. The amplitude spectrum exhibits accentuated minima as an evidence that transmission losses here are important.

Now, let us examine the effect of including all the multiples in the impulse response. This is shown in figure 3.14. Again, it can be seen that this is not an important problem for a transitional case, multiples die quite soon as the reflection coefficients are not large enough. Therefore, the amplitude spectrum is still quite similar to the reflection coefficient series. Instead, for the cyclic case the contribution of multiples is quite important. They reinforce the primary signal and they overcome it, as it was shown on section 3.1.2 (figure 3.3). The

effects of the multiples trapped inside thin layers with high reflection coefficients cause the presence of notches in the amplitude spectrum, just as it was shown for a single layer, but here the complexity of the model mark the presence of few important notches.

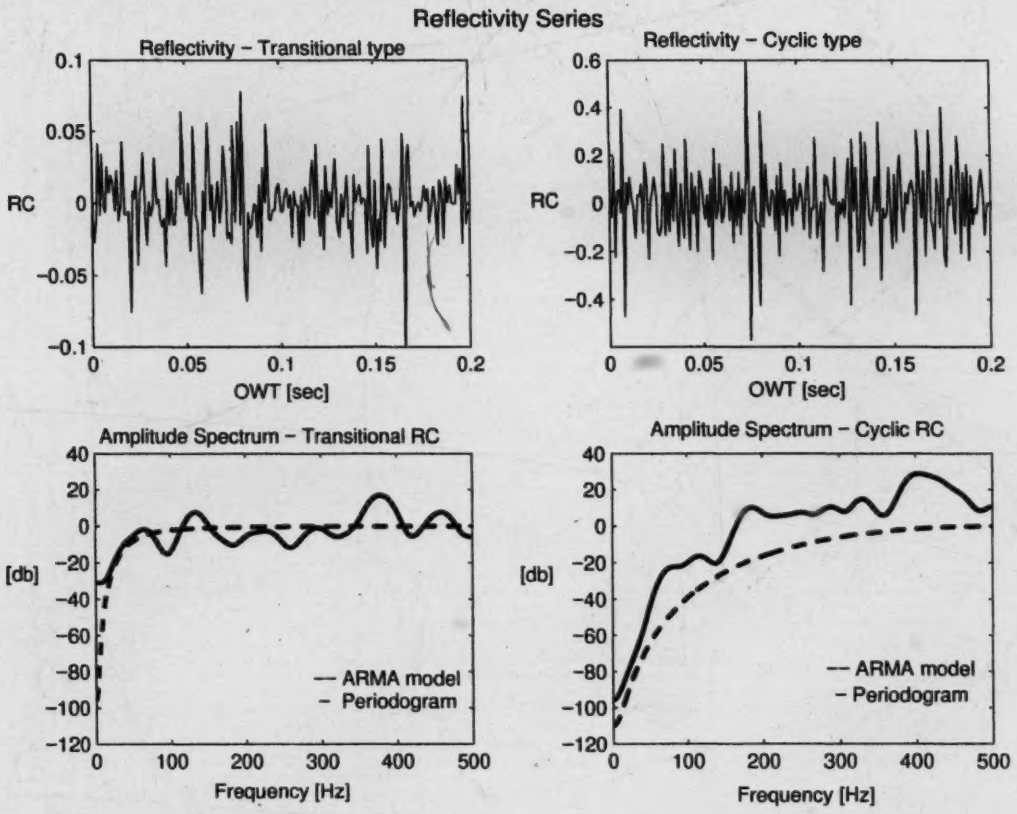

Figure 3.12: Top: transitional and cyclic reflectivity sequences. Bottom: corresponding amplitude spectra.

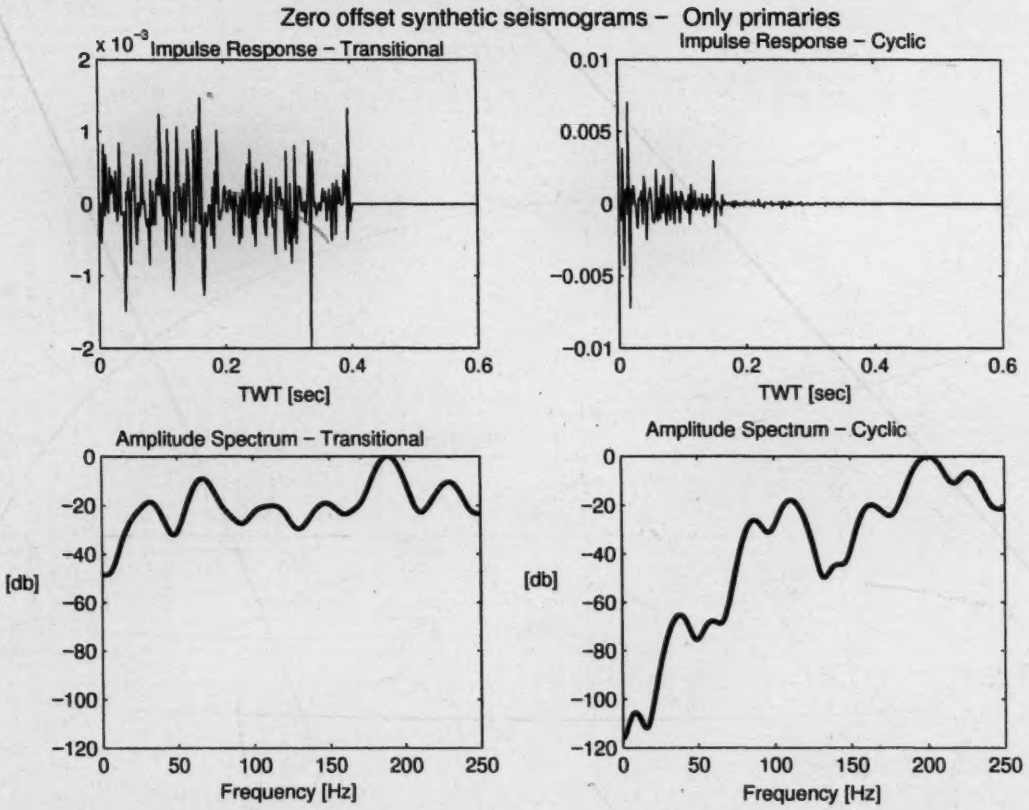

Figure 3.13: Top: impulse response with transmission loss and no multiples for a transitional and cyclic reflectivity sequences. Bottom: corresponding amplitude spectra.

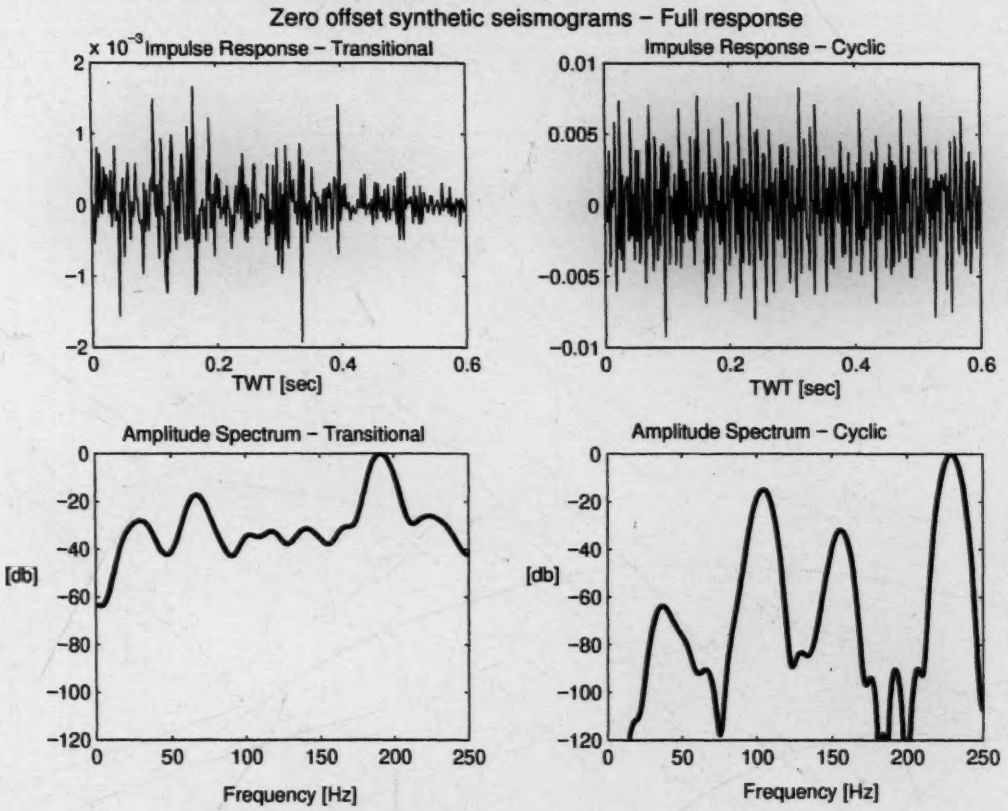

Figure 3.14: Top: impulse response with transmission loss and all multiples for a transitional and cyclic reflectivity sequence. Bottom: corresponding amplitude spectra.

3.3 Seismic attenuation due to layering

In the previous section it was shown, the difference between the impulse response of a transitional and cyclic layering in terms of their amplitude spectra. It becomes clear that layering is an important point when dealing with attenuation. It is worth to clarify that with attenuation due to layering I am not implying intrinsic attenuation. The first one is only caused by the concept of a geometrical disposition of a package of layers, where their thickness and impedance contrast are responsible for the observed apparent attenuation. Intrinsic attenuation Q, which is mainly caused by energy loss due to friction (Lay and Wallace, 1995). Seismic attenuation due to layering alone arises from a combination of the transmission losses through the interfaces of a layered subsurface and the generation of intrabed multiples. Such a statement was concluded by O'Doherty and Anstey (1971) and confirmed by Schoenberger and Levin (1974). Following their approach it is possible to visualize the effects of transmission losses and intrabed multiples in cases like the idealized model of coal seams used in the previous section. An instantaneous transmission loss due to layering only (no multiples considered) can be obtained as the ratio of a point on the primary time trace to the same point of the input time trace. Understanding by *input time trace* the one that contains all the primary reflections without transmission losses (it would be just the convolution of spike with the reflectivity series). The *primary time trace* will contain all the primary reflections including transmission losses. In a similar way, it can be obtained the effect of adding multiple reflections by computing the ratio between the primary time trace and the *multiple time trace*, seeing that part or all the attenuation on seismograms can be attributed to intrabed multiple reflections rather than to the intrinsic properties of rock materials. On the other hand, as it was mentioned before, short-period multiples tend to compensate for simple reflection losses due to transmission across

the layers.

Figure 3.15 shows how important is the attenuation due to transmission loss in a case that behaves like coal seams. As for the effects of multiples, the multiple time trace correspond to the full response considering multiples up to order 50. As it can be seen this short multiples tend to raise the amplitude of the transmitted signal but, on the other hand, some of the minima on the spectrum became more pronounced than in the primary trace spectrum. This could be attributed to the interference between this short delay multiples and the direct signal.

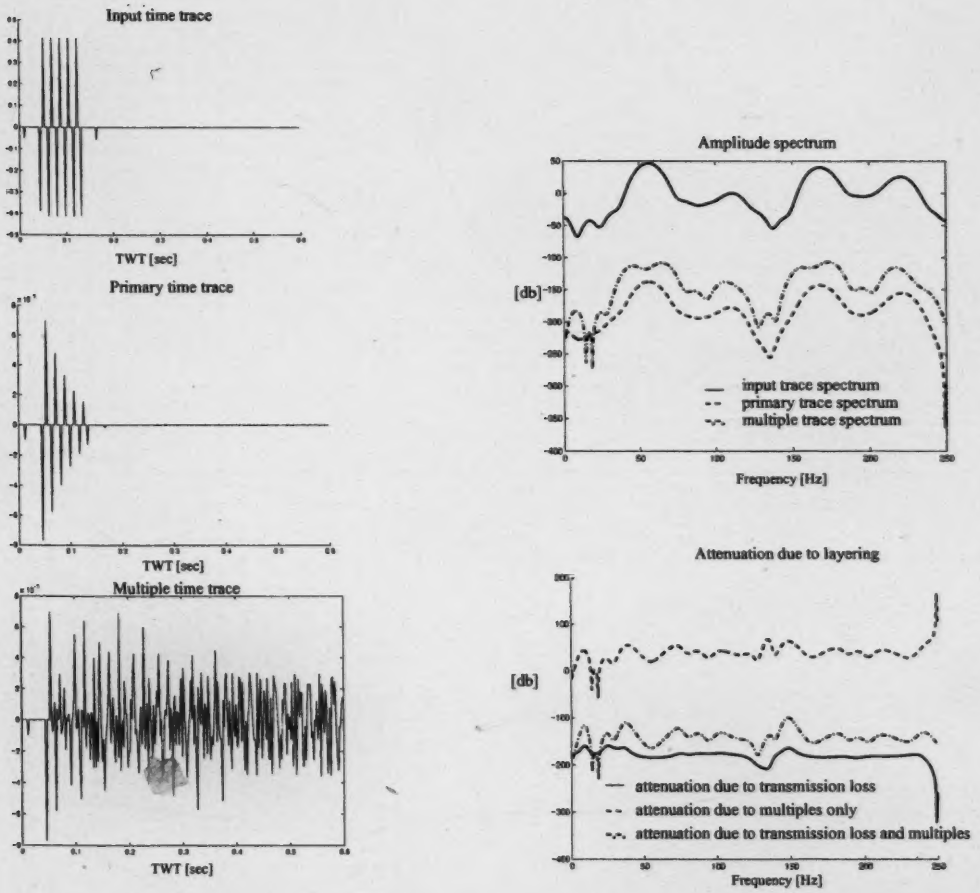

Figure 3.15: Attenuation due to layering only. Attenuation due to transmission loss computed as the spectra ratio of primary time trace to input time trace. Attenuation due to multiples only computed as the spectra ratio of multiple time trace to primary time trace. Attenuation due to layering (transmission + multiples) computed as multiple time trace to input time trace.

3.4 Summary

This chapter provided several examples of impulse response for transitional and cyclic layering. The transitional type has an impulse response that resembles the original reflectivity series. Transmission losses are not significant and the amplitude of multiple reflections die quite fast.

The cyclic case, as it would be the case of a succession of coal seams, leads to more complicated impulse responses. In this case, the impedance contrast between layers is high, therefore transmission losses are very important. A succession of thin layers cause short-period multiples that overlap with the primary wave causing two effects on the amplitude spectrum of the transmitted signal. First, multiples tend to raise the amplitude of the primaries and overtake it. Secondly, for certain frequencies this interference between multiples and primary can be destructive, causing notches for some frequencies on the amplitude spectrum. Frequency minima depend on the thickness and impedance of the layers; also the number of layers since this would be directly connected with the number of multiples interfering.

Apparent attenuation due to layering alone can be said to have two components, one due to transmission loss and the other due to multiple interference. The first one can be estimated computing the ratio between amplitude spectra of the primary trace (primary reflections with transmission loss) to the input trace (primary reflections without transmission loss). The second one can be computed with the ratio between amplitude spectra of the multiple trace (primary reflections with transmission losses and all multiples included) to the primary trace (primary reflections with transmission loss). Well data can be used to compute the corresponding traces to have an estimate of this apparent attenuation.

Chapter 4

Deconvolution

4.1 Introduction

The main idea behind this chapter is to propose a way to overcome the effects caused by cyclic reflectivity, not only in terms of its color but specially in terms of its filtering behavior.

So far, in the previous chapters I explained two different types of reflectivities, transitional and cyclic. Real log data are often composed of a mixture of these reflectivities. The coal seams in the WCB are better represented by a cyclic type. It was explained in chapter two that neither transitional or cyclic reflectivities are white, but they do have some color. This non-white character should be contemplated at the deconvolution step. In chapter 3 it was shown how the impulse response is distorted when a cyclic reflectivity is present. When a wave is traveling through such a profile it will suffer distortions, mainly in the amplitude spectrum. The main consequence will be the nonstationarity of the signal. The signal looses frequency content and experiences a phase change while is passing through what it is called *stratigraphic filter*. However, it is possible to design a filter that is able to compensate for most of this effect.

The chapter is organized as follows. First, a review of deconvolution methods is provided. Then, a description of some of the techniques to take the reflectivity color into account at this processing step. Next, it is proposed a way to compensate for the effects of stratigraphic filtering due to cyclic non resolvable layering. Following this, it is a discussion about the nonstationarity of the signal. Finally, an example and a summary are provided.

4.2 Deconvolution

Deconvolution is a process that improves the temporal resolution of seismic data by compressing the basic seismic wavelet (Yilmaz, 1987). A recorded seismogram can be modeled as a convolution of the Earth's impulse response with the seismic wavelet. This wavelet has many components, including source signature, recording filter, surface reflections, and geophone response. The earth's impulse response comprises primary reflections (reflectivity series) and all possible multiples. Ideally, deconvolution should compress the wavelet components and eliminate multiples, leaving only the earth's reflectivity in the seismic trace. Of course, to be able to compress the wavelet, first it has to be known or approximately estimated. Some assumptions are to be made about the seismic model in order to be able to solve this problem. Different deconvolution methods make different assumptions.

Deconvolution methods include least squares deconvolution (being predictive deconvolution the most important, which includes spiking deconvolution as a special case), maximum-likelihood deconvolution, maximum-entropy deconvolution, homomorphic deconvolution, minimum-entropy deconvolution, iterative deconvolution, surface-consistent deconvolútion, deterministic deconvolution and various deconvolution methods based on other criteria.

The seismic convolutional model has two components, namely the reflection

sequence and the wavelet, each of the deconvolution methods mentioned, make assumptions on these two components which validity will strongly depend on the area of interest. One of the most common assumptions made deals with white reflectivity. As it was explained in chapter two, it was found in many wells around the world that the reflectivity is not white (Walden and Hosken, 1985). For the type of geology whose seismic response is analyzed in this thesis, the hypothesis of a white reflectivity series is a very weak one.

The following section provides a brief review of the most widely used type of deconvolution and the most robust under a variety of input conditions (Jurkevics and Wiggins, 1984), this is the least squares deconvolution. After this, methods for deconvolving signal with non-white reflectivity series will be discussed and it will be found which would be the best for the case of an area with coal seams.

4.3 Least squares deconvolution

The standard method of performing seismic deconvolution is based on least-squares prediction-error filtering (Robinson, 1957). In its usual form, this method assumes that the seismic wavelet is minimum-delay and that the reflectivity is white. Wiener spiking deconvolution works under the same seismic model (Robinson and Treitel, 1967). One of the main limitations of this type of deconvolution is the assumption of a white reflectivity series. Walden and Hosken (1985) found that reflectivities series are more like a pseudo-white series. After their work talking about white reflectivity is very questionable. In chapter two it was shown that in the case of a transitional reflectivity, this assumption could still work, but for a cyclic case (coal seams) is critical. Let us review briefly the Wiener deconvolution (Robinson and Treitel, 1967; Leinbach, 1996) to understand why those assumptions are made. The simplest representation of a trace $s(t)$ consists of a wavelet $w(t)$ convolved with a reflection coefficient series $r(t)$.

The noise-free trace is given by

$$s(t) = w(t) * r(t), \tag{4.3.1}$$

where $*$ stands for discrete convolution. The reflection coefficients are represented by sharp spikes generated by the acoustic impedance between different rock types. Each spike is convolved with the seismic wavelet as it passes through the earth. Since reflection spikes are close together than a wavelet length, the spike locations become confused. Adjacent wavelets overlap each other, producing a tangle of constructive and destructive interference. Spiking deconvolution attempts to compress these wavelet in time, unravel confusion and resolve each sharp reflection. Spiking deconvolution assumes that wavelet properties do not change with time (are stationary). The least squares deconvolution filter then attempts to shape the input seismic trace $s(t)$ into the desired output $r(t)$ by minimizing the mean squared error between the desired output and the actual filter output $y(t)$. The actual output is simply the input $s(t)$ convolved with the filter $f(t)$. The equation defining the filter are:

$$\phi_{ss}(\tau) * f(\tau) = \phi_{rs}(\tau), \tag{4.3.2}$$

where ϕ_{ss} is the auto-correlation of the trace and ϕ_{rs} is the cross-correlation between the the reflectivity and the trace. The auto-correlation of the trace can be written as:

$$\phi_{ss} = \phi_{rr} * \phi_{ww}. \tag{4.3.3}$$

While the cross-correlation of the trace and the reflectivity is written as:

$$\phi_{rs}(\tau) = \phi_{rr}(\tau) * w(-\tau). \tag{4.3.4}$$

The normal equations can now be rewritten as:

$$[\phi_{rr}(\tau) * \phi_{ww}(\tau)] * f(\tau) = \phi_{rr}(\tau) * w(-\tau). \tag{4.3.5}$$

Here comes the assumption to solve for the filter. First, is assumed that the reflectivity series has the statistical properties of random white noise. This means that its auto-correlation is given by a spike at zero lag scaled by its power P,

$$\phi_{rr}(\tau) = P\delta(0). \tag{4.3.6}$$

This is a paradox of spiking deconvolution: one first makes a questionable statistical assumption concerning the reflectivity of the earth in order to subsequently estimate this reflectivity. Now the normal equations became,

$$\phi_{ww}(\tau) * f(\tau) = w(-\tau). \tag{4.3.7}$$

Second,the wavelet is assumed minimum phase. Then, we can estimate this minimum phase wavelet from its left side auto-correlation function (ϕ_{ww}). Finally the filter can now be computed and afterward apply to the trace to compress the wavelet and recover the reflectivity.

Todoeschuck and Jensen (1988) studied the predictive deconvolution problem and proposed what they called a Joseph filter [1]. This filter was intended to recover a reflection sequence which power spectrum is proportional to the frequency f and presents negative auto-correlation at small lags. Their results seems to work better when comparing with those using prediction error filter. This could be one approach to be tested with the Rosebud data. The approximations made in that method are valid for small values of the reflection coefficients, $\mid r \mid < 0.4$. This is within the range of the well data from Rosebud area (figures 2.1 and 2.3).

Other contributions on this type of deconvolution focus on the amplitude distribution of the reflectivity series. In chapter two it was mentioned that seismic

[1] Joseph as referring to the statistics of the floods of the Nile, specifically the tendency of periods of flood or drought to persist. The power spectra of the flow of the Nile and of other rivers show a dependency on frequency f of $1/f^{\beta}$ with β between 0.5 and 1.1.

processing usually assumes Gaussianity for its convenience. However, Walden and Hosken (1986) found that the distribution is essentially symmetric but has a sharper central peak and larger tails than a Gaussian distribution. This concept is exploited in higher order statistical methods for wavelet estimation (Lazear, 1993; Velis and Ulrych, 1996; Sacchi and Ulrych, 1998; Sacchi, 1999). Besides, assuming that the reflectivity sequence is Gaussian inhibits wavelet phase estimation. Tenorio (2002) proposed a generalized Wiener-Levinson deconvolution using non-Gaussian modeling. The main idea behind this assumption is to be able to recover wavelet phase information. This non-Gaussian distribution is simulated by a mixture of Gaussian distributions. This method leads to better amplitude and phase estimates for high signal to noise ratios, meaning that spikeness of the reflectivity is above the noise level, but still assumes a white reflectivity sequence.

Besides the limitations of the assumptions made on the seismic model, one seek for a deconvolution method able to get rid of the multiple energy, specially short-delay multiples. Robinson (1966) study the problem of short-delay multiples in the water layer. This author proposed the statistical method of predictive deconvolution to keep the front part of the minimum-delay seismic wavelet but destroys the back part, getting rid of the water reverberations. Since intrabed multiples due to coal seams have a behavior similar to those inside a water layer, one can think that this could be a nice solution. Unfortunately, one extra problem comes from the very fine thickness of the coal layers. On the contrary of the thickness of a water layer, coal beds have a thickness in the order of 2-10m, beyond seismic resolution what makes things difficult to solve.

4.4 Deconvolution for non-white reflectivity

Saggaf and Robinson (2000), provided a review on deconvolution methods for non-white reflectivity. They suggested processes that include ARMA, scaling Gaussian noise, fractional Brownian motion, fractional Gaussian noise and fractionally integrated noise to face the problem on non-whiteness. The idea behind all these methods is to find a model for the reflection coefficients that honor their correlation structure better than white noise.

Let us first analyze the case when the non-white reflectivity component is taken into account in the conventional deconvolutional method. The trace is taken to be the convolution of the Earth's reflection coefficients r with the effective wavelet w (which will be assumed to be minimum phase)

$$s = w * r. \tag{4.4.1}$$

The reflectivity can be factored into a minimum-phase non-white-noise component r_m and an all pass component r_a that is white noise:

$$r = r_m * r_a. \tag{4.4.2}$$

When reflectivity is a non white process, the minimum-phase component r_m does not vanish. Denoting the auto-correlation function as ϕ, and since r_a is white, then the auto-correlation of the trace is given by:

$$\phi(s) = \phi(w * r_m). \tag{4.4.3}$$

Then, the filter used to recover the reflectivity from the trace is given by:

$$f \approx (w * r_m)^{-1}, \tag{4.4.4}$$

$$f * s \approx r_a. \tag{4.4.5}$$

This will be the error inflicted on the deconvolution by the assumption of white reflectivity, the output of the conventional deconvolution is not the whole reflectivity but only its white component. The conventional filter removes the minimum-phase component of reflectivity as it compresses the wavelet.

One way to tackle this problem is to find a way to model the stochastic properties of the reflection coefficients. It will be useful to make the distinction between the probability distribution structure of a process (described by the probability density function, e.g. being Gaussian) and the correlation structure (described by the auto-correlation function, e.g. being white noise). Saggaf and Robinson (2000) showed different ways of modeling a nonwhite reflectivity with a Gaussian distribution although some of the processes need not to be Gaussian. In chapter 2 we show that modeling with an ARMA process allow as to include a non-Gaussian density distribution like a mixture of two Laplace distributions. As for the models presented in their paper include ARMA models, Scaling Gaussian noise, that is the same idea mentioned in the previous section in the case of the Joseph filters (Todoeschuck and Jensen, 1988), Fractional Brownian Motion (FBM), Fractional Gaussian Motion (FGM) and the Fractionally Integrated Noise (FIN) . Methods like FBM and FGM present the complexity of not having an analytical expression for the power spectrum. The FIN not only has analytical expressions for both the auto-correlation function and the power spectrum but has the advantage of requiring only one parameter for its definition. Instead, ARMA models have the disadvantage of requiring two parameters for their definition. Taking into account the advantages and disadvantages of each method choosing the one that better fits the data would certainly depends in its type and complexity.

Once a suitable model was found for the data, the next step is to construct a filter to generalize the conventional deconvolution method. Four equivalent

methods for constructing and applying the filter were proposed (Saggaf and Robinson, 2000) and will be reviewed in the following section.

4.4.1 Reflectivity whitening filter

As it was explained before, conventional deconvolution only recovers the white part of the reflectivity. In other to be able to properly apply this type of deconvolution, one can whiten the trace before applying it. A filter g can be designed as the least squares inverse of the minimum-phase component of reflectivity r_m

$$g \approx r_m^{-1}. \tag{4.4.6}$$

When this filter is applied to the trace,

$$g * s = g * w * r_m * r_a, \tag{4.4.7}$$

$$g * s \approx w * r_a, \tag{4.4.8}$$

$$\phi(g * s) \approx \phi(w). \tag{4.4.9}$$

Now, the auto-correlation of the wavelet is well estimated and from here it can be used the typical approach to design the deconvolution filter $\hat{f}$ to compress the wavelet

$$\hat{f} \approx w^{-1} \tag{4.4.10}$$

Notice, that this filter is computed from the output of the reflectivity whitening filter rather than from the original trace. Once it was computed, it is applied to the original trace to recover the reflectivity.

$$\hat{f} * s \approx \hat{f} * w * r, \tag{4.4.11}$$

$$\hat{f} * s \approx r. \tag{4.4.12}$$

This method is the most natural generalization of the conventional deconvolution procedure. However, its disadvantage is that it complicates the deconvolution routines since the filter $\hat{f}$ is computed from a trace different from the one to which it is applied.

4.4.2 Frequency domain filtering

From (4.3.1) the power spectrum of the trace $P_s(\omega)$ can be written as:

$$P_s(\omega) = P_w(\omega).P_r(\omega). \tag{4.4.13}$$

By modeling the rc series by a process that well approximates its stochastic properties, a good estimate of its power spectrum can be obtained. Calling $\hat{P}_r(\omega)$ this estimate can be written as:

$$\frac{P_s(\omega)}{\hat{P}_r(\omega)} \approx P_w(\omega). \tag{4.4.14}$$

Then a good estimate of the auto-correlation of the wavelet can be obtained by spectral division. Transforming the trace to the frequency domain, dividing by the power spectrum of the process used to model the rc series, and then going back to the time domain. This method has the same disadvantage than the previous one, plus some numerical inaccuracies when $\hat{P}_r(\omega)$ is very small.

4.4.3 Double filtering

In order to re-use existing deconvolution routines, another way is to compute the deconvolution filter $\hat{f}$ as in the first method but then apply it on the output of the reflectivity whitening filter (the same from which it was computed) rather than on the original trace.

$$\hat{f} * g * s \approx g * r \tag{4.4.15}$$

$$(\hat{f} * g * s) * g^{-1} \approx r \tag{4.4.16}$$

The disadvantage of this method is that it requires the application of two additional filters (g before deconvolution and g^{-1} after it) rather than just one.

4.4.4 Spectral compensation filter

Another way to approach the problem caused by conventional deconvolution would be to design a filter that restores the minimum phase component of reflectivity to the output of conventional deconvolution. From equation 4.46 we have,

$$g^{-1} \approx r_m. \tag{4.4.17}$$

Convolving g^{-1} with equation 4.4.5,

$$g^{-1} * f * s \approx g^{-1} * r_a, \tag{4.4.18}$$

then,

$$g^{-1} * f * s \approx r_m * r_a. \tag{4.4.19}$$

Finally, we were able to recover both components of the reflectivity series r,

$$g^{-1} * f * s \approx r. \tag{4.4.20}$$

Where f is the conventional deconvolution operator computed from the original trace and g^{-1} is the spectral compensation filter, since it compensates for the spectral distortion of reflectivity caused by conventional deconvolution. This method is the easiest to implement and use, since it reuses existing deconvolution codes and requires only to apply one extra filter.

4.5 Deconvolution in the presence of layering filtering

In the presence of layering filtering, conventional deconvolution is not capable of recovering the "right wavelet" below the stratigraphic filter. It is clear that it is necessary to explore the data by windows and compensate somehow the effect due to this layering filter. This could be achieved by taking time windows above and below the stratigraphic filter from the stack seismogram $s_{above}(t)$ and $s_{below}(t)$. Then, we compute the amplitude spectrum above $A_{above}(\omega)$ and below $A_{below}(\omega)$ the transmission filter using the periodogram technique. Then, a transfer function can be computed by dividing these spectra in the frequency domain for the range of frequency of interest.

$$TRF(\omega) = \frac{A_{above}(\omega)}{A_{below}(\omega)}, \tag{4.5.1}$$

$TRF(\omega)$ being the amplitude spectrum of the filter to be applied to the window below the stratigraphic filter. Using the Hilbert transform $\mathcal{H}$ (Claerbout, 1976) it is possible to determine a minimum phase filter $trf_{min}(t)$ for the given amplitude spectrum $TRF(\omega)$

$$trf_{min}(t) = \mathcal{H}[TRF(\omega)]. \tag{4.5.2}$$

Once the transfer filter $trf_{min}(t)$ was computed, it can be convolved with the data below the stratigraphic filter, $s_{below}(t)$

$$s_{below}^{filtered}(t) = s_{below}(t) * trf_{min}(t). \tag{4.5.3}$$

Now, applying conventional deconvolution to the windows above and below should yield to approximate the same wavelet. This approach could be a simple

way to compensate the problems of the non stationarity of the wavelet due to the stratigraphic filtering. The main difficulty on this technique is the criteria on choosing the windows length involved, not only for the data above and below the layering filter but also for the computation of the transfer function in the frequency domain. In the following section, I illustrate this technique with an example.

4.6 Non-stationarity of the signal

Deconvolution as it was said has the task to improve resolution of the data. In the presence of a cyclic reflectivity this task becomes quite difficult due to the interference between the primary signal and many short-period multiples coming from that cyclic pattern. Understanding by short period that the time difference between primary and first multiple is less than the width of the propagating wavelet. Then the multiple overlies the primary and modifies it by this superposition. Since we are dealing with multiples beyond seismic resolution, NMO (normal moveout correction) and deconvolution fails to isolate the primary arrival.

Since real data present a mixture of transitional and cyclic reflectivities, the wavelet will be distorted as it travels through the earth, changing its phase and amplitude spectrum, being this effect more critical under the presence of a cyclic pattern. There were shown in chapter 3, examples where exploring the full impulse response for a cyclic reflectivity give rise to the appearance of a notch in the high frequencies in the amplitude spectrum of the signal. The cyclic system therefore acts like a low pass filter. The low frequencies see a nearly homogeneous system and pass through it with little attenuation. Higher frequencies begin to see the velocity structure and are multiply reflected within it. Consequently, higher frequencies are delayed and ultimately removed from

the transmitted pulse (Spencer et al., 1977). Besides this filtering effect, the concept of colored reflectivity cannot be avoid in the case of cyclic reflectivities. Although transitional reflectivities are not white, the whiteness assumption still works as a good approximation. Instead, for the cyclic case this becomes a critical assumption leading to a wrong estimation of the wavelet. Therefore, in a mixture reflection coefficient series this change in its character should be taken into account. Windowed deconvolution seems to be the best way to deal with non-stationarity. Identifying different windows that should be compensated for color or lack of frequency content in order to recover a wavelet consistent within the complete seismogram.

4.7 Examples

This synthetic example is generated using a model illustrated in figure (4.1). Coal layers are characterized with low density and velocity ($\rho_{coal} = 1.7g/cc$ and $v_{coal} = 2400m/s$), while the background has velocity and density almost twice the former ones ($\rho_{background} = 2.2g/cc$ and $v_{background} = 4200m/s$) for the stratigrafic filter.

The package of layers within the transmission filter were designed taking into account the condition of non-resolvable layers. That is to say, the thickness is less than about $\lambda/8$, where λ is the (predominant) wavelength computed using the velocity of the layer. As a source for the propagation of waves it was used a $50Hz$ Ricker wavelet, the sampling interval chosen is $0.002sec$.

First, I compute the amplitude spectrum of the O'Doherty and Anstey theoretical transmission filter generated by the present reflectivity. This spectrum helps to visualize the possible frequency notches caused by this example.

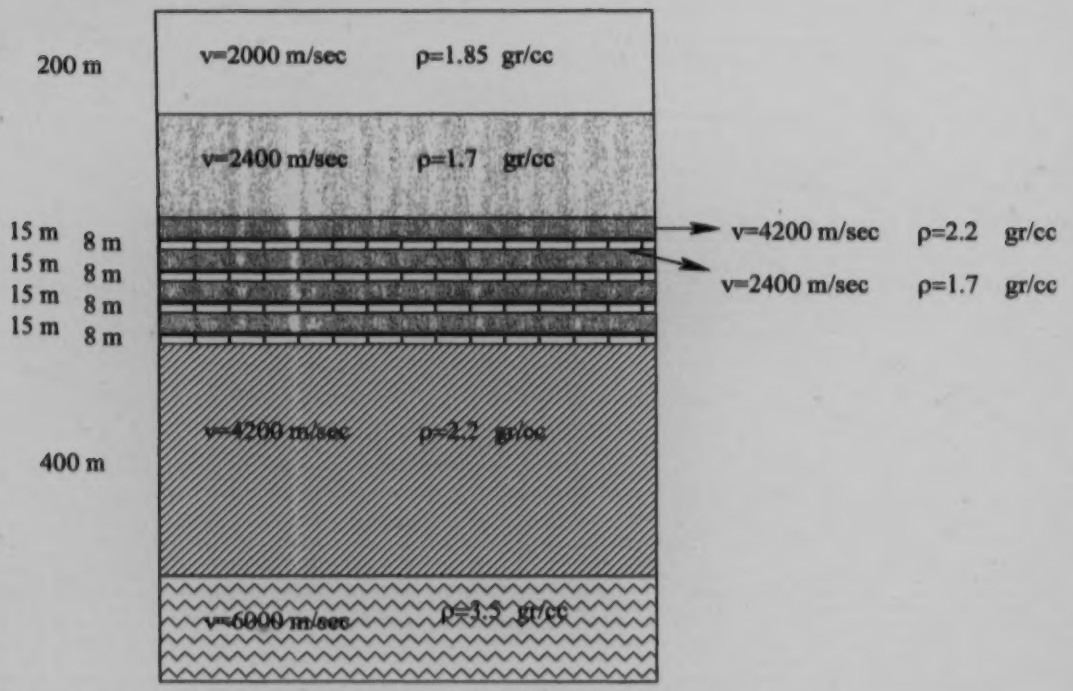

Figure 4.1: Earth model for a transmission filter.

Then, zero offset simulation with and without multiples were made. Simulations were done using the algorithm proposed by Mendel et al. (1979). Details of this algorithm are given in the following chapter, section 5.1. Figure 4.2 portrays the input reflectivity model and the output impulse response for the Ricker wavelet traveling through such reflectivity. From figure 4.3 illustrates the O'Doherty and Anstey theoretical amplitude spectrum and the computed spectrum for the transmitted signal. Based on the theoretical amplitude spectrum it should be expected to find a drop in the amplitude between $50Hz$ up to $90Hz$. The computed periodogram for the zero offset data corroborates this lack of frequency content in a window between $0.5 - 0.7sec$.

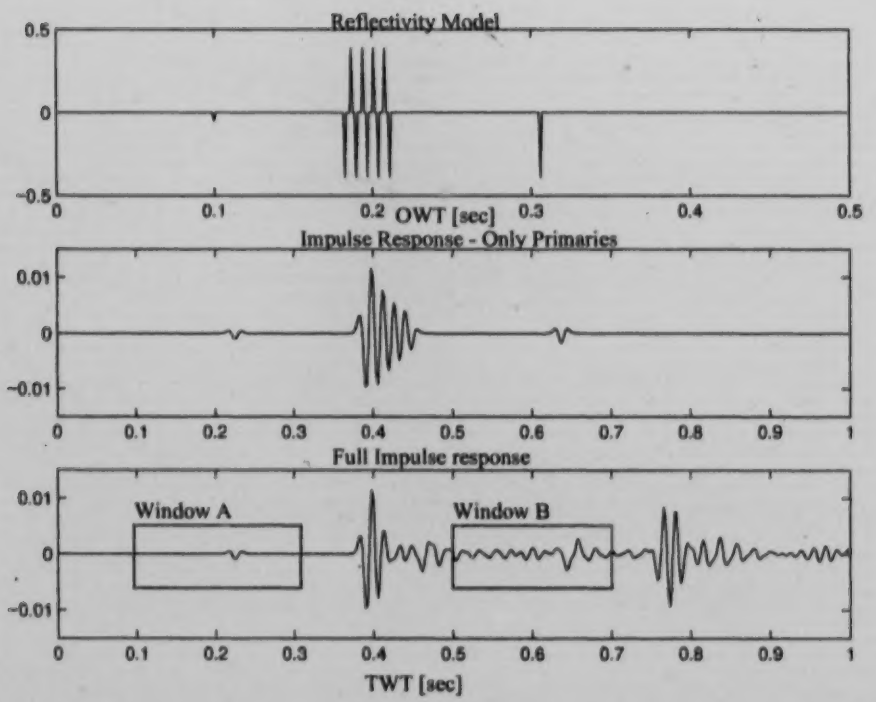

Figure 4.2: Top: reflectivity model. Middle: zero offset-impulse response (only primaries). Bottom: zero offset-full response. Window A stands for 'Above the transmission filter' and B stands for 'Below the transmission filter'.

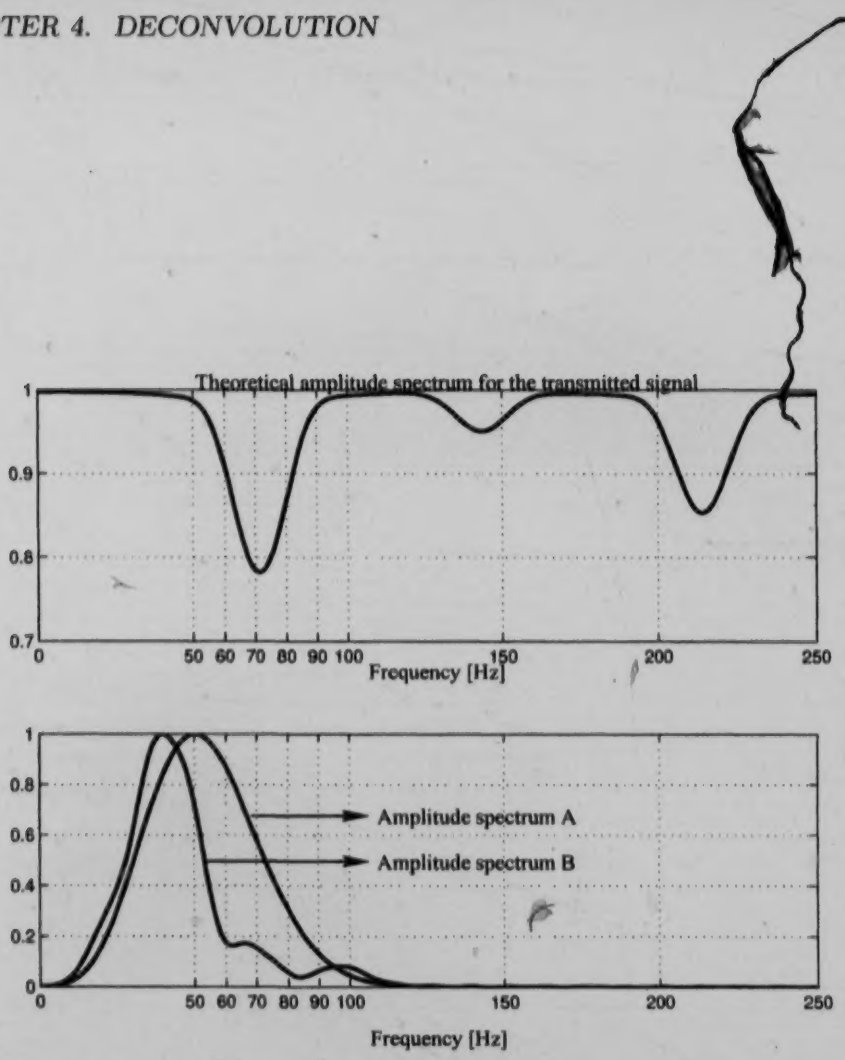

Figure 4.3: Top: O'Doherty and Anstey theoretical amplitude spectrum for the transmitted signal.Bottom: amplitude spectrum A for data between 0.1-0.3 sec overlying amplitude spectrum B for data between 0.5-0.7 sec.

A simulation with offset was also performed by means of a wave propagator method, working in this case only with acoustic waves. The propagator method used here is called the reflectivity method. This is based on the algorithm proposed by Kennet (1983). A derivation of the algorithm used is given in next chapter, section 5.2.

Shot gather data corroborates the drop in the amplitude spectrum observed for the same reflectivity model at zero offset simulations. It is interesting to note that, as observed by Perz (2000), the effect of the transmission filter does not seem to have a strong dependency on offset (figure 4.5).

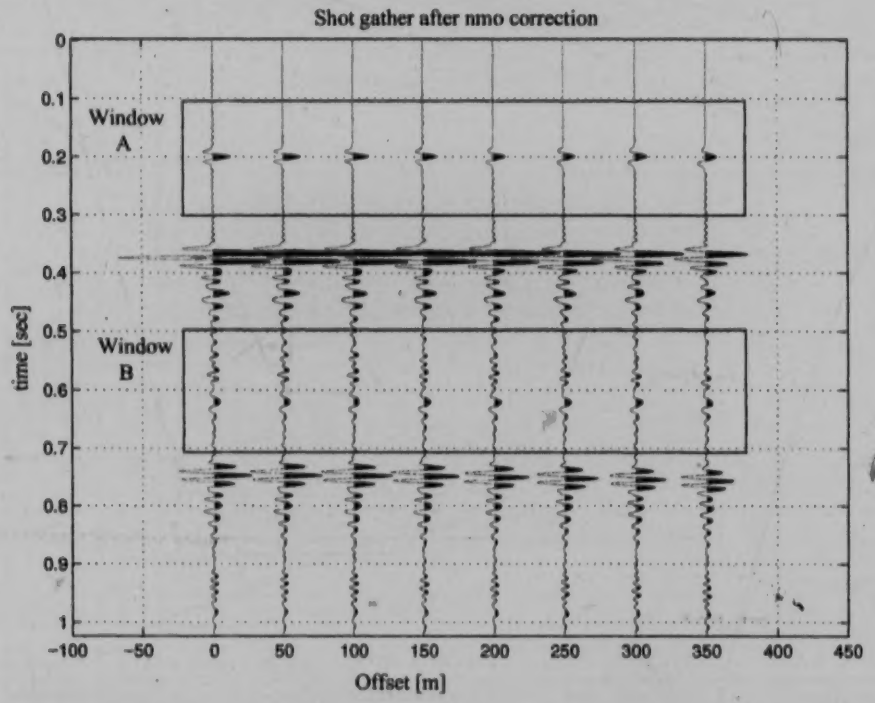

Figure 4.4: Full impulse response with offset. Window A stands for 'Above the transmission filter' and B stands for 'Below the transmission filter'.

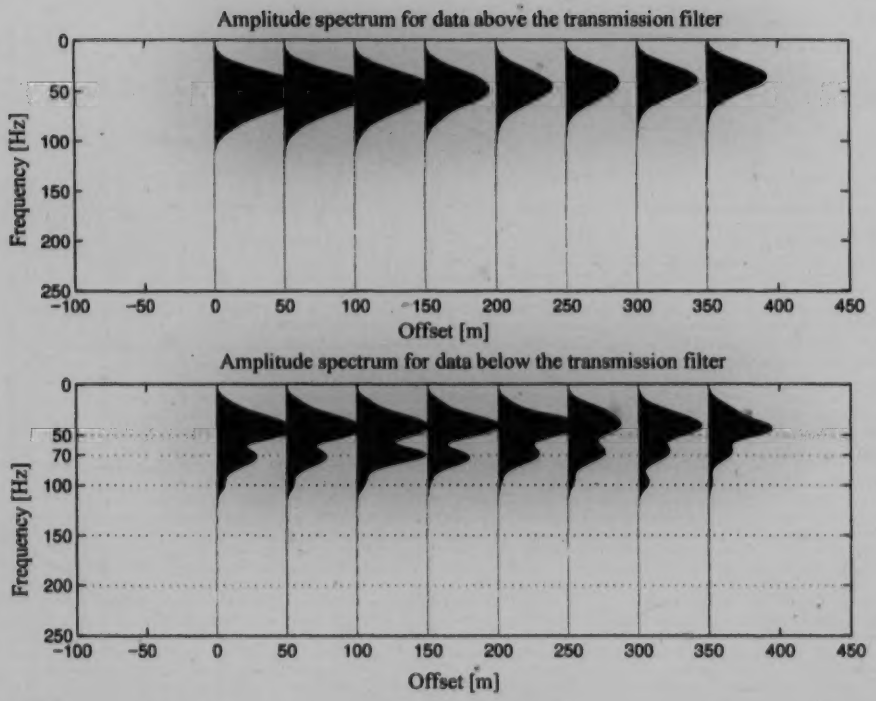

Figure 4.5: Top: amplitude spectrum for data between 0.1-0.3 sec. Bottom: amplitude spectrum for data between 0.5-0.7 sec, below transmission filter .

Next, the normal moveout correction (nmo) was applied and data was stacked to minimize the effect of multiples. However, since we are working beyond the limits of resolution there are still some remnants of multiple energy in the stack section. Notice that the arrival below the transmission filter is delayed by almost 90 degrees, being a trough instead of a peak at $t = 0.612sec$. This effect on the phase of the signal was pointed out by Banik (1985b), Coulombe and Bird (1996) and by Perz (2000).

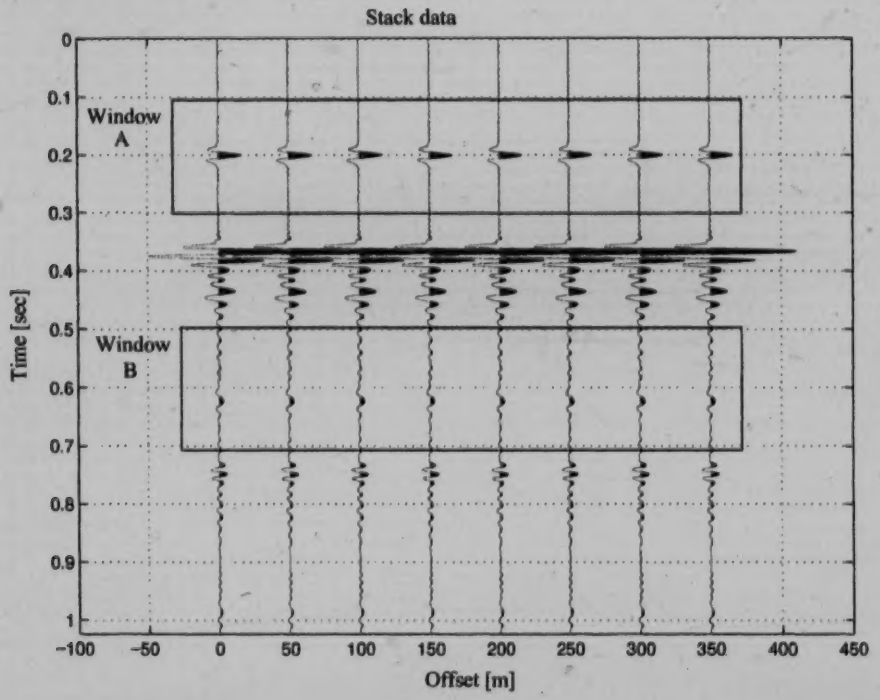

Figure 4.6: Full impulse response-stack data. Window A stands for 'Above the transmission filter' and B stands for 'Below the transmission filter'. Stacked trace was repeated for plotting purposes.

This example is intended to illustrate the technique from section 4.5 to compensate for the effect of the transmission filter. A window above the transmission filter was chosen between $0.1 - 0.3sec$ (window A). Another window below the transmission filter was chosen between $0.5 - 0.7sec$ (window B). Data and the amplitude spectrum for these windows is shown in figure 4.7. We define the transfer function $TRF(\omega)$ in the frequency domain as the one computed by dividing the spectra from window A and window B in the frequency range between $25 - 75Hz$.

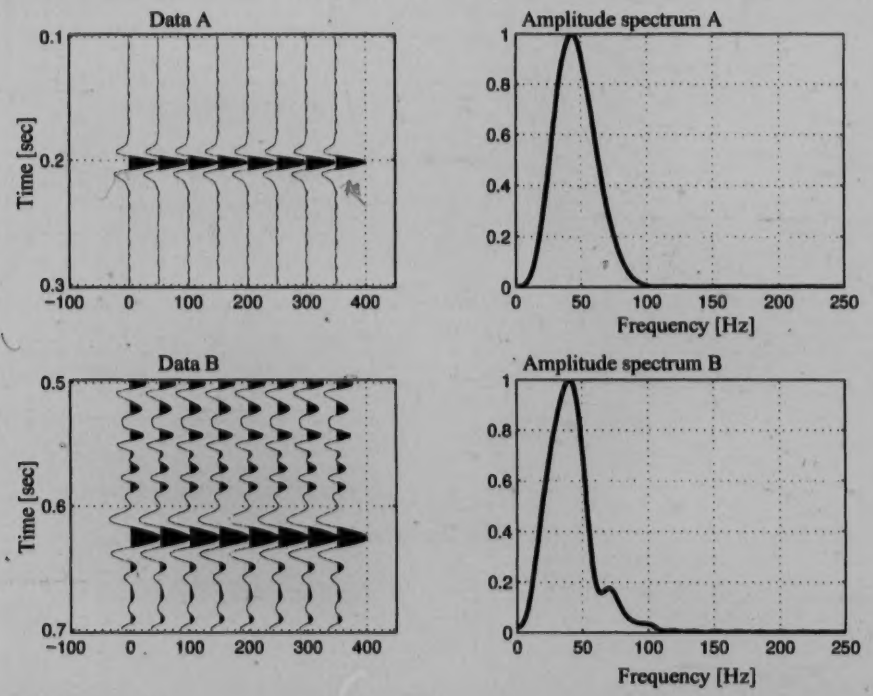

Figure 4.7: Top left: data A (Above transmission filter). Top right: amplitude spectrum A for data A. Bottom left: data B (Below transmission filter). Bottom right: amplitude spectrum B for data B.

Using conventional deconvolution, the corresponding wavelets above and below the transmission filter were extracted. Figures 4.8 and 4.9 present the extracted wavelet for each case with their corresponding amplitude spectrum. It can be seen from them that the amplitude spectrum of the wavelet below the transmission filter is shifted toward the low frequencies.

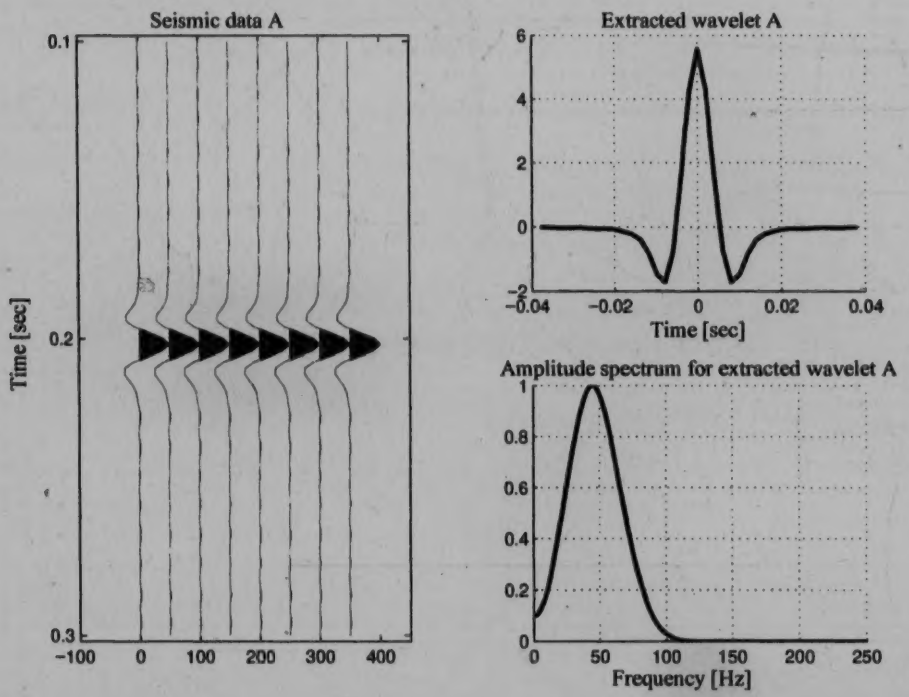

Figure 4.8: Right: data A (Above transmission filter). Left top: extrated wavelet from data A by conventional deconvolution. Left bottom: amplitude spectrum of extracted wavelet A.

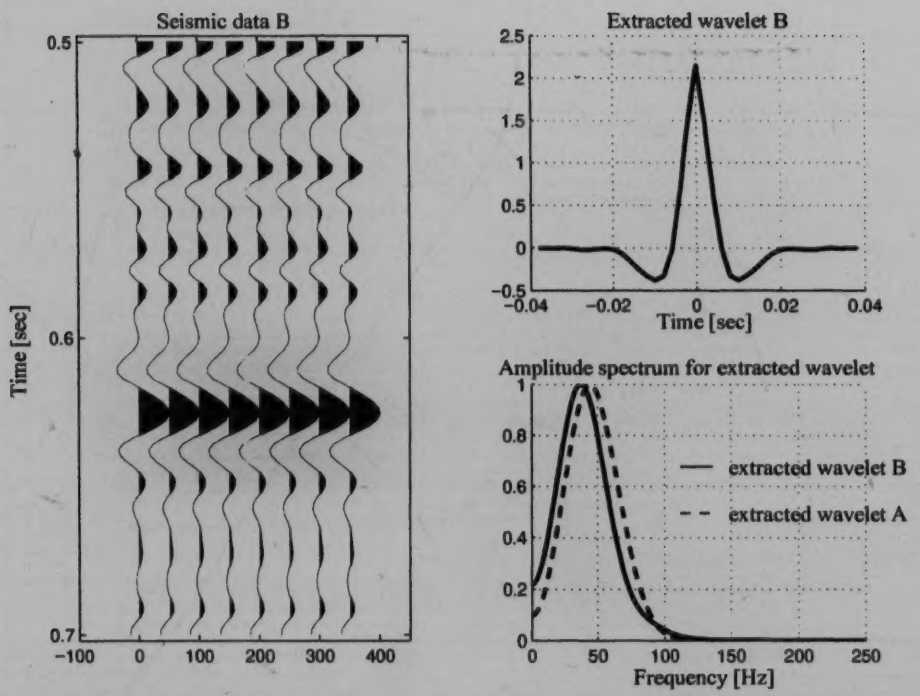

Figure 4.9: Right: data B (Below transmission filter). Left top: extrated wavelet from data B by conventional deconvolution. Left bottom: amplitude spectrum of extracted wavelet B overlying amplitude spectrum of extracted wavelet A.

Next, the transfer filter $trf_{min}(t)$ was computed and convolved with the data below the transmission filter. Figure (4.10) compared data below transmission filter before and after applying the compensatory filter. It can be seen an increment in frequency content after filtered and also notice that the signal was slighty correct in terms of phase. In terms of the amplitude spectrum of the signal below the transmission filter, after convolution with $trf_{min}(t)$, it was possible to boost up the spectrum at the notch window. However, the result overestimates the amplitude for frequencies towards the end of the spectrum.

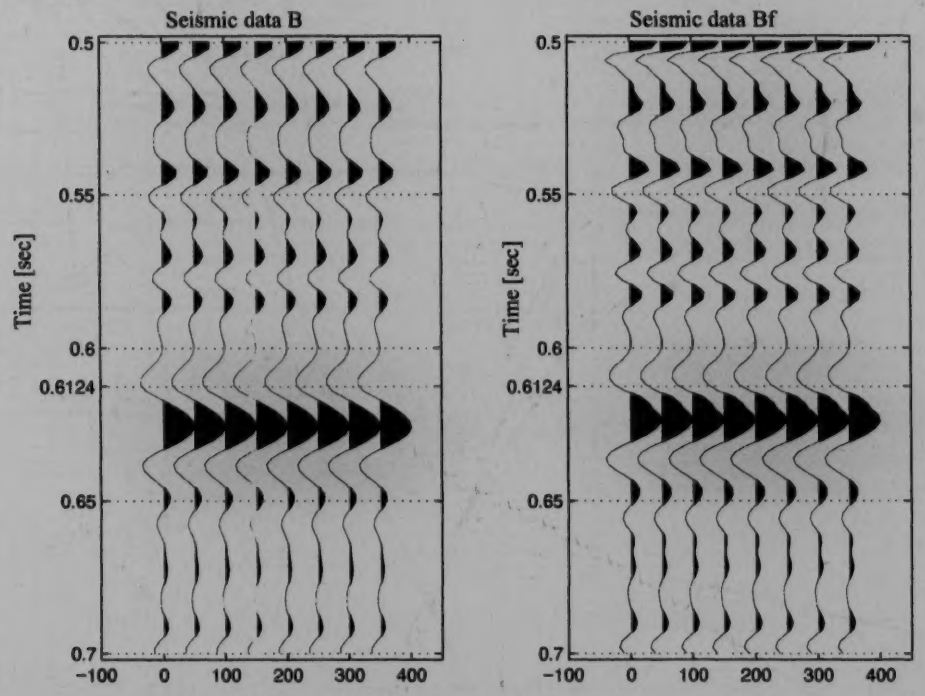

Figure 4.10: Left:seismic data B, Below transmission filter. Right: seismic data Bf, Below transmission Filter after applying compensatory filter to overcome the loss in frequency content trf_{min} (equation 4.5.4).

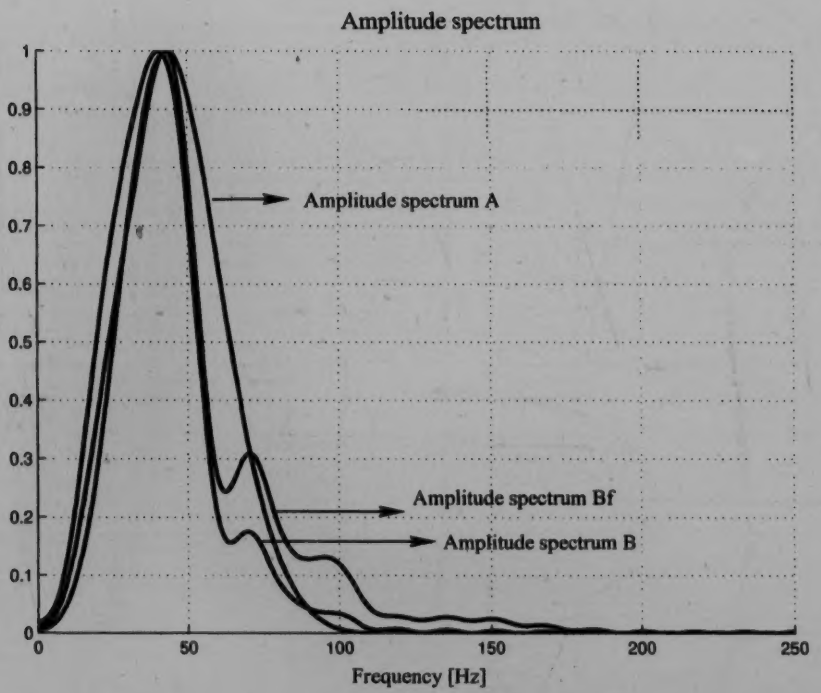

Figure 4.11: Amplitude spectrum A for the data above the transmission filter, overlying the amplitude spectrum B for data below the transmission filter and amplitude spectrum Bf for data below transmission filter after applying compensatory filter trf_{min}.

Finally, conventional deconvolution was applied to extract the corresponding wavelet from the data below the transmission filter after compensatory filtering (figure 4.12). The amplitude spectrum of the filtered wavelet seem to be a better approximation for the extracted wavelet above the transmission filter.

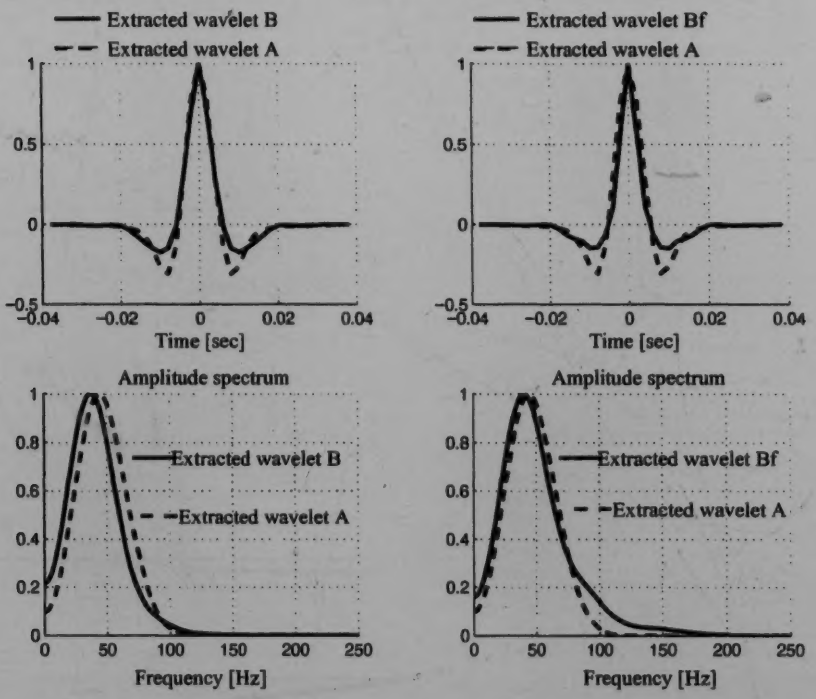

Figure 4.12: Top left: extrated wavelet B from data below the transmission filter. Bottom left: amplitude spectrum of the extracted wavelet B overlying amplitude spectrum from extracted wavelet A (Above transmission filter). Top right:extrated wavelet Bf from data below the transmission filter, after compensatory filter. Bottom right: amplitude spectrum of the extracted wavelet Bf, overlying amplitude spectrum from extracted wavelet A.

4.8 Summary

The first sections of this chapter provided a review on conventional deconvolution techniques. It was explained how deconvolution can be improved to overcome the weak assumption on autocorrelation structure of the reflectivity component. Works on deconvolution with non-white reflectivity were reviewed (Todoeschuck and Jensen, 1988; Saggaf and Robinson, 2000). Generally, all of them proposed a way to whiten the seismic trace before applying conventional deconvolution. The most practical approach to the problem of nonwitheness seems to be the *spectral compensation filter*. This method is the easiest to implement and use, since it re-uses existing deconvolution codes and requires only one extra filter to apply.

The second part of this chapter is intended to suggest a way to overcome the effect of stratigraphic filtering. The approach proposed here is easy to implement and able to improve the signal below the stratigraphic filter. It is recommended to apply this technique after stack to minimize multiple contribution. The example given in section 4.7 illustrates the apparent attenuation due to stratigraphic layering. The computed amplitude spectrum for the signal below the transmission filter corroborates the predicted notches from the theoretical amplitude spectrum given by O'Doherty and Anstey. Data below the transmission filter was convolved with the compensatory filter and afterward conventional deconvolution was used for wavelet extraction. Comparisons between extracted wavelets below the transmission filter before and after applying the compensatory filter show the effectiveness of the applied compensation. The extracted wavelet and its amplitude spectrum below transmission filter after compensatory filter resembles better the wavelet above transmission filter. So far, the existent literature on this subject propose to include a post stack two gate deconvolution (gate above and below the transmission filter) to remove the effects caused by the presence

of coals (Coulombe and Bird, 1996). The approach presented in this chapter is easy to implement and could be a way to normalize the wavelet along the seismogram.

Chapter 5

Modeling techniques

5.1 Synthetic seismograms at zero offset

Zero offset synthetic seismograms for a layered-media system were computed following the method proposed by Mendel et al. (1979) and extended to synthetic vertical seismic profile (SVSP) by Wyatt (1981). This method not only allows to place source and sensors at different depth but also the usage of non equal one way travel times. Earlier approaches for zero offset modeling, like Wuenschel (1960), Robinson (1968) and Claerbout (1976) used uniform travel times, source and sensor are located at the surface. Those methods recursively connect adjacent layers by means of frequency domain relationships. The approach used here treat all of the equations that describe a layered-media system together in the time domain. Details of this method are explained in the following section.

5.1.1 Interface equations

As it was defined in the previous chapter the reflection coefficient at zero offset is given by:

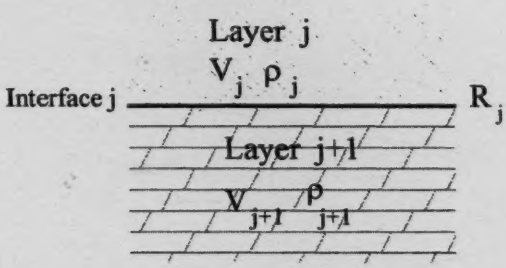

Figure 5.1: Reflection coefficient model.

$$r_j = \frac{\rho_j V_j - \rho_{j+1} V_{j+1}}{\rho_j V_j + \rho_{j+1} V_{j+1}}. \tag{5.1.1}$$

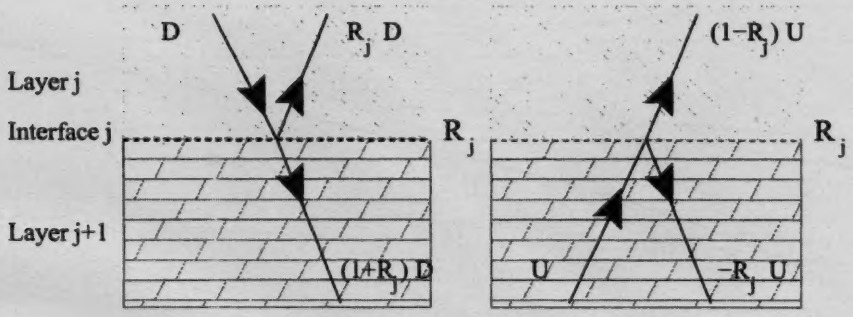

Figure 5.2: Reflection and transmission coefficients.

At any interface a down-going wave with amplitude d will be reflected and transmitted as it is depicted in figure 5.2 (left), being $(1 + r_j)$ the downward transmission coefficient. Similarly situation is illustrated in figure 5.2 (right) for an up-going wave of amplitude u where the upward transmission coefficient will be $(1 - r_j)$. For this modeling technique we use the convention that the reflection coefficient from below the interface is $-r_j$ and and from above the interface is $+r_j$. The algorithm used for zero offset seismograms starts with the ray diagram at figure 5.4.

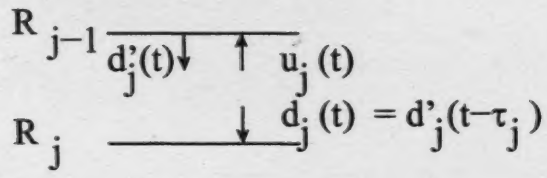

Figure 5.3: Waves at a layer j, time t.

First, notice that the down-going wave d_j is just a time delayed version of $d'_j(t-\tau)$. Having this in mind, now focus on figure 5.4.

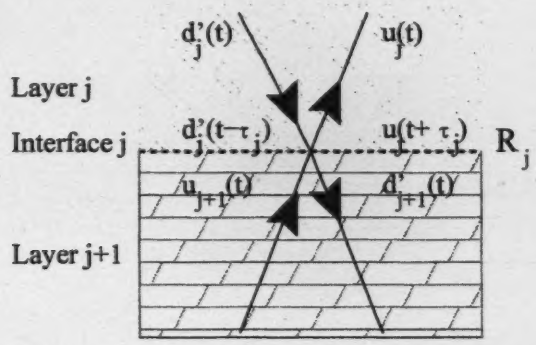

Figure 5.4: Reflected and transmitted waves at interface j.

The up-going wave is made up of two contributions, one due to the reflected part of $d'_j(t-\tau)$ and the other one coming from the transmitted portion of $u_{j+1}(t)$, then it can be written

$$u_j(t+\tau) = r_j d'_j(t-\tau) + (1-r_j)u_{j+1}(t), \tag{5.1.2}$$

similarly for the down-going wave,

$$d'_{j+1}(t) = (1+r_j)d'_j(t-\tau) - r_j u_{j+1}(t). \tag{5.1.3}$$

These two equations conform the "interface equations" and they are the ones that will propagate the wave field for a model of k layers. In a system of k

layers the previous equations are valid for layers $2...k-1$. A few considerations should be made for the first interface (surface) and the last one (k) in terms of the boundary conditions of the system. The example in chapter four considered source and receiver at the surface, the algorithm for such configuration is explained as follows. At the surface, the source impinge on the layered-media with a signal $m(t)$ that propagates through the layers. Then, the up-going wave to the receiver at the surface is given by:

$$y(t) = r_0 m(t) + (1 - r_0)u_1(t), \tag{5.1.4}$$

and the down-going wave is given by:

$$d_1'(t) = (1 + r_0)m(t) - r_0 u_1(t), \tag{5.1.5}$$

where r_0 is the reflection coefficient at the surface.

Boundary conditions for last layer set that there should be no up-going waves coming from below this interface since no source o reflector are there. Then, $u_{j+1}(t) = 0$ and the corresponding equations for this layer are:

$$u_k(t + \tau) = r_k d_k'(t - \tau), \tag{5.1.6}$$

and the down-going wave will be given by:

$$d_{k+1}'(t) = (1 + r_k) d_k'(t - \tau). \tag{5.1.7}$$

So far we delineate the basic equations involved in this algorithm. Next section explains the dynamic of the method for a full response modeling.

5.1.2 Full response model

To clearly show the dynamic of the algorithm it is convenient to group the previous equations in a layer ordering.

$$d'_1(t) = (1 + r_0)m(t) - r_0 u_1(t), \tag{5.1.8}$$

$$u_1(t + \tau) = r_1 d'_1(t - \tau) + (1 - r_1 u_2(t)), \tag{5.1.9}$$

$$d'_j(t) = (1 + r_{j-1})d'_{j-1}(t - \tau) - r_{j-1} u_j(t), \tag{5.1.10}$$

$$u_j(t + \tau) = r_j d'_j(t - \tau) + (1 - r_j)u_{j+1}(t), \tag{5.1.11}$$

$$d'_k(t) = (1 + r_{k-1})d'_{k-1}(t - \tau) - r_{k-1} u_k(t), \tag{5.1.12}$$

$$u_k(t + \tau) = r_k d'_k(t - \tau). \tag{5.1.13}$$

It is useful to re-arrange these equations in such a way that on the left hand side we place all the events that occur at time $t + \tau$ and on the right hand side all the events that occur at time t. In order to do this, notice that

$$d_k(t) = d'_{k-1}(t - \tau). \tag{5.1.14}$$

Then, the system of equations can be re-written as follows:

$$d_1(t + \tau) = (1 + r_0)m(t) - r_0 u_1(t), \tag{5.1.15}$$

$$u_1(t+\tau) = r_1 d_1(t) + (1 - r_1 u_2(t), \tag{5.1.16}$$

$$d_j(t+\tau) = (1 + r_{j-1}) d_{j-1}(t) - r_{j-1} u_j(t), \tag{5.1.17}$$

$$u_j(t+\tau) = r_j d_j(t) + (1 - r_j) u_{j+1}(t), \tag{5.1.18}$$

$$d_k(t+\tau) = (1 + r_{k-1}) d_{k-1}(t) - r_{k-1} u_k(t), \tag{5.1.19}$$

$$u_k(t+\tau) = r_k d_k(t). \tag{5.1.20}$$

Then, the the wave field at the surface $y(t)$ is given by the sum of the reflected portion of the energy source $r_0\ m(t)$ and the transmitted portion of the up-going wave at the top of the first layer $(1 - r_0)\ u_1(t)$, i.e.,

$$y(t) = r_0 m(t) + (1 - r_0) u_1(t), \tag{5.1.21}$$

where $u_1(t)$ is computed using the previous set of equations (5.1.15-5.1.20). The signal $y(t)$ includes transmission loss and all possible multiples for the time of simulation. One can also choose the order of multiples to be included in the impulse response by slightly modifying the algorithm (Wyatt, 1981). This is the method used to generated the zero offset examples in chapters three and four.

Synthetic VSP algorithm

The extension to SVSP made by Wyatt (1981) lead to the following algorithm. At the top of the first layer

$$y(t) = r_0 m(t) + (1 - r_0) u_1(t). \tag{5.1.22}$$

And for a layer j,

$$y_j(t) = u_j(t+\tau) + d_j(t) = (1 + r_j) d_j(t) + (1 - r_j) u_{j+1}(t). \tag{5.1.23}$$

These equations express the complete wave field for a vertical seismic profile, including all multiples and transmission loss.

5.2 The reflectivity method (including offset)

Several different methods have been developed to calculate theoretical seismograms in realistic, horizontally stratified models (Fuchs and Müller, 1971; Müller, 1985; Kennet, 1983). The reflectivity method is a wave number or slowness integration method (Chapman and Orcutt, 1985; Mallick and Frazer, 1987). The name of the method stands for the fact that the function which is integrated is the reflectivity of a layered medium (Müller, 1985). Originally this method was valid for a layered medium without a free surface and a source on one side of those layers whose reflections are sought (Fuchs and Müller, 1971). This method was mainly applied to seismic prospecting problems with special focus on coal-mining problems (Fertig and Müller, 1978). Later, Kennet (1983) found a recursively formula for the calculation of reflection coefficients. Kennet and Kerry (1979) expanded the method for the case of a layered half-space including a free surface and a source at arbitrary depth. They showed that the integrand of the slowness integral in such a case can be expressed mainly by the reflectivities of two partitions of the medium, the layers above the source and those below.

The example in chapter 4 was generated by the reflectivity method as it is presented by Chapman and Orcutt (Chapman and Orcutt, 1985), and Kennet (1983) .

The reflectivity method allows to compute offset dependent synthetic seismograms by integrating the momentum equation,

$$-\rho\,\omega^2\,\mathbf{u} \;=\; \nabla.\sigma + \mathbf{f}, \tag{5.2.1}$$

and the constitutive equation

$$\sigma \;=\; \mathbf{c} \;:\; \varepsilon, \tag{5.2.2}$$

where σ and ε are the infinitesimal stress and strain tensors, ρ is the density, $\mathbf{u}$ is the elastic displacement, $\mathbf{f}$ is the body-force density, and $\mathbf{c}$ is the four-order

elastic tensor. Since our elastic medium is stratified, we can transform out the dependence of $\mathbf{u}$ and σ on radius x and azimuth ϕ by expanding them as series of cylindrical harmonics via the Fourier-Hankel transform (Takeuchi and Saito, 1972). The details of this procedure can be found in many books and papers (Kennet, 1983; Chapman and Orcutt, 1985). Then problem is converted to an ordinary differential equation in z. The system to solve is a two boundary value problem. For a model with n layers, it has at the surface ($z = 0$) zero stress and at the last interface ($z = z_n$) absence of incoming waves since they are no sources or other interfaces below it. The resulting equation is written as:

$$\partial_z \mathbf{y}(z) \;=\; \omega\, \mathbf{A}(z)\, \mathbf{y}(z) \;+\; \mathbf{F}, \tag{5.2.3}$$

where $\mathbf{y}(z)$ is the stress-displacement vector, each of its components has been expanded as series of cylindrical harmonics via the Fourier-Hankel transform. $\mathbf{F}$ is the term corresponding to the source. And $\mathbf{A}(z)$ is given by:

$$\begin{pmatrix} 0 & p\frac{\lambda}{\lambda+2\mu} & 0 & \frac{1}{\lambda+2\mu} & 0 & 0 \\ -p & 0 & 0 & 0 & \frac{1}{\mu} & 0 \\ 0 & 0 & 0 & 0 & 0 & \frac{1}{\mu} \\ -\rho & \frac{p\rho g}{\omega} & 0 & 0 & p & 0 \\ \frac{p\rho g}{\omega} & \delta p^2 - \rho & 0 & -\rho\frac{\lambda}{\lambda+2\mu} & 0 & 0 \\ 0 & 0 & \mu p^2 - \rho & 0 & 0 & 0 \end{pmatrix} \tag{5.2.4}$$

$$\delta = 4\rho\beta^2(1 - \frac{\beta^2}{\alpha^2}), \tag{5.2.5}$$

where ω is frequency, $p = k/\omega$ is the ray parameter with k as the wave number, $\alpha(z)$ stands for the compressional wave (p-wave) velocity and $\beta(z)$ for the shear wave (s-wave) velocity, $\lambda(z)$ and $\mu(z)$ are the Lame parameters.

Each component of stress-displacement vector can be recovered in the offset domain by the inverse Fourier-Hankel transform:

$$\mathbf{y}(x,\omega) \;=\; \int_0^\infty \omega^2\, p\, dp\, \tilde{\mathbf{y}}(p,\omega)\, J_0(\omega p x) \tag{5.2.6}$$

J_0 is the Bessel function of order zero. The Inverse Fourier transform is used to recovered the components in the time domain.

$$\mathbf{y}(x,t) \;=\; \frac{1}{2\pi} \int_{-\infty}^{\infty} d\omega\, e^{-i\omega t}\, \mathbf{y}(x,\omega) \tag{5.2.7}$$

Finally, $y(x,t)$ gives the complete wave field at the surface including all multiples, transmission loss included. This method allows the user to choose which waves to propagate. In the example shown in chapter four we only consider the acoustic case.

5.2.1 Homogeneous differential system

Let us consider first the solution of the homogeneous differential system:

$$\partial_z \mathbf{y}(z) \;=\; \omega\, \mathbf{A}(z)\mathbf{y}(z). \tag{5.2.8}$$

The stress displacement vector can be written in terms of the eigenvectors of A as,

$$\mathbf{y} = \mathbf{N}.\mathbf{w}, \tag{5.2.9}$$

where, $\mathbf{w}$ is called the "wave vector". $\mathbf{N}$ is the eigenvector matrix as defined in Appendix 1. The elements of N are scaled so that $i\, N^+ = N^{-1}$ [1]

[1] N^+ satisfies the following property,

$$\mathbf{N}^+ \;=\; -\mathbf{J}\mathbf{N}^{\mathbf{T}}\mathbf{J}, \tag{5.2.10}$$

Replacing $\mathbf{y}$ in the equation of motion 5.2.3, we obtain:

$$\partial_z(\mathbf{Nw}) = \omega\,\mathbf{A}\,\mathbf{N}\,\mathbf{w}, \tag{5.2.12}$$

$$\partial_z\mathbf{w} = [\omega\,\mathbf{N}^{-1}\mathbf{AN} - \mathbf{N}^{-1}\partial_z\mathbf{N}]\mathbf{w}. \tag{5.2.13}$$

Since

$$\omega\mathbf{N}^{-1}\,\mathbf{A}\,\mathbf{N} = i\omega\mathbf{q}, \tag{5.2.14}$$

where $i\mathbf{q}$ is the the diagonal matrix of eigenvalues of $\mathbf{A}$,

$$\mathbf{q} = \mathrm{diag}[q_\alpha, q_\beta, q_\beta, -q_\alpha, -q_\beta, -q_\beta], \tag{5.2.15}$$

with,

$$q_\alpha(p,z) = [\alpha^{-2}(z) - p^2]^{1/2} \tag{5.2.16}$$

$$q_\beta(p,z) = [\beta^{-2}(z) - p^2]^{1/2} \tag{5.2.17}$$

with, $Im(\omega q_\alpha) \geq 0$ and $Im(\omega q_\beta) \geq 0$ [2].

In a uniform medium the coefficient matrix $\mathbf{A}$ is constant so the eigenvector matrix $\mathbf{N}$ is independent of z. Therefore

$$\mathbf{N}^{-1}\partial_z\mathbf{N} = 0. \tag{5.2.18}$$

Then the wave vector $\mathbf{w}$ is governed by

$$\partial_z\mathbf{w} = i\omega\,\mathbf{q}\,\mathbf{w}, \tag{5.2.19}$$

$$\mathbf{J} = \begin{pmatrix} 0 & -I \\ I & 0 \end{pmatrix}, \tag{5.2.11}$$

[2] Im stands for the imaginary part of the complex number

a solution can be written as,

$$\mathbf{w}(z) = e^{\omega(z-z_0)\mathbf{q}}\,\mathbf{w}(z_0), \tag{5.2.20}$$

then,

$$\mathbf{w}(z) = \mathbf{S}(z-z_0)\,\mathbf{w}(z_0). \tag{5.2.21}$$

In the last equation we have introduced the "wave propagator" $\mathbf{S}$. Now, the stress-displacement solution is given by

$$\mathbf{y}(z) = \mathbf{N}_z\, e^{\omega(z-z_0)\mathbf{q}}\,\mathbf{N}_{z_0}^{-1}\,\mathbf{y}(z_0). \tag{5.2.22}$$

We define the Propagator matrix P, commonly known as the Haskell matrix as (Haskell, 1953):

$$\mathbf{P}(z,z_0) = \mathbf{N}_z\, e^{\omega(z-z_0)\mathbf{q}}\,\mathbf{N}_{z_0}^{-1} = i\mathbf{N}_z\, e^{\omega(z-z_0)\mathbf{q}}\,\mathbf{N}_{z_0}^{+} \tag{5.2.23}$$

The propagator will propagate the solution from one layer to the other like

$$\mathbf{y}(z) = \mathbf{P}(z,z_0)\,\mathbf{y}(z_0). \tag{5.2.24}$$

Once that we have introduced this concept for a uniform medium, we can apply it to a layered-media as it is explained in the following section.

5.2.2 Layered medium

Let us first start with the solution $\mathbf{y}(z)$ propagating through a single interface z_ℓ. The propagator $\mathbf{P}$ will be expressed as:

$$\mathbf{P}(z_m,z_n) = \mathbf{P}(z_m,z_\ell)\,\mathbf{P}(z_\ell,z_n). \tag{5.2.25}$$

Replacing the propagator by its expression 5.2.23 into equation 5.2.25 we obtain,

$$\mathbf{P}(z_m,z_n) = \mathbf{N}_{z_{m-0}}\, e^{i\omega\int_{z_\ell}^{z_m}\mathbf{q}\,d\xi}\,[i\,\mathbf{N}_{z_{\ell+0}}^{+}\,\mathbf{N}_{z_{\ell-0}}]\, e^{i\omega\int_{z_n}^{z_\ell}\mathbf{q}\,d\xi}\, i\mathbf{N}_{z_{n+0}}^{+}. \tag{5.2.26}$$

Notice that we used $e^{i\omega \int_{z_\ell}^{z_m} \mathbf{q}\, d\xi}$ instead of $e^{i\omega(z-z_0)\mathbf{q}}$ since we are dealing with a not-uniform layered media.

We recall the wave propagator to be,

$$\mathbf{S}_\ell = \mathbf{S}(z_{\ell+0}, z_{\ell-0}) = i\, \mathbf{N}^+_{z_{\ell+0}}\, \mathbf{N}_{z_{\ell-0}}, \tag{5.2.27}$$

which connects the waves across the interface at z_ℓ.

Similarly,

$$\mathbf{S}(z_{m-0}, z_{\ell+0}) = e^{i\omega \int_{z_\ell}^{z_m} \mathbf{q}\, d\xi} = \wedge_\ell \oplus \wedge_\ell^{-1}, \tag{5.2.28}$$

propagates the waves across the layer from z_ℓ to z_m ($\oplus$ is used to denote a generalization of the usual direct sum). Where $\wedge$ is a 3x3 matrix of the positive phase factors,

$$\wedge_\ell = exp\left\{ i\omega \int_{z_\ell}^{z_m} \begin{pmatrix} q_\alpha & 0 & 0 \\ 0 & q_\beta & 0 \\ 0 & 0 & q_\beta \end{pmatrix} d\xi \right\} \tag{5.2.29}$$

Then, we can express the propagator $\mathbf{P}$ in terms of the wave propagator $\mathbf{S}$ as,

$$\mathbf{P}(z_m, z_n) = \mathbf{N}(z_{m-0})\, \mathbf{S}(z_{m-0}, z_{\ell+0})\, \mathbf{S}_\ell\, \mathbf{S}(z_{\ell-0}, z_{n+0})\, i\, \mathbf{N}(z_{n+0}). \tag{5.2.30}$$

The interesting point of this expression resides on the fact that the wave propagator $\mathbf{S}$ can be written in terms of the reflection and transmission coefficients (Kennet, 1983). In this way, the algorithm will be more stable, avoiding growing exponentials what was usually the problem with propagator theory (Thomson, 1950; Haskell, 1953; Knopoff, 1964).

Consider an incident wave of unit amplitude at an interface z_ℓ. this will generate reflected and transmitted waves as it shown in this figure

Then, the continuity of the solution through the interface requires,

$$\mathbf{N}_{z_\ell-0}\, \mathbf{I} + \mathbf{N}_{z_\ell-0}\, \mathbf{R}_U = \mathbf{N}_{z_\ell+0}\, \mathbf{T}_U, \tag{5.2.31}$$

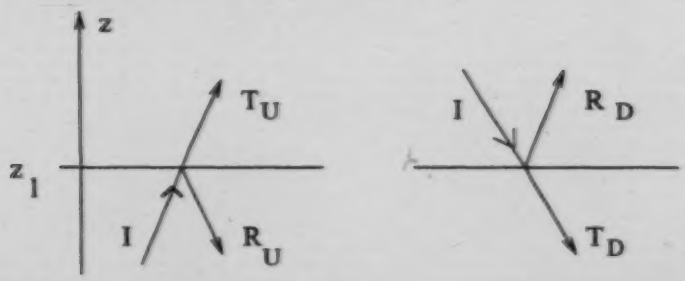

Figure 5.5: Reflected and transmitted ray at an interface z_ℓ. Subscript indicates the incident wave direction.

and

$$\mathbf{N}_{z_\ell - 0}\,\mathbf{T}_D \;=\; \mathbf{N}_{z_\ell + 0}\,\mathbf{R}_D + \mathbf{N}_{z_\ell + 0}\,\mathbf{I}. \tag{5.2.32}$$

The continuity of the solution vector **y** at the interface for the six possible incident wave conditions can be expressed in a matrix equation,

$$\mathbf{N}_{z_\ell - 0} \begin{pmatrix} \mathbf{I} & 0 \\ \mathbf{R}_U & \mathbf{T}_D \end{pmatrix} = \mathbf{N}_{z_\ell + 0} \begin{pmatrix} \mathbf{T}_U & \mathbf{R}_D \\ 0 & \mathbf{I} \end{pmatrix} \tag{5.2.33}$$

Where $\mathbf{R}_U$,$\mathbf{R}_D$,$\mathbf{T}_U$,$\mathbf{T}_D$ are reflection and transmission matrices for incident waves traveling in the upward and downward directions. i.e.,

$$\mathbf{R}_U \;=\; \begin{pmatrix} R_U^{pp} & R_U^{vp} & 0 \\ R_U^{pv} & R_U^{vv} & 0 \\ 0 & 0 & R_U^{hh} \end{pmatrix}, \tag{5.2.34}$$

where the first superscript refers to the incident wave type, in this case traveling in an upward direction from below the interface. The second superscript refers to the reflected ray type. P refers to a P-wave, v to an SV-wave and h to an SH-wave. It was included the separation of the P-SV and SH systems by setting some coefficients to zero. The elements of the other matrices are similarly defined. Appendix 2 will show the explicit form of the reflection and transmission coefficients.

We recall the wave propagator from equation 5.2.27,

$$\mathbf{S}_\ell \;=\; \mathbf{N}^{-1}_{z_\ell+0}\,\mathbf{N}_{z_\ell-0}. \tag{5.2.35}$$

Combining this equation with equation 5.2.33 we obtain,

$$\mathbf{S}_\ell \;=\; \begin{pmatrix} \mathbf{T}_U - \mathbf{R}_D\,\mathbf{T}_D^{-1}\,\mathbf{R}_U & \mathbf{R}_D\,\mathbf{T}_D^{-1} \\ -\mathbf{T}_D\,\mathbf{R}_U & \mathbf{T}_D^{-1} \end{pmatrix} \tag{5.2.36}$$

The wave propagator $\mathbf{S}$ can be used to expand the propagator $\mathbf{P}$ in terms of the reflection and transmission coefficients in a recursively formula due to Kennett (1983).

Suppose we have found the solution for a stack of layers from z_m to z_{n-1} and we add a new layer from z_{n-1} to z_n.

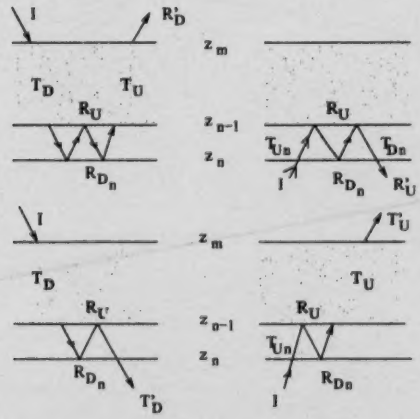

Figure 5.6: The generation of the ray expansion when an extra layer $z_{n-1} < z < z_n$ is added to a stack of layers $z_m < z < z_{n-1}$. One ray in each set of reverberations is illustrated.

In terms of the wave propagator we can write,

$$\mathbf{S}(z_m - 0, z_n - 0) = \mathbf{S}(z_m - 0, z_{n-1} - 0)\mathbf{S}(z_{n-1} - 0, z_n + 0)\mathbf{S}_n \tag{5.2.37}$$

Replacing equation 5.2.36 into equation 5.2.37 we obtain,

$$\begin{pmatrix} \mathbf{T}'_U - \mathbf{R}'_D\mathbf{T}'^{-1}_D\mathbf{R}'_U & \mathbf{R}'_D\mathbf{T}'^{-1}_D \\ -\mathbf{T}'_D\mathbf{R}'_U & \mathbf{T}'^{-1}_D \end{pmatrix} = \begin{pmatrix} \mathbf{T}_U - \mathbf{R}_D\mathbf{T}_D^{-1}\mathbf{R}_U & \mathbf{R}_D\mathbf{T}_D^{-1} \\ -\mathbf{T}_D\mathbf{R}_U & \mathbf{T}_D^{-1} \end{pmatrix} \times$$
$$\times \begin{pmatrix} \wedge_n & 0 \\ 0 & \wedge_n^{-1} \end{pmatrix} \begin{pmatrix} \mathbf{T}_{U_n} - \mathbf{R}_{D_n}\mathbf{T}_{D_n}^{-1}\mathbf{R}_{U_n} & \mathbf{R}_{D_n}\mathbf{T}_{D_n}^{-1} \\ -\mathbf{T}_{D_n}\mathbf{R}_{U_n} & \mathbf{T}_{D_n}^{-1}. \end{pmatrix} \tag{5.2.38}$$

Where $\mathbf{T}'$ refers to the complete stack from z_m to z_n, $\mathbf{T}$ refers to the stack from z_m to z_{n-1} and $\mathbf{T}_n$ refers to the interface at z_n. Solving this system we obtain Kennett's recursive formula between reflection and transmission coefficients from a stack of layers.

5.2.3 The Source term

So far, we deal with the solution of the homogeneous differential system. Now let us incorporate the contribution of the seismic source. Then equation 5.2.8 will be modified as,

$$\partial_z \mathbf{y}(z) \;=\; \omega \mathbf{A}(z) y(z) + \mathbf{F} \tag{5.2.39}$$

where $\mathbf{F}$ is the source contribution.

The complete solution of this equation (Chapman and Orcutt, 1985) is given by,

$$\mathbf{y}(z) \;=\; \mathbf{P}(z, z_n)\, \mathbf{y}(z_n) \;+\; \int_{z_n}^{z} \mathbf{P}(z,\xi)\, \mathbf{w}_s(\xi) d\xi \tag{5.2.40}$$

where

$$\mathbf{w}_s^T = [\, 0, 0, 0, -F_k^m(z), -G_k^m(z), -H_k^m(z)] \tag{5.2.41}$$

The source force f_0 has been expanded in the harmonic functions F_k^m, G_k^m,H_k^m. Let us take the case of an infinitesimal point source at $x = x_0$. We consider the

seismic source as being due to a stress glut $\Gamma(x,t)$ (Backus and Mulcahy, 1976),

$$\mathbf{f}_0 = -\nabla.\Gamma \tag{5.2.42}$$

Then, we define the moment tensor $\mathbf{m}(t)$ as the volume integral of the stress glut

$$\mathbf{m}(t) = \int_v \Gamma(\mathbf{x},t)d\mathbf{x}. \tag{5.2.43}$$

We write the source force for the idealized point source as (Gilbert, 1971),

$$\mathbf{f}_0 = \mathbf{f}(t)\delta(\mathbf{x}-\mathbf{x}_0) - \nabla.\mathbf{m}(t)\delta(\mathbf{x}-\mathbf{x}_0). \tag{5.2.44}$$

For the cylindrical system the delta function is given by

$$\delta(\mathbf{x}-\mathbf{x_0}) = \lim_{x_0\to 0} \frac{\delta(z-z_0)\delta(x-x_0)\delta(\phi)}{x} \tag{5.2.45}$$

where the harmonic coefficients for order m=0 are (Kennet and Kerry, 1979),

$$\eta^{-1}F_k^0(z) = \hat{f}_z(\omega)\delta(z-z_0) - \hat{m}_{zz}(\omega)\delta'(z-z_0) \tag{5.2.46}$$

$$\eta^{-1}G_k^0(z) = -(k/2)[\hat{m}_{xx}(\omega)+\hat{m}_{\phi\phi}(\omega)]\delta(z-z_0) \tag{5.2.47}$$

$$\eta^{-1}H_k^0(z) = 0 \tag{5.2.48}$$

with,

$$\eta = (\frac{k}{2\pi})^{1/2} = (\frac{p\omega}{2\pi})^{1/2}. \tag{5.2.49}$$

The relevant quantity when including the source is the discontinuity in component waves at that point. The saltus in the component vector can be written as:

$$[\mathbf{r}(z_0)] = \int_{z_0-0}^{z_0+0} \mathbf{F}^{-1}(\xi)\mathbf{w_s}(\xi)d\xi, \tag{5.2.50}$$

using that

$$\mathbf{F} = \mathbf{N} e^{[i\omega \int^z \mathbf{q}(p,\xi)\, d\xi]}, \tag{5.2.51}$$

then,

$$[\mathbf{r}(z_0)] = i \int_{z_0-0}^{z_0+0} e^{[-i\omega\tau(\xi)]} \mathbf{N}^+(\xi) \mathbf{w}_s(\xi) d\xi. \tag{5.2.52}$$

Replacing the expressions of $\mathbf{w}_s$ from equation 5.2.41 and the harmonic functions from equations 5.2.46, 5.2.47 and 5.2.48 we get,

$$\begin{aligned}[\mathbf{r}(z_0)] = \mathbf{W}\, [&(q_\alpha,\ ip,\ 0,\ q_\alpha,\ -ip,\ 0)^T\ \hat{f}_z(\omega) - \\ -i\omega\, &(q_\alpha^2,\ -ipq_\beta,\ 0,\ -q_\alpha^2,\ -ipq_\beta,\ 0)^T\ \hat{m}_{zz}(\omega) - \\ -i\omega &(p^2,\ ipq_\beta,\ 0,\ -p^2,\ ipq_\beta,\ 0)^T\ \frac{\hat{m}_{xx}(\omega) + \hat{m}_{\phi\phi}(\omega)}{2}\end{aligned} \tag{5.2.53}$$

Terms on the right hand side (RHS) are evaluated at the source depth z_0. $\mathbf{W}$ is a diagonal matrix that contains the phase at the source and the eigenvector weighting,

$$\mathbf{W} = \eta e^{[-i\omega\tau(z_0)]} \begin{pmatrix} (2pq_\alpha)^{-1/2} & & & & & \\ & (2pq_\beta)^{-1/2} & & & 0 & \\ & & (2\mu q_\beta)^{-1/2} & & & \\ & & & (2pq_\alpha)^{-1/2} & & \\ & 0 & & & (2pq_\beta)^{-1/2} & \\ & & & & & (2\mu q_\beta)^{-1/2} \end{pmatrix} \tag{5.2.54}$$

Since these expressions are the change in waves across the source depth, the first three components of $[\mathbf{r}(z_0)]$ are the amplitudes of the source waves propagating in the positive direction from the source and the last three components are minus the amplitudes of source waves propagating in the negative direction. Then we can write the jump due to the source as,

$$[\mathbf{y}(z_0)] = \mathbf{N}(z_0) e^{[-i\omega\tau(z_0)]} [\mathbf{r}(z_0)] \tag{5.2.55}$$

Normally we take the phase of the source $\tau(z_0)$ as zero. Now, in the case of an explosive source, the moment tensor is diagonal

$$\hat{m}(\omega) = \hat{m}_{zz}(\omega) = \hat{m}_{xx}(\omega) = \hat{m}_{\phi\phi}(\omega). \tag{5.2.56}$$

Then for this case equation 5.2.53 for $[\mathbf{r}(z_0)]$ ca be simplified as,

$$[\mathbf{r}(z_0)] = \frac{-i\omega\, \hat{m}(\omega)\, \eta}{\alpha_0^2\, (2\rho_0\, q_{\alpha_0})^{1/2}}\, [1, 0, 0, -1, 0, 0]^T. \tag{5.2.57}$$

Where we consider for W a source that generates only p-waves. In the example shown in chapter four we also consider a zero phase source.

5.2.4 Complete solution

Once the source term was defined, we can look for the complete solution of the in-homogeneous differential equation:

$$\partial_z \mathbf{y} \;=\; \omega \mathbf{A}\mathbf{y} + \mathbf{F} \tag{5.2.58}$$

Under the following boundary conditions:

- Top($z = 0$) : Free surface, stress components→zero
- Bottom($z = z_n$): only downward propagation. There are no sources or reflected energy.

Then, the solution can be written as

$$\underbrace{\begin{pmatrix} \mathbf{y}(0) \\ 0 \end{pmatrix}}_{\textit{stress set to zero}} = \mathbf{Y}_{(z_n)} \underbrace{\begin{pmatrix} 0 \\ \mathbf{w}_D(z_n) \end{pmatrix}}_{\textit{upoing waves set to zero}} + \mathbf{Y}_{(z_0)} \underbrace{\begin{pmatrix} \mathbf{r}_U \\ \mathbf{r}_D \end{pmatrix}}_{\textit{upward and downward source contribution}} \tag{5.2.59}$$

Where

$\mathbf{Y}_{(z)} = \mathbf{P}(0,z)\mathbf{N}(z)$

$\mathbf{w}_D$ down-going wave field at $z = z_n$.

$z_0 \rightarrow$ source depth.

$\mathbf{r}_U \rightarrow$ up-going waves from the source.

$\mathbf{r}_D \rightarrow$ down-going waves from the source.

In terms of propagators, the solution at the surface is given by:

$$\mathbf{y}(z_0+0) = \underbrace{\mathbf{P}(0,z_n)\mathbf{N}(z_n)}_{\mathbf{N}(z_0)\mathbf{S}(0,z_n)}\ \mathbf{w}(z_n) \ - \ \underbrace{\mathbf{P}(0,z_0)\mathbf{N}(z_0)}_{\mathbf{N}(z_0)\mathbf{S}(0,z_0)}\ \mathbf{w}_{source} \tag{5.2.60}$$

Since we know how to write the wave propagator $\mathbf{S}$ in terms of the reflection and transmission coefficients, we rewrite the solution as:

$$\begin{pmatrix}\mathbf{y}(0)\\ 0\end{pmatrix} = \begin{pmatrix}\mathbf{N}_{11} & \mathbf{N}_{12}\\ \mathbf{N}_{21} & \mathbf{N}_{22}\end{pmatrix}_{z_0}\begin{pmatrix}\mathbf{S}_{11} & \mathbf{S}_{12}\\ \mathbf{S}_{21} & \mathbf{S}_{22}\end{pmatrix}_{z_n}\begin{pmatrix}0\\ \mathbf{w}_D\end{pmatrix} - \begin{pmatrix}\mathbf{N}_{11} & \mathbf{N}_{12}\\ \mathbf{N}_{21} & \mathbf{N}_{22}\end{pmatrix}_{z_0}\begin{pmatrix}\mathbf{S}_{11} & \mathbf{S}_{12}\\ \mathbf{S}_{21} & \mathbf{S}_{22}\end{pmatrix}_{z_0}\begin{pmatrix}\mathbf{r}_U\\ \mathbf{r}_D\end{pmatrix} \tag{5.2.61}$$

We want solve the system for the displacement at the surface ($\mathbf{y}(0)$). Our unknowns are actually $\mathbf{y(0)}$ and the escaping waves $\mathbf{w_D}$. Solving for these vectors we obtain:

$$\mathbf{y}(0) = [\mathbf{N}^0_{11}\mathbf{S}^n_{12} + \mathbf{N}^0_{12}\mathbf{S}^n_{22}]\mathbf{w}_D - [\mathbf{N}^0_{11}\mathbf{S}^0_{11} + \mathbf{N}^0_{12}\mathbf{S}^0_{21}]\mathbf{r}_U + [\mathbf{N}^0_{11}\mathbf{S}^0_{12} + \mathbf{N}^0_{12}\mathbf{S}^0_{22}]\mathbf{r}_D. \tag{5.2.62}$$

$$0 = [\mathbf{N}^0_{21}\mathbf{S}^n_{12} + \mathbf{N}^0_{22}\mathbf{S}^n_{22}]\mathbf{w}_D - [\mathbf{N}^0_{21}\mathbf{S}^0_{11} + \mathbf{N}^0_{22}\mathbf{S}^0_{21}]\mathbf{r}_U + [\mathbf{N}^0_{21}\mathbf{S}^0_{12} + \mathbf{N}^0_{22}\mathbf{S}^0_{22}]\mathbf{r}_D. \tag{5.2.63}$$

Where we used the notation,

$\mathbf{N}^0_{ij} = \mathbf{N}_{ij}(z_0)$

$\mathbf{S}^n_{ij} = \mathbf{S}_{ij}(z_n)$

$\mathbf{S}^0_{ij} = \mathbf{S}_{ij}(z_0)$

Now, calling $\mathbf{S}_W$ and $\mathbf{S}_T$ the contributions of the source,

$$\mathbf{S}_W = [\mathbf{N}^0_{11}\mathbf{S}^0_{11} + \mathbf{N}^0_{12}\mathbf{S}^0_{21}]\mathbf{r}_U + [\mathbf{N}^0_{11}\mathbf{S}^0_{12} + \mathbf{N}^0_{12}\mathbf{S}^0_{22}]\mathbf{r}_D \tag{5.2.64}$$

$$\mathbf{S}_T = [\mathbf{N}^0_{21}\mathbf{S}^0_{11} + \mathbf{N}^0_{22}\mathbf{S}^0_{21}]\mathbf{r}_U + [\mathbf{N}^0_{21}\mathbf{S}^0_{12} + \mathbf{N}^0_{22}\mathbf{S}^0_{22}]\mathbf{r}_D \tag{5.2.65}$$

We solve for $\mathbf{w}_D$ from equation 5.2.63 and we obtain,

$$\mathbf{w}_D = [\mathbf{N}^0_{21}\mathbf{S}^n_{12} + \mathbf{N}^0_{22}\mathbf{S}^n_{22}]^{-1}\mathbf{S}_T, \tag{5.2.66}$$

replacing this expression of $\mathbf{w}_D$ on equation 5.2.62 leads to,

$$\mathbf{y}(0) = [\mathbf{N}^0_{11}\mathbf{S}^n_{12} + \mathbf{N}^0_{12}\mathbf{S}^n_{22}][\mathbf{N}^0_{21}\mathbf{S}^n_{12} + \mathbf{N}^0_{22}\mathbf{S}^n_{22}]^{-1}\mathbf{S}_T - \mathbf{S}_W. \tag{5.2.67}$$

Now, we recall $\mathbf{S}$

$$\mathbf{S}_\ell = \begin{pmatrix} \mathbf{S}_{11} & \mathbf{S}_{12} \\ \mathbf{S}_{21} & \mathbf{S}_{22} \end{pmatrix} = \begin{pmatrix} \mathbf{T}_U - \mathbf{R}_D\,\mathbf{T}_D^{-1}\,\mathbf{R}_U & \mathbf{R}_D\,\mathbf{T}_D^{-1} \\ -\mathbf{T}_D\,\mathbf{R}_U & \mathbf{T}_D^{-1}, \end{pmatrix} \tag{5.2.68}$$

replacing the wave propagators for their expressions in terms of reflection and transmission coefficients in equation 5.2.67 and re-arranging terms we obtain the solution at the surface in the (ω,p) domain as:

$$\mathbf{y}(0) = [\mathbf{N}^0_{12}\mathbf{T}^{-1}_{D_n} + \mathbf{N}^0_{11}\mathbf{R}_{D_n}\mathbf{T}^{-1}_{D_n}][\mathbf{N}^0_{21}\mathbf{R}_{D_n}\mathbf{T}^{-1}_{D_n} + \mathbf{N}^0_{22}\mathbf{T}^{-1}_{D_n}]^{-1}\mathbf{S}_T - \mathbf{S}_W \tag{5.2.69}$$

Finally, introducing the free surface reflection matrix,the solution at the surface is given by:

$$\mathbf{y}(0) = (\mathbf{N}_{12} + \mathbf{N}_{11}\mathbf{R}_{D_n})(\mathbf{I} - \tilde{\mathbf{R}}\mathbf{R}_{D_n})^{-1}\mathbf{N}^{-1}_{22}\mathbf{S}_T - \mathbf{S}_\omega \tag{5.2.70}$$

$\tilde{\mathbf{R}} = -\mathbf{N}^{-1}_{22}\mathbf{N}_{21}$ free surface reflection matrix.

This solution is given in the (ω,p) domain, to get the solution in the time-offset (t,x) domain we have to apply the inverse Fourier-Hankel transform, as it will be shown in next section.

5.2.5 Inverse Transforms

In order to obtain the expression of equation 5.2.70 in the time-offset domain a number of analytical and numerical techniques have been developed. We can divide the existing methods according to the order of integration. If the p integral is evaluated first, the intermediate result is a complex spectrum, and we call it a *spectral method.* If the ω integral is evaluated first, the intermediate result is a time series for a given p. We call this a *slowness method.* The method I used for the example shown follows the slowness method.

Each component of the vector $\mathbf{y}$ from equation 5.2.70 is a function of horizontal wave-number and azimuthal order m and and can be recovered by inverting the Fourier-Hankel transform. Here it is enough to consider only the term $m = 0$ so that the inverse Fourier-Hankel transform is given by:

$$\mathbf{y}(x,\omega) \;=\; \int_0^\infty \omega^2\, p\, dp\, \tilde{\mathbf{y}}(p,\omega)\; J_0(\omega p x), \tag{5.2.71}$$

J_0 is the Bessel function of order zero and $\tilde{\mathbf{y}}(p,\omega)$ is referred as the reflectivity function. In this equation p is the horizontal slowness, ω is radian temporal frequency and x is the distance of the receiver from the source. There are several techniques to solve equation 5.2.71 (Chapman and Orcutt, 1985; Mallick and Frazer, 1987). In this case I used the standard trapezoidal method, for that the integrand can be rewritten as:

$$\mathbf{y}(x,\omega) \;=\; \int_\gamma \frac{\omega^2}{2}\, p\, dp\, \tilde{\mathbf{y}}(p,\omega)\; H_0^1(\omega p x), \tag{5.2.72}$$

where the Bessel function is approximate by the Hankel function of type 1 and order zero . To simplify the integral to apply the trapezoidal rule, it can be written,

$$\int_\gamma \mathbf{f}(p)\; e^{Sg(p)} dp, \tag{5.2.73}$$

where,

$$\mathbf{f}(p) = \frac{\omega^2}{2}\, p\, \tilde{\mathbf{y}}(p,\omega)\, H_0^1(\omega p x) e^{-i\omega p x}, \tag{5.2.74}$$

$$S = i\omega x \tag{5.2.75}$$

and

$$g(p) = p. \tag{5.2.76}$$

Then, application of the standard trapezoidal rule to the integral in the equation 5.2.71, between the limits a and b, gives the quadrature formula,

$$\int_a^b \mathbf{f}(p)\, e^{Sg(p)} dp = \frac{1}{2}[f(a)e^{Sg(a)} + f(b)e^{Sg(b)}]\delta p. \tag{5.2.77}$$

When the integral from equation 5.2.71 has been computed for a range of frequencies, we recover the time domain version of $\mathbf{y}$ by and inverse Fourier transform,

$$\mathbf{y}(x,t) \;=\; \frac{1}{2\pi} \int_{-\infty}^{\infty} d\omega\, e^{-i\omega t}\, \mathbf{y}(x,\omega). \tag{5.2.78}$$

Finally, expression 5.2.78 gives the wave field at the surface in the time-offset domain[3].

[3]The numerical implementation of equation 5.2.78 uses a fast Fourier transform (FFT) (Strang, 1986)

Chapter 6

Conclusions

Within this thesis, the problem of *stratigraphic filtering* due to the presence of a cyclic reflectivity has been studied. An example of such an effect can be found in areas with thin coal beds in the Western Canadian Sedimentary Basin. The presence of coal seams can be identified with a cyclic impedance layering responsible for notches in the frequency content of the transmitted signal. The impulse response of such a cyclic reflectivity is contaminated by short-period multiple impossible to isolate and eliminate. Destructive interference between this multiple energy and the primary signal is the main reason for the loss of frequency content in the transmitted signal. Therefore, seismic processing faces a challenging task at the time of overcoming this problem.

As as secondary complication at the processing stage there is the concept of *non-white reflectivity* associated with a cyclic impedance sequence. Conventional deconvolution assumes a white reflectivity to compress the wavelet and recover the Earth's reflection response. However, in the presence of a cyclic impedance layering the whiteness assumption is invalid and deconvolution should be somehow corrected for this.

The effect of short-delay multiple reflections on primary reflection ampli-

tude and spectra are critically dependent on the type of the impedance layering present. Chapter two, introduces the concepts of *cyclic* and *transitional* impedance stratification. O'Doherty and Anstey (1971) clearly explained the difference between these two types of reflectivity. The cyclic type is the one that tends to alternate rapidly high and low values of impedance. In this context, "rapidly" refers to a layer thickness less than about $\lambda/8$, where λ is the (predominant) wavelength computed using the velocity of the layer. In contrast, a transitional reflectivity is characterized by a smooth (at least on the scale of a wavelength) change in impedance with depth.

O'Doherty and Anstey (1971) found that there is an anti-correlation between the power spectrum of the reflection coefficient series and the amplitude spectrum of the pulse transmitted through it. This approximation implies that in the case of a cyclic reflectivity, characterized by a low frequency cut, the signal transmitted through it has an inverse high-frequency cut. Such an effect is observed in the presence of coal seams in the Western Canadian Sedimentary Basin. Therefore, it seems to be important to study the properties of this type of reflectivity to be able to understand the associated impulse response.

In this sense, Walden and Hosken (1985; 1986) studied the statistical properties of the reflectivities from many wells all around the world. They found that neither transitional or cyclic types have a white spectrum. It was found that the reflection series are pseudo-white only above a corner frequency, below which their power spectrum falls away according to a power law f^{β}, where β is between 0.5 and 1.5. They proposed that ARMA(1,1) models would be the best way to model the amplitude spectrum observed on real log reflectivities.

Besides that, their work show that the probability distribution structure of these types of reflectivity is not Gaussian. It was found that the distribution is essentially symmetric but has a sharper central peak and larger tails than a

Gaussian distribution. Walden and Hosken (1986) proposed that a mixture of two Laplace distributions provides a good fit to the amplitude distribution of the primary reflection coefficients.

It is interesting to point out that by trying to understand the nature of stratigraphic filtering we come across to the concept of non-whiteness associated to cyclic reflectivities. However, it is important to avoid confusion about this subject. The non-whiteness characteristic of a cyclic reflectivity is not responsible for the observed layering filtering. The idea of a non-white reflectivity deals with its correlation structure, meaning that the sequence is not completely random but presents certain order. Instead, layering filtering is associated with the distortions that arise when a wave is traveling through such a profile. Nevertheless both concepts complicate conventional processing and one should be aware of this problem at the processing stage.

Once the idea of cyclic reflectivity was explained, chapter 3 focus on the main factors responsible for stratigraphic layering. In the presence of a cyclic impedance layering, stratigraphic filtering would arise from the combination of two factors: *transmission loss* and the presence of *short-period multiples*. The concept of short-period implies that the time difference between primary and first multiple is less than the width of the propagating wavelet.

As it was mentioned, O'Doherty and Anstey (1971) proposed an approximate relationship between the amplitude spectrum of the transmitted pulse and the power spectrum of the reflection coefficients series associated with the transmission filter. Later on, many other papers appear for a more clear derivation of such a relation. Banik (1985b; 1985a) derived the classic O'Doherty and Anstey formula using traditional methods of statistical mechanics as it is shown in Appendix B. Others, like Schoenberger (1974), Spencer (1977), Mateeva (2001), just accept the original derivation and study with more detail the attenuation

effect. They found that the main factor on the frequency attenuation is based on the interference between primary and short-path multiples. Such an interference would be constructive for some frequencies and destructive for others causing notches in the amplitude spectrum of the transmitted signal as it is observed in the WCB. The idea behind this effect is that the impulse response is associated to a cyclic impedance layering, characterized by high reflection coefficients. In this case, transmission losses might be so severe that the primary signal is reduced to negligible values. However, the short-period multiples immediately following the primary have significant amplitudes and the same polarity. The cyclic system acts like a low pass filter. The low frequencies see a almost homogeneous system and pass through it with little attenuation. Higher frequencies begin to see the velocity structure and are multiply reflected within it. Consequently, higher frequencies are delayed and ultimately removed from the transmitted signal. Chapter 3 explicitly illustrate these effects with several examples.

Finally, after getting a sense of what is causing the stratigraphic filtering observed in the WCB data, we analyzed possible approaches to overcome this effect from the seismic processing point of view. As it was mentioned before, the stratigraphic filtering is characterized by a correlation structure that deviates from the common used whiteness assumption. Chapter four reviewed some of the known techniques to face this weakness in the conventional seismic processing (Saggaf and Robinson, 2000). The *Spectral compensation filter* seems to be the easiest technique to implement and use.

As for the stratigraphic filtering effect itself it is proposed a way to compensate for the lack of frequency content in the transmitted signal below the transmission filter. This method consists of designing a minimum phase filter by using the Hilbert transform of the spectral factorization (spectra above and below the transmission filter). Results obtained by this technique seem to be

reasonable when comparing the extracted wavelets above and below the transmission filter after applying the minimum phase filter. However, the technique is very sensitive to the selection of the window length for the spectral factorization.

In conclusion, a way to improve the seismic image affected by transmission filtering could contemplate the following ideas. As it was mentioned within the thesis, conventional deconvolution is based on a seismic model with two components, wavelet and reflectivity. Processing data in the presence of stratigraphic filtering requires extra steps to improve the incomplete seismic model it is usually assumed.

In terms of the wavelet component, the spectral factorization technique presented here will help to compensate for the distortions experienced by the wavelet through the transmission filter. As a result non-stationarity of the signal should be reduced. The recommendation is to apply this technique after stack to minimize the effects of multiple energy. As for the reflectivity component, we know that the whiteness assumption is invalid specially in the presence of a cyclic reflectivity sequence. To compensate for this effect the application of a spectral compensation filter seems to be the most practical solution.

The important point in these techniques is that they imply a generalization of the conventional processing by just adding an extra step in the processing flow.

Layering filtering is still a topic under study, since the interference between multiples and primary is beyond seismic resolution. The success of the technique recommended here is sensitive to the area under study and it has to be adjusted for each case. For a better understanding of its performance, more tests with different datasets should be conducted.

References

Backus, G. E., and Mulcahy, M., 1976, Moment tensors and other phenomenological descriptions of seismic sources, I, continuous displacements.: Geophys. J. R. Astron. Soc., **46**, 341–361.

Banik, N., Lerche, I., Resnick, J. R., and Shuey, R. T., 1985a, Stratigraphic filtering, part II: Model spectra: Geophysics, **50**, 2775–2783.

—— 1985b, Stratigraphic filtering, part I: Derivation of the o'doherty-anstey formula: Geophysics, **50**, 2768–2774.

Box, G., and Jenkins, G., 1970, Time series analysis, forecasting and control: Holdenday, San Francisco.

Chapman, C., and Orcutt, J. A., 1985, The computation of body wave synthetic seismograms in laterally homogeneous media: Reviews of Geophysics, **23**, 105–163.

Chatfield, C., 1996, The analysis of time series, an introduction: Chapman and Hall/CRC.

Claerbout, J. F., 1976, Fundamentals of geophysical data processing: New York, McGraw-Hill Book Co. Inc.

Coulombe, C., and Bird, D. N., 1996, Transmission filtering by high-amplitude

reflection coefficients:theory,parctice,and processing considerations: The Leading Edge, **15**, 1037–1042.

Fertig, J., and Müller, G., 1978, Computations of synthetic seismograms for coal seams with the reflectivity method: Geophysical Prospecting, **26**, 868–883.

Fuchs, K., and Müller, G., 1971, Computation of synthetic seismograms with the reflectivity method and comparison with observations.: Geophys. J. R. Astron. Soc., **23**, 417–433.

Gilbert, F., 1971, Excitation of the normal modes of the earth by earthquake sources: Geophys. J. R. Astron. Soc., **22**, 223–226.

Haskell, N. A., 1953, The dispersion of surface waves on multilayered media.: Bull. seism. Soc. Am., **43**, 17–34.

Jurkevics, A., and Wiggins, R., 1984, A critique of seismic deconvolution methods: Geophysics, **49**, 2109–2116.

Kennet, B., and Kerry, N., 1979, Seismic waves in a stratified half-space: Geophys. J. R. Astron. Soc., **57**, 557–583.

Kennet, B., 1983, Seismic wave propagation in stratified media: Cambridge University Press.

Knopoff, L., 1964, A matrix method for elastic wave problems.: Bull. seism. Soc. Am., **54**, 431–438.

Lay, T., and Wallace, T. C., 1995, Modern global seismology: Academic Press.

Lazear, D., 1993, Mixed-phase wavelet estimation using fourth-order cumulants.: Geophysics.

Leinbach, J., 1996, Deconvolution 2: Society of Exploration Geophysicits.

Mallick, S., and Frazer, N., 1987, Practical aspects of reflectivity modeling: Geophysics, **52**, 1355–1364.

Mateeva, A., 2001, Spectral footprint of intrabed multiples: Center for wave phenomena, Department of Geophysics, Colorado School of Mines, **CWP-377**, 1–14.

Mendel, N., and Chan, 1979, Synthetic seismograms using the state-space approach: Geophysics, **44**, 880–895.

Müller, G., 1985, The reflectivity method: a tutorial: Journal of Geophysics, **58**, 153–174.

O'Doherty, and Anstey, 1971, Reflections on amplitudes: Geophysical Prospecting, **19**, 430–458.

Perz, M., 2000, Angle-dependent coal transmission filtering in the western canadian basin:a numerical study: SEG 2000 Expanded Abstracts, **12**, 2020–2023.

Robinson, E. A., and Treitel, S., 1967, Principles of digital wiener filtering.: Geophysical Prospecting, **15**, 311–333.

Robinson, E. A., and Treitel, S., 1980, Geophysical signal analysis: Englewood Cliffs,N.J., McGraw-Hill Book Co. Inc.

Robinson, E. A., 1957, Predictive decomposition of seismic traces: Geophysics, **22**, 767–778.

Robinson, E. A., 1966, Multichannel z-transforms and minimum-delay: Geophysics, **31**, 482–500,(erratum in Geophysics,31,992).

Robinson, E. A., 1968, Basic equations for synthetic seismograms using the z-transform approach.: Geophysics, **33**, 521–523.

Sacchi, M., and Ulrych, T. J., 1998, Nonminimum-phase wavelet estimation using polycepstra.: Journal of seismic exploration, **15**, 80–83.

Sacchi, M., and Ulrych, T. J., 2000, Nonminimum-phase wavelet estimation using higher order statistics: The Leading Edge, **15**, 80–83.

Sacchi, M., 1999, A procedure for wavelet estimation based on second and fourth order statistics.: CSEG Annual meeting abstracs.

Saggaf, M. M., and Robinson, E. A., 2000, A unified framework for the deconvolution of traces of non-white reflectivity: Geophysics, **65**, 1660–1676.

Schoenberger, M., and Levin, F. K., 1974, Apparent attenuation due to intrabed multiples: Geophysics, **39**, 278–291.

Smith, G. G., Cameron, A. R., and Bustin, R. M., 1994, Coal resources of the western canada sedimentary basin,*in* geological atlas of the western canada sedimentary basin: Canadian Society of Petroleum Geologists.

Smith, G. G., 1989, Coal formation and resources in the foreland basin: Canadian Society of Petroleum Geologists, **Special Volume**, 307–320.

Spencer, T. W., Edwards, C. M., and Sonnad, J. R., 1977, Seismic wave attenuation in nonresolvable cyclic stratification: Geophysics, **42**, 939–949.

Strang, G., 1986, Introduction to applied mathematics: Wellesley-Cambridge Press.

Takeuchi, H., and Saito, M., 1972, Seismic surface waves, *in* bolt, b. a.,ed.,methods of computational physics: Academic Press, Inc.

Tenorio, L., 2002, Modeling non-gaussian reflectivities: Generalizing wiener-levinson deconvolution: Geophysics, **66**, 1913–1920.

Thomson, W. T., 1950, Transmission of elastic waves through stratified medium.: J. appl. Phys., **21**, 89–93.

Todoeschuck, J. P., and Jensen, O. G., 1988, Joseph geology and seismic deconvolution: Geophysics, **53**, 1410–1414.

Velis, D., and Ulrych, T., 1996, Imulated annealing wavelet estimation via fourth-order cumulant matching.: Geophysics.

Walden, A. T., and Hosken, J., 1985, An investigation of the spectral properties of primary reflection coefficients: Geophysical Prospecting, **33**, 400–435.

Walden, A. T., and Hosken, J., 1986, The nature of non-gaussianity of primary reflection coefficients and its significance in deconvolution: Geophysical Prospecting, **34**, 1038–1066.

Widess, M., 1973, How thin is a thin bed?: Geophysics, **38**, 1176–1180.

Wuenschel, P. C., 1960, Seismogram synthesis including multiples and transmission coefficients.: Geophysics, **25**, 106–129.

Wyatt, K., 1981, Synthetic vertical seismic profile: Geophysics, **46**, 880–891.

Yilmaz, 1987, Seismic data processing: Society of Exploration Geophysicits.

Appendix A

The reflectivity method

A.1 Non-zero elements of the eigenvector matrix

The elements of the eigenvectors N of the matrix A are given by (Chapman and Orcutt, 1985):

$$N_{11} = -N_{14} = \frac{iq_\alpha}{(2\rho q_\alpha)^{1/2}}, \tag{A.1.1}$$

$$N_{21} = N_{24} = \frac{p}{(2\rho q_\alpha)^{1/2}}, \tag{A.1.2}$$

$$N_{41} = N_{44} = \frac{-\Omega}{(2\rho q_\alpha)^{1/2}}, \tag{A.1.3}$$

$$N_{51} = -N_{54} = \frac{2i\mu p q_\alpha}{(2\rho q_\alpha)^{1/2}}, \tag{A.1.4}$$

$$N_{12} = N_{15} = \frac{p}{(2\rho q_\beta)^{1/2}}, \tag{A.1.5}$$

$$N_{22} = -N_{25} = \frac{iq_\beta}{(2\rho q_\beta)^{1/2}}, \tag{A.1.6}$$

$$N_{42} = -N_{45} = \frac{2i\mu p q_\beta}{(2\rho q_\beta)^{1/2}}, \tag{A.1.7}$$

$$N_{52} = N_{55} = \frac{-\Omega}{(2\rho q_\beta)^{1/2}}, \tag{A.1.8}$$

$$N_{33} = N_{36} = \frac{1}{(2\mu q_\beta)^{1/2}}, \tag{A.1.9}$$

$$N_{63} = -N_{66} = \frac{i\mu q_\beta}{(2\mu q_\beta)^{1/2}}, \tag{A.1.10}$$

where,

$$\Omega = \rho - 2\mu p^2, \tag{A.1.11}$$

where ρ is the density, μ is the Lamé elastic parameter. The eigenvalues q_α and q_β are given by,

$$q_\alpha(p,z) = [\alpha^{-2}(z) - p^2]^{1/2}, \tag{A.1.12}$$

$$q_\beta(p,z) = [\beta^{-2}(z) - p^2]^{1/2}, \tag{A.1.13}$$

where p the ray parameter is given by $p = \frac{k}{\omega}$, with k as the wavenumber and ω the angular frequency.

The compressional wave velocity α is given by

$$\alpha(z) = (\frac{\lambda + 2\mu}{\rho})^{1/2}, \tag{A.1.14}$$

and the shear wave velocity β is,

$$\beta(z) = (\frac{\mu}{\rho})^{1/2}, \tag{A.1.15}$$

with λ and μ as the Lamé elastic parameter.

The elements are scaled in such a way that,

$$N^{-1} = iN^{+}. \tag{A.1.16}$$

A.2 Reflection and transmission coefficients

The reflection and transmission coefficients are computed whenever the waves go through a new interface. Here, one can select the type of waves to propagate, i.e. if we have an incident p-wave, we can select either to propagate only p-waves or include the sv-waves.

In the following formulas signs + and - are to indicate top and bottom of an interface respectively (Chapman and Orcutt, 1985).

$$R_D^{pp} = (A_{\alpha-} A_{\beta+} + C_{1-} C_{2+} - D) \; / \; \Delta^{pv}, \tag{A.2.1}$$

$$R_U^{pp} = (-A_{\alpha-} A_{\beta+} + C_{1+} C_{2-} - D) \; / \; \Delta^{pv}, \tag{A.2.2}$$

$$R_D^{vv} = (A_{\alpha+} A_{\beta-} + C_{1+} C_{2-} - D) \; / \; \Delta^{pv}, \tag{A.2.3}$$

$$R_U^{vv} = (-A_{\alpha+} A_{\beta-} + C_{1+} C_{2-} - D) \; / \; \Delta^{pv}, \tag{A.2.4}$$

$$R_U^{hh} = -R_D^{hh} = (\mu_2 \; q_{\beta 2} - \mu_1 \; q_{\beta 1}) \; / \; \Delta^{h}, \tag{A.2.5}$$

$$T_U^{pp} = T_D^{pp} = F_{\alpha 1} \; F_{\alpha 2} (q_{\beta 1} E_2 + q_{\beta 2} E_1 \; / \; \Delta^{pv}, \tag{A.2.6}$$

$$T_U^{vv} = T_D^{vv} = F_{\beta 1} \; F_{\beta 2} (q_{\alpha 1} E_2 + q_{\alpha 2} E_1 \; / \; \Delta^{pv}, \tag{A.2.7}$$

$$T_U^{hh} = T_D^{hh} = 2(\mu_2\, q_{\beta 2}\, \mu_1\, q_{\beta 1})^{1/2} \,/\, \Delta^h, \tag{A.2.8}$$

$$R_D^{pv} = R_D^{vp} = ipF_{\alpha 1}\, F_{\beta 1}(2q_{\alpha 2}\, q_{\beta 2} E_1 B_2 + E_2(E_2 - \rho_1)) \,/\, (\rho_1 \Delta^{pv}), \tag{A.2.9}$$

$$R_U^{pv} = R_U^{vp} = -ipF_{\alpha 2}\, F_{\beta 2}(2q_{\alpha 1}\, q_{\beta 1} E_1 B_1 + E_1(E_1 - \rho_2)) \,/\, (\rho_2 \Delta^{pv}), \tag{A.2.10}$$

$$T_D^{pv} = T_U^{vp} = -ipF_{\alpha 1}\, F_{\beta 2}(2B_2\, q_{\beta 1}\, q_{\alpha 2} + E_1 - \rho_2)) \,/\, \Delta^{pv}, \tag{A.2.11}$$

$$T_D^{vp} = T_U^{pv} = ipF_{\alpha 2}\, F_{\beta 1}(2B_1\, q_{\beta 2}\, q_{\alpha 1} + E_2 - \rho_1)) \,/\, \Delta^{pv}, \tag{A.2.12}$$

where,

$$\Delta^h = (\mu_1\, q_{\beta 1} + \mu_2\, q_{\beta 2}), \tag{A.2.13}$$

$$\Delta^{pv} = A_{\alpha +} A_{\beta +} - C_{1+} C_{2+} + D, \tag{A.2.14}$$

$$A_{\alpha +} = \rho_2\, q_{\alpha 1} + \rho_1\, q_{\alpha 2}, \tag{A.2.15}$$

$$A_{\beta -} = \rho_2\, q_{\beta 1} - \rho_1\, q_{\beta 2}, \tag{A.2.16}$$

$$B_1 = \mu_1 - \mu_2, \tag{A.2.17}$$

$$B_2 = \mu_2 - \mu_1, \tag{A.2.18}$$

$$C_{1+} = 2p[B_1(q_{\alpha 1}\, q_{\beta 1} + p^2) - \rho_1], \tag{A.2.19}$$

$$C_{2-} = 2p[B_2(-q_{\alpha 2}\, q_{\beta 2} + p^2) - \rho_2], \tag{A.2.20}$$

$$D = p^2(\rho_1 + \rho_2)^2, \tag{A.2.21}$$

$$E_1 = \rho_1 - 2p^2 B_1, \tag{A.2.22}$$

$$E_2 = \rho_2 - 2p^2 B_2, \tag{A.2.23}$$

$$F_{\alpha 1} = (2\ \rho_1\ q_{\alpha 1})^{1/2}, \tag{A.2.24}$$

$$F_{\beta 1} = (2\ \rho_2\ q_{\beta 2})^{1/2}. \tag{A.2.25}$$

The subscripts 1 and 2 refer to the medium just above and below the interface, i.e.

$$\mu_1 = \mu(z_\ell + 0), \tag{A.2.26}$$

$$\mu_2 = \mu(z_\ell - 0). \tag{A.2.27}$$

[(Chapman and Orcutt, 1985), pages 120,121]

Appendix B

O'Doherty-Anstey formula

B.1 Derivation of the O'Doherty-Anstey formula

I follow the derivation given by Banik (1985b) where they treat the medium as a continuum rather that as discrete layers, the advantage is that the result is independent of sample interval.

Let's start with the one-dimensional wave equation in the frequency domain:

$$\frac{\partial}{\partial z}\left[\frac{1}{\rho}\frac{\partial p}{\partial z}\right] + \frac{\omega^2}{\rho V^2}\, p \;=\; 0 \qquad \text{(B.1.1)}$$

Where $p =$ is pressure, $\omega =$ the angular frequency, $z =$ is depth, $\rho =$ density and $V =$ velocity.

Introducing the one way traveltime T as a new independent variable instead of depth

$$T = \int \frac{dz}{V}, \qquad \text{(B.1.2)}$$

and expressing the impedance Z as,

$$Z(T) = \rho V. \qquad \text{(B.1.3)}$$

Replacing this in the wave equation becomes,

$$\frac{\partial^2 p}{\partial T^2} - \frac{\partial p}{\partial T}\frac{\partial (lnZ)}{\partial T} + \omega^2 p = 0 \qquad \text{(B.1.4)}$$

Then, they postulate that the impedance Z at each depth T is a random variable. Assuming that lnZ is a stationary process, then its expectation value is independent of depth:

$$E[lnZ(T)] \equiv lnZ_0 \qquad \text{(B.1.5)}$$

Denoting the fluctuations in lnZ as,

$$\delta\mu = lnZ - E[lnZ] = ln(Z/Z_0) \qquad \text{(B.1.6)}$$

then, the wave equation can be re-written as,

$$\frac{\partial^2 p}{\partial T^2} + \omega^2 p = \frac{\partial p}{\partial T}\frac{\partial (\delta\mu)}{\partial T}. \qquad \text{(B.1.7)}$$

Another consequence of assuming lnZ is stationary is that its autocorrelation only dependent on the lags:

$$E[\delta\mu(T)\,\delta\mu(T')] \equiv M(T - T') \qquad \text{(B.1.8)}$$

Although equation B.1.5 and B.1.8 are not necessarily well honored by nature, the two assumptions are commonly made to facilitate mathematical results comparable to field data. Both are also implicit in the derivation given by O'Doherty and Anstey (1971).

The analogy between O'Doherty-Anstey formula, where they use a discrete rc series, can be found in the continuous field with a valid discrete aproximatiom. For that, the depth T can be divided into small, equals intervals and Z can be

considered constant at each interval. The discontinuity between intervals is given by the reflection coefficients,

$$r_\ell = \frac{Z_{\ell+1} - Z_\ell}{Z_{\ell+1} + Z_\ell}. \tag{B.1.9}$$

For small reflection coefficients ($| r | \ll 1$) which are related to the spatial change in lnZ

$$r \approx \frac{1}{2}\Delta lnZ = \frac{\tau}{4}\frac{\partial(lnZ)}{\partial T} \tag{B.1.10}$$

where τ is the two way time for the sample interval. Now, using equation B.1.6, becomes

$$r \approx \frac{\tau}{4}\frac{\partial(\delta\mu)}{\partial T}. \tag{B.1.11}$$

O'Doherty and Anstey (1971) defined the spectrum $R(\omega)$ of the series of reflection coefficients as,

$$R(\omega) = \frac{1}{\tau}\sum_\ell e^{+i\omega\ell\tau} E[r_n r_{n+\ell}]. \tag{B.1.12}$$

The analogy to this formula as a continuous quantity, replace equation B.1.11 into equation B.1.12 and let the sum approximate an integral.

$$R(\omega) = \frac{1}{8}\int_{-\infty}^{+\infty} dT\, e^{-i2\omega(T-T')}\frac{\partial^2}{\partial T\,\partial T'}E[\delta\mu(T)\delta\mu(T')]. \tag{B.1.13}$$

The autocorrelation in equation B.1.13 is written as $M(T-T')$ in equation B.1.8. Defining its Fourier transform $\hat{M}$ such that

$$M(T-T') = \frac{1}{2\pi}\int_{-\infty}^{+\infty} dx e^{+ix(T-T')}\hat{M}(x) \tag{B.1.14}$$

Substituting equations B.1.8 and B.1.14 into equation B.1.13 gives,

$$R(\omega) = \frac{1}{2}\omega^2 \hat{M}(2\omega) \tag{B.1.15}$$

Equations B.1.13 or B.1.15 defines the continuous quantity that corresponds to the spectrum employed by O'Doherty and Anstey (1971), essentially is the spectrum of $\frac{\partial(\delta\mu)}{\partial T}$.

Banik (1985b) used the mean-field theory for waves in random media, obtaining results identical to those of O'Doherty and Anstey. In this way, the pressure p at each depth T is a random variable, connected to the impedance fluctuation with equation B.1.14. Denoting the mean field $E[p]$ as p_0 and the fluctuating part δp, then

$$p = p_0 + \delta p \tag{B.1.16}$$

Following an standard procedure they obtain a Kramers-Kronig dispersion relation for p_0. For temporal dependence $e^{-i\omega t}$ the spatial dependence is a damped plane wave of the form $e^{-i\Omega t}$ with spatial frequency Ω. Then they obtain the following results (details of their derivation can be found in the Appendix B of their paper (Banik et al., 1985b))

$$\Omega = \pm\omega(1 + F), \tag{B.1.17}$$

where the signs correspond to upward and downward modes of propagation. The real and imaginary parts of F are given by,

$$F_I = \frac{1}{2}\omega \hat{M}(2\omega), \tag{B.1.18}$$

$$F_R = \frac{1}{pi}\int_{-\infty}^{+\infty} dy \frac{F_I(y)}{(y-\omega)}. \tag{B.1.19}$$

From equations B.1.15 and B.1.18 it also valid the expression,

$$F_I = \frac{R(\omega)}{\omega} \tag{B.1.20}$$

The mean-field dispersion relation can be interpreted as stratigraphic filtering by considering a downward propagating wavelet. For a case like a succession of fine layers, when the waveform travels through it is contaminated by short-period multiples. The waveform is then continuously modified by the superposition of these short-delay multiples. In a distance ΔT the component of temporal frequency ω is multiplied by,

$$e^{+i\Omega\Delta T} = e^{+iw\Delta T} A(\omega) \tag{B.1.21}$$

where,

$$A(\omega) = e^{i\omega F \Delta T} \tag{B.1.22}$$

Finally, by replacing equation B.1.20 in equation B.1.22, it gives the formula of O'Doherty and Anstey (1971)

$$\mid A(\omega) \mid = e^{-i\Delta T R(\omega)}. \tag{B.1.23}$$